بسم الله الرحمن الرحيم



Palestine Polytechnic University

Deanship of Graduate Studies and Scientific Research

Master of Civil Engineering- Earthquake Engineering

RESPONSE MODIFICATION FACTOR IN REINFORCED CONCRETE SPECIAL MOMENT RESISTING FRAME BUILDINGS

Name of student

Majdi Osama Ahmaro

Supervisor

Dr. Haitham Ayyad

Thesis submitted in partial fulfillment of the requirements of the degree of Master of Science in civil engineering to the faculty of Graduate Studies at Palestine Polytechnic University.

November 2026

The undersigned hereby certify that they have read, examined, and recommended to the Deanship of Graduate Studies and Scientific Research at Palestine Polytechnic University

RESPONSE MODIFICATION FACTOR IN REINFORCED CONCRETE SPECIAL MOMENT RESISTING FRAME BUILDINGS

Majdi Osama Ahmaro

In partial fulfillment of the requirements for the degree of Master of Civil Engineering - Earthquake Engineering.

Graduate Advisory Committee:

Prof./Dr. ……, (Supervisor), University.

Signature: _____ Date: _____

Prof./Dr. ……, (Internal committee member), University.

Signature: _____ Date: _____

Prof./Dr. ……, (External committee member), University.

Signature: _____ Date: _____

Thesis Approved by:

Name: _____

Dean of Graduate Studies & Scientific Research
Palestine Polytechnic University

Signature: _____ Date: _____

RESPONSE MODIFICATION FACTOR IN REINFORCED CONCRETE SPECIAL MOMENT RESISTING FRAME BUILDINGS

ABSTRACT

The response modification factor R = 8 that ASCE 7-16 assigns to reinforced concrete (RC) special moment-resisting frames is a single value, applied regardless of height, period or detailing. This study estimates the factor for seven three-dimensional frames designed to ASCE 7-16 and detailed to ACI 318-19, for a rock site with the hazard of seismic Zone 3 of Palestine (Z = 0.30): frames of four, six and fifteen stories, and four variants of the fifteen-story frame (wider hoop spacing with lower concrete strength, higher column reinforcement, and reduced column sections at two locations). The frames were designed in ETABS and analyzed by pushover analysis in SAP2000, with the hinge properties and acceptance criteria of ASCE 41-17. The factor was computed as $R = R_\mu \times \Omega$ from an equal-area bilinear idealization, under three code-based definitions of the maximum displacement: the amplified displacement of ASCE 7-16 (Method A), the target displacement of FEMA 356 (Method B), and the displacement at which the first component reaches the Collapse-Prevention limit of ASCE 41-17 (Method C). Because the prototype is in Risk Category III, the estimated factor is R / I_e and is compared with 8 / 1.25 = 6.40. Methods A and B give 3.30 to 4.19 and 2.24 to 3.74, below 6.40, because their demand displacements are only 1.1 to 1.6 times the effective yield displacement. Method C gives 10.21 to 13.50, above 6.40 in every model, with ductility ratios of 1.99 to 2.92; under the first-mode load pattern the five models that reached the limit give 9.98 to 11.08. Wider hoop spacing with lower concrete strength lowered the capacity-based factor by 12.1 percent, higher column reinforcement raised it by 9.5 percent, and reducing column sections away from the first story changed it by less than 0.5 percent. For the seven frames examined and under the stated assumptions, R = 8 is conservative with respect to the capacity available up to Collapse Prevention, and the estimated factor depends strongly on the definition of the maximum displacement, which should always be stated. Nonlinear dynamic analysis is recommended to confirm these results.

Keywords: response modification factor; special moment-resisting frame; pushover analysis; overstrength; displacement ductility; ASCE 7-16; ASCE 41-17; ACI 318-19; collapse prevention.

معامل تعديل الاستجابة في المباني ذات الإطارات الخرسانية المسلحة الخاصة المقاومة للعزوم

الملخص

يحدد الكود ASCE 7-16 لمعامل تعديل الاستجابة R في الإطارات الخرسانية المسلحة الخاصة المقاومة للعزوم قيمة واحدة هي 8، تُطبق مهما كان ارتفاع المبنى أو دوره أو تفاصيل تسليحه. تقدّر هذه الدراسة المعامل لسبعة إطارات ثلاثية الأبعاد صُممت وفق ASCE 7-16 وفُصّل تسليحها وفق ACI 318-19، لموقع صخري له خطر المنطقة الزلزالية 3 في فلسطين (Z = 0.30): إطارات من أربعة وستة وخمسة عشر طابقًا، وأربعة نماذج معدلة من الإطار ذي الخمسة عشر طابقًا (تباعد أكبر للكانات مع مقاومة خرسانة أقل، وتسليح أعلى للأعمدة، وتصغير مقاطع الأعمدة في موضعين). صُممت الإطارات في ETABS وحُللت بتحليل الدفع الجانبي في SAP2000، بخصائص المفاصل ومعايير القبول في ASCE 41-17. حُسب المعامل من العلاقة $R = R_\mu \times \Omega$ اعتمادًا على منحنى ثنائي الخطية متساوي المساحة، وفق ثلاثة تعريفات للإزاحة القصوى مأخوذة من الأكواد: الإزاحة المضخمة في ASCE 7-16 (الطريقة A)، والإزاحة الهدف في FEMA 356 (الطريقة B)، والإزاحة التي يبلغ عندها أول عنصر حد منع الانهيار في ASCE 41-17 (الطريقة C). ولأن المبنى من فئة الخطورة III، فالمعامل المقدَّر هو R / I_e ويُقارن بالقيمة 6.40 = 1.25 / 8. أعطت الطريقتان A وB قيمًا من 3.30 إلى 4.19 ومن 2.24 إلى 3.74، وهي أقل من 6.40، لأن إزاحتي الطلب فيهما لا تزيدان على 1.1 إلى 1.6 مرة من إزاحة الخضوع الفعالة. وأعطت الطريقة C قيمًا من 10.21 إلى 13.50، أعلى من 6.40 في النماذج كلها، بنسب مطاوعة من 1.99 إلى 2.92؛ وتحت نمط التحميل الموافق للنمط الأول أعطت النماذج الخمسة التي بلغت الحد قيمًا من 9.98 إلى 11.08. خفّض تباعد الكانات الأكبر مع مقاومة الخرسانة الأقل المعامل المبني على القدرة بنسبة 12.1%، ورفعه تسليح الأعمدة الأعلى بنسبة 9.5%، وغيّره تصغير مقاطع الأعمدة بعيدًا عن الطابق الأول بأقل من 0.5%. تخلص الدراسة إلى أن القيمة R = 8 محافظة، للإطارات السبعة المدروسة وضمن الافتراضات المذكورة، قياسًا بالقدرة المتاحة حتى حد منع الانهيار، وأن المعامل المقدَّر يعتمد بقوة على تعريف الإزاحة القصوى، فيجب ذكره دائمًا. وتوصي الدراسة بالتحليل الديناميكي اللاخطي لتأكيد هذه النتائج.

الكلمات المفتاحية: معامل تعديل الاستجابة؛ الإطارات الخاصة المقاومة للعزوم؛ تحليل الدفع الجانبي؛ المقاومة الزائدة؛ مطاوعة الإزاحة؛ ASCE 7-16؛ ASCE 41-17؛ ACI 318-19؛ حد منع الانهيار.

DECLARATION

I declare that the Master Thesis entitled “Response Modification Factor in Reinforced Concrete Special Moment Resisting Frame Buildings” is my own original work, and I hereby certify that unless stated, all work contained within this thesis is my own independent research and has not been submitted for the award of any other degree at any institution, except where due acknowledgement is made in the text.

Student Name: Majdi Osama Ahmaro

Signature: _____ Date: _____

DEDICATION

To the soul of my mother, whose prayers reached further than she ever knew, and whose memory carried this work through every difficult night. May Allah have mercy upon her.

To my father, who taught me that patience and knowledge are the same virtue wearing two names, and who never once let me doubt that this day would come.

To my wife, my steady support through every stage of this research, who carried the weight of ordinary days so that I could carry this one.

To my brothers, my sisters and my friends, and to everyone who offered a sincere prayer or a kind word along the way.

ACKNOWLEDGEMENT

First, I thank Allah, who granted me the strength and patience to complete this work.

I extend my sincere gratitude to my supervisor, Dr. Haitham Ayyad, whose guidance shaped this thesis at every stage. His questions were as valuable as his answers, and the discipline he asked of the analysis is reflected in every result reported here.

I also thank Dr. Bilal Al-Masri, coordinator of the Master program in Civil Engineering at Palestine Polytechnic University, and the faculty members of the program, for the knowledge and the environment that made this research possible.

Finally, I thank my family for their patience over the months this work demanded, and my colleagues for every discussion that sharpened an idea.

TABLE OF CONTENTS

ABSTRACT IV
الملخص V
DECLARATION VI
CHAPTER 1 INTRODUCTION 1
1.1 Background 1
1.2 Seismic Hazard of the Study Region 3
1.3 Problem Statement 5
1.4 Research Objectives 6
1.5 Research Methodology 7
1.6 Scope and Limitations 8
1.7 Research Significance 9
1.8 Thesis Organization 10
CHAPTER 2 LITERATURE REVIEW 12
2.1 Introduction 12
2.2 The Response Modification Factor: Concept, Formulation, and Components 12
2.2.1 Historical Development of the R-Factor 12
2.2.2 Mathematical Formulation 13
2.2.3 The Ductility Reduction Factor and Its Period Dependence 14
2.2.4 The Overstrength Factor 16
2.2.5 The Redundancy Factor 17
2.3 Methods of Estimating R from Nonlinear Analysis 17
2.3.1 Nonlinear Static (Pushover) Analysis 17
2.3.2 Bilinear Idealization and Extraction of the R-Components 18
2.3.3 Nonlinear Dynamic and Incremental Dynamic Analysis 19
2.3.4 The Maximum-Displacement Problem 19
2.4 Critical Review of Previous Studies 20
2.4.1 Effect of Building Height and Period 20
2.4.2 Effect of Bay Configuration and Global Geometry 21
2.4.3 Effect of Reinforcement Detailing and Confinement 22
2.4.4 Effect of Vertical Irregularity and Redundancy 22
2.4.5 Influence of the Estimation Method and Target-Displacement Definition 23
2.4.6 Code Comparison and the Developing-Country Context 23
2.4.7 Collapse-Risk and Post-Earthquake Functionality Approaches 24
2.5 Research Gap and Positioning of the Present Study 27
2.6 Summary 28

CHAPTER 3 STUDY DESCRIPTION 29
3.1 Introduction 29
3.2 Prototype Structure Description 29
3.3 Material Properties 34
3.4 Gravity Loading 34
3.5 Seismic Design Parameters 35
3.6 Seismic Force-Resisting System and Design Coefficients 36
3.7 Design Base Shear and Load Combinations 37
3.8 Parametric Study Framework 38
CHAPTER 4 VALIDATION OF THE NONLINEAR MODELING PROCEDURE 40
4.1 Introduction 40
4.2 Nonlinear Analysis Framework in SAP2000 40
4.2.1 Solution Strategy 40
4.2.2 Material Constitutive Models 41
4.2.3 Plastic Hinge Definitions 42
4.3 Validation Case 1: Single-Span Beam (Bresler and Scordelis, 1963) 43
4.3.1 Geometry and Test Configuration 43
4.3.2 Material Properties 43
4.3.3 Numerical Model Setup and Results 44
4.4 Validation Case 2: Two-Span Continuous Beam (Duddeck-Mueller) 45
4.4.1 Geometry and Test Configuration 45
4.4.2 Material Properties 46
4.4.3 Numerical Model Setup and Results 46
4.5 Validation Case 3: One-Story Reinforced Concrete Frame (Xiao et al., 2006) 47
4.5.1 Geometry and Test Configuration 47
4.5.2 Material Properties 48
4.5.3 Numerical Model Setup and Results 49
4.6 Consolidated Assessment of Modeling Accuracy 50
4.7 Chapter Summary 51
CHAPTER 5 SPECIAL MOMENT RESISTING FRAME MODELING AND NONLINEAR ANALYSIS 53
5.1 Introduction 53
5.2 Prototype Geometry 53
5.3 Material Properties of the Nonlinear Model 55
5.3.1 Acceptance criteria for plastic hinges 56
5.4 Components of the Response Modification Factor 58
5.4.1 Ductility and ductility reduction factor 58

5.4.2 Overstrength factor 59
5.4.3 Definition of the Maximum Displacement: Three Methods 60
5.5 Performance Levels and Bilinear Idealization 64
5.5.1 Effective Stiffness K_e 66
5.6 Reinforcement Detailing of the Prototype Models 66
5.6.1 Four-story and six-story models 67
5.6.2 Fifteen-story reference model 68
5.6.3 Parametric variants of the fifteen-story frame 68
5.7 Numerical Modeling 70
5.7.1 Analysis platform and design transfer 70
5.7.2 Plastic hinge formulation 71
5.7.3 Loading protocol and second-order effects 72
5.8 Chapter Summary 73
CHAPTER 6 ESTIMATION OF THE RESPONSE MODIFICATION FACTOR 75
6.1 Introduction and Decomposition Framework 75
6.1.1 The reduced identity and the condition for its use 77
6.1.2 Source of the three definitions of the maximum displacement 78
6.2 Elastic Design Quantities 79
6.3 Bilinear Idealization of the Capacity Curve 80
6.3.1 The area A, and how it is obtained 80
6.3.2 Derivation of the equal-area equation 81
6.3.3 The anchor displacement 82
6.3.4 Admissibility of the construction 82
6.3.5 The effective stiffness 83
6.4 Method A: the Code-Amplified Displacement 83
6.4.1 Definition 83
6.4.2 Numerical chain 84
6.4.3 The role of the importance factor in the reported factor 85
6.5 Method B: the FEMA 356 Target Displacement 87
6.5.1 Definition 87
6.5.2 Numerical chain 87
6.5.3 The ductility mobilized under this method 88
6.6 Method C: the Collapse-Prevention Displacement Capacity 89
6.6.1 The hinge inventory 89
6.6.2 Definition 90
6.6.3 Locating the limit state between two analysis steps 91
6.6.4 The components that govern 93

6.6.5 Sensitivity to a criterion based on a fraction of the hinges 94
6.7 Model-by-Model Calculation 95
6.7.1 Four-story frame 97
6.7.2 Six-story frame 100
6.7.3 Fifteen-story reference frame 103
6.7.4 Model 4: wider hoop spacing and lower concrete strength 106
6.7.5 Model 5: about 2 percent longitudinal reinforcement 109
6.7.6 Model 6: reduced columns in stories 3 to 5 112
6.7.7 Model 7: reduced columns in stories 13 to 15 115
6.8 Consolidated Results 117
6.8.1 Uniform pattern 117
6.8.2 First-mode load pattern and the envelope of the two patterns 119
6.9 Comparative Discussion 122
6.9.1 The three definitions compared 122
6.9.2 Comparison with the tabulated value of ASCE 7-16 122
6.9.3 The effect of building height 124
6.9.4 The parametric variants 125
6.9.5 The effect of the load pattern 125
6.10 Limitations of the Estimation 126
6.11 Summary of Findings 127
CHAPTER 7 CONCLUSIONS AND RECOMMENDATIONS 129
7.1 Summary of the Study 129
7.2 Conclusions 129
7.3 Limitations 130
7.4 Recommendations 131
REFERENCES 132
APPENDIX A ELASTIC DESIGN CALCULATIONS AND CODE CHECKS 139
A.1 Seismic Design Parameters 139
A.2 Design Base Shear 139
A.3 Story Drift Check 140
A.4 Stability Coefficient 142
APPENDIX B COLUMN CONFINEMENT: DESIGN AND MANDER PARAMETERS 144
B.1 Design of the Column Hoops 144
B.2 Mander Parameters of a Representative Column 145
B.3 Volumetric Confinement Ratio 145
B.4 Derived Confined Properties 145

B.5 Internal Consistency Check _____ 146
APPENDIX C PLASTIC HINGE PROPERTIES _____ 147
C.1 Hinge Assignment Scheme _____ 147
C.2 Representative Hinges _____ 147
C.3 Evolution of the Hinge Demand-Capacity Ratio, Fifteen-Story Reference Frame _____ 148
APPENDIX D FEMA 356 DISPLACEMENT COEFFICIENT METHOD: COEFFICIENT VALUES _____ 149
D.1 Basis of Each Coefficient _____ 149
D.2 Computation of C_0 _____ 149

ABBREVIATIONS AND SYMBOLS

Abbreviations and Acronyms

ACI	American Concrete Institute
ASCE	American Society of Civil Engineers
ATC	Applied Technology Council
BS 8110	British Standard 8110, structural use of concrete
CP	Collapse Prevention performance level
DST	Dead Sea Transform fault system
ECP	Egyptian Code of Practice; in the studies cited, ECP-201 (2012), the Egyptian code for calculating loads and forces in structural work and masonry
ELF	Equivalent Lateral Force procedure, ASCE 7-16 Section 12.8
EQX	Earthquake load case applied in the longitudinal (x) direction
ETABS	Extended Three-Dimensional Analysis of Building Systems, the elastic design software
FEMA	Federal Emergency Management Agency
IBC	International Building Code
IDA	Incremental Dynamic Analysis
IDARC	Inelastic Damage Analysis of Reinforced Concrete, software used in a cited study
IO	Immediate Occupancy performance level
IS 1893	Indian Standard 1893, criteria for earthquake-resistant design of structures
LS	Life Safety performance level
MCE_R	Risk-Targeted Maximum Considered Earthquake
MRF	Moment-Resisting Frame
NEHRP	National Earthquake Hazards Reduction Program
NLTHA	Nonlinear Time-History Analysis
OMRF	Ordinary Moment-Resisting Frame
RC	Reinforced Concrete
SAP2000	Structural Analysis Program 2000, the nonlinear pushover software
SCWB	Strong-Column Weak-Beam
SDC	Seismic Design Category
SEI	Structural Engineering Institute
SMRF	Special Moment-Resisting Frame
SNI	Standard Nasional Indonesia, the Indonesian national standard; in the studies cited, SNI 1726:2019 (seismic design)
UBC	Uniform Building Code

Roman Symbols

A	Area enclosed by the capacity curve up to the anchor displacement, kN·mm
a, b, c	Modeling parameters of a plastic hinge, ASCE 41-17 Tables 10-7 and 10-8
A_c	Area of the concrete core measured to the centerline of the perimeter hoop, mm²
A_e	Area of effectively confined concrete core, mm²
A_{sh}	Total cross-sectional area of transverse reinforcement within the spacing s, mm²
b_c	Core dimension measured to the centerline of the perimeter hoop, mm
C_0, C_1, C_2, C_3	Displacement modification coefficients of FEMA 356, Equation 3-15
D/C	Demand-capacity ratio of a plastic hinge, θ_p / θ_{CP}
C_d	Deflection amplification factor, taken as 5.5 for the special moment-resisting frame
C_s	Seismic response coefficient
C_t, x	Period parameters of ASCE 7-16 Equation 12.8-7, taken as 0.0466 and 0.9
C_u	Coefficient for the upper limit on the calculated period, taken as 1.5
E_c	Modulus of elasticity of concrete, MPa
E_s	Modulus of elasticity of reinforcing steel, MPa
E_{sec}	Secant modulus of confined concrete at peak stress, f'_{cc} / ε_{cc}, MPa
f'_c	Specified compressive strength of unconfined concrete, MPa
f'_{cE}	Expected compressive strength of concrete used in the nonlinear models, MPa
f'_{cc}	Compressive strength of confined concrete, MPa
f_y	Specified yield strength of longitudinal reinforcement, MPa
f_{yE}	Expected yield strength of reinforcement used in the nonlinear models, MPa
f_{yh}	Yield strength of transverse reinforcement, MPa
g	Acceleration of gravity
h_{sx}	Story height below the level considered, mm
I_e	Importance factor, taken as 1.25 for Risk Category III
K_d	Elastic design stiffness, V_d / Δ_d, kN/mm
K_e	Effective lateral stiffness, secant to 0.6 V_y, kN/mm
k_e	Confinement effectiveness coefficient of the Mander model

N	Total number of plastic hinges in the model
N_{UD}	Axial force of a column under the gravity load case of the nonlinear analysis, kN
n	Axial load ratio of a column, $N_{UD} / (A_g f'_{cE})$
P_x	Total unfactored vertical design load at and above the level considered, kN
R	Response modification factor
R_A, R_B, R_C	Response modification factor obtained by Methods A, B and C respectively
R_μ	Ductility reduction factor
r	Curve-shape parameter of the Mander model, $E_c / (E_c - E_{sec})$
S_a	Spectral acceleration at the effective fundamental period, g
S_d	Spectral displacement, mm
S_s, S_1	Mapped risk-targeted spectral accelerations at short period and at 1 s, g
S_{MS}, S_{M1}	Spectral accelerations adjusted for site class at short period and at 1 s, g
S_{DS}, S_{D1}	Design spectral accelerations at short period and at 1 s, g
s	Centre-to-center spacing of transverse reinforcement, mm
T	Fundamental period; design period $C_u T_a$ where capped, s
T_a	Approximate fundamental period of ASCE 7-16 Equation 12.8-7, s
T_e	Effective fundamental period taken from the SAP2000 model, s
T_L	Long-period transition period, s
T_s	Corner period of the design spectrum, S_{D1} / S_{DS}, s
V_d	Design base shear, kN
V_u	Base shear at the anchor point of the bilinear idealization, kN
V_x	Seismic design shear acting at the level considered, kN
V_y	Effective yield base shear, kN
W	Effective seismic weight of the structure, kN

Greek Symbols

α	Tensile stiffness coefficient of the concrete material model (Chapter 4)
β	Ratio of shear demand to shear capacity in Equation 12.8-16, taken as unity
Γ	Modal participation factor in the direction of loading
Δ	Design story drift, mm
Δ_a	Allowable story drift, mm
Δ_d	Elastic design roof displacement, mm
$\Delta_{max,A}$	Maximum roof displacement under Method A, mm

$\Delta_{max,C}$	Maximum roof displacement under Method C: the roof displacement at which the first component reaches its Collapse-Prevention criterion, mm
Δ_u	Roof displacement at the anchor point, mm
Δ_y	Effective yield roof displacement, mm
δ_t	Target displacement of the FEMA 356 displacement coefficient method, mm
δ_x	Amplified story displacement of ASCE 7-16 Equation 12.8-15, mm
δ_{xe}	Elastic story displacement obtained from the analysis, mm
ε_{cc}	Strain at the peak stress of confined concrete
ε_{cu}	Ultimate compressive strain of confined concrete
ε_{su}	Strain at the ultimate tensile strength of the transverse reinforcement
θ	Stability coefficient of ASCE 7-16 Equation 12.8-16
θ_{max}	Limiting value of the stability coefficient
θ_p, θ_{CP}	Plastic rotation of a hinge and its Collapse-Prevention plastic rotation, rad
μ	Displacement ductility ratio
ν	Poisson’s ratio
ξ	Damping-related multiplier in the four-term decomposition reported in the cited literature
ρ	Redundancy factor of ASCE 7-16 Section 12.3.4
ρ_{bal}	Balanced reinforcement ratio of a beam section
ρ_l	Longitudinal reinforcement ratio
ρ_s	Volumetric ratio of transverse confining reinforcement to the confined core
ρ_t	Transverse reinforcement ratio of a column, A_v / (b s), ASCE 41-17 Table 10-8
Φ	Nominal bar diameter designation, for example Φ14
φ_{roof}	Mode-shape ordinate at the roof under the adopted normalization
Ω	Overstrength factor
Ω_0	Overstrength factor tabulated by the code, taken as 3.0

LIST OF FIGURES

Figure 1.1 Ductile and brittle global response of a structure. 1
Figure 1.2 Principal faults of Palestine and the surrounding region (Sharon et al., 2020). 3
Figure 1.3 Seismic hazard map of the Levant (An-Najah National University, n.d.). 4
Figure 2.1 Decomposition of the response modification factor on the capacity curve. 14
Figure 2.2 Newmark-Hall ductility reduction factor against period. 15
Figure 2.3 Capacity-spectrum method (after ATC-40, 1996). 18
Figure 3.1 Plan and three-dimensional views of the prototype structure. 30
Figure 3.2 Four-story frame (ETABS). 31
Figure 3.3 Six-story frame (ETABS). 32
Figure 3.4 Fifteen-story reference frame (ETABS). 32
Figure 3.5 Elevation of the fifteen-story reference frame (SAP2000). 33
Figure 4.1 Elastic-perfectly plastic and linear-hardening stress-strain curves. 42
Figure 4.2 Single-span beam of Bresler and Scordelis (1963). 43
Figure 4.3 Load-deflection curve of the single-span beam. 45
Figure 4.4 Cross section of the two-span beam. 46
Figure 4.5 Load-deflection curve of the two-span beam. 47
Figure 4.6 One-story frame tested by Xiao et al. (2006). 48
Figure 4.7 Load-deflection response of the one-story frame. 50
Figure 5.1 Fifteen-story reference model (SAP2000). 54
Figure 5.2 Confined and unconfined concrete (after Mander et al., 1988). 56
Figure 5.3 Generalized force-deformation relation (ASCE 41-17, Figure 10-1a). 57
Figure 5.4 Displacement ductility ratio. 59
Figure 5.5 Overstrength factor on the capacity curve. 60
Figure 5.6a ASCE 7-16 Equation 12.8-15 (Method A). 61
Figure 5.6b FEMA 356 Equation 3-15 (Method B). 62
Figure 5.6c ASCE 41-17 Table 10-7, beams (Method C). 63
Figure 5.6d ASCE 41-17 Table 10-8, columns (Method C). 63
Figure 5.7 Secant-stiffness bilinear idealization (Paulay and Priestley, 1992). 65
Figure 5.8 Equal-area rule on the capacity curve of the four-story frame. 65
Figure 5.9 Effective stiffness and bilinear idealization (FEMA 356, Figure 3-1). 66
Figure 5.10 First-story column sections of the fifteen-story reference frame. 70
Figure 5.11 Beam sections of the fifteen-story frames. 70
Figure 5.12 Deformed shape and plastic hinge state (SAP2000). 72
Figure 5.13 Lateral load distribution of ASCE 41-17 Section 7.4.3.2.3. 73

Figure 5.14 Lateral load distribution of FEMA 356 Section 3.3.3.2.3. 73
Figure 6.1 Area A and the equal-area idealization, four-story frame. 81
Figure 6.2 Acceptance criteria of ASCE 41-17 Section 7.5.3.2.2. 91
Figure 6.3 Base hinge of column 2801 in SAP2000. 91
Figure 6.4 Largest hinge D/C ratio against roof displacement. 93
Figure 6.5 Hinge D/C ratios of the reference frame at $\Delta_{max,C}$. 94
Figure 6.6 R_C against the criterion that defines $\Delta_{max,C}$. 95
Figure 6.7 Four-story frame: capacity curve and bilinear idealizations. 99
Figure 6.8 Six-story frame: capacity curve and bilinear idealizations. 102
Figure 6.9 Reference frame: capacity curve and bilinear idealizations. 105
Figure 6.10 Model 4: capacity curve and bilinear idealizations. 108
Figure 6.11 Model 5: capacity curve and bilinear idealizations. 111
Figure 6.12 Model 6: capacity curve and bilinear idealizations. 114
Figure 6.13 Model 7: capacity curve and bilinear idealizations. 117
Figure 6.14 Capacity curves of Models 4 to 7 and the reference frame. 119
Figure 6.15 Capacity curves under the two load patterns. 121
Figure 6.16 Estimated factors of the seven models. 122

LIST OF TABLES

Table 2.1 Representative studies on the R-factor of RC moment frames. 25
Table 3.1 Geometric and material properties of the prototype. 34
Table 3.2 Seismic design parameters. 36
Table 3.3 Seismic design coefficients of the SMRF system. 36
Table 3.4 Design base shear of the three frames. 37
Table 4.1 Material properties of the single-span beam. 44
Table 4.2 Material properties of the two-span beam. 46
Table 4.3 Material properties of the one-story frame. 48
Table 4.4 Numerical and experimental capacities. 50
Table 5.1 Confined-concrete parameters of a representative column. 55
Table 5.2 Material properties of the design and nonlinear models. 56
Table 5.3 Reinforcement of the four- and six-story frames. 67
Table 5.4 Column schedule of the fifteen-story reference frame. 68
Table 5.5 Column sections of the parametric variants. 69
Table 5.6 Beam schedule of the fifteen-story frames. 69
Table 6.1 Notation and origin of each quantity. 76
Table 6.2 Elastic design quantities of the seven models. 79
Table 6.3 Method A, seven models. 84
Table 6.4 Method A in terms of the two stiffnesses. 84
Table 6.5 Reference frame under two risk categories. 85
Table 6.6 Basis of the coefficients of Equation (6.12). 87
Table 6.7 Method B, seven models. 88
Table 6.8 Plastic hinge inventory. 89
Table 6.9 Sensitivity of R_C to the criterion that defines $\Delta_{max,C}$. 95
Table 6.10 Inputs common to the seven models. 96
Table 6.11 Calculation for the four-story frame. 97
Table 6.12 Calculation for the six-story frame. 100
Table 6.13 Calculation for the fifteen-story reference frame. 103
Table 6.14 Calculation for Model 4. 106
Table 6.15 Calculation for Model 5. 109
Table 6.16 Calculation for Model 6. 112
Table 6.17 Calculation for Model 7. 115
Table 6.18 Consolidated results, uniform pattern. 118
Table 6.19 Results under the first-mode pattern. 120
Table 6.20 Present ranges and published estimates of R. 124

Table A.1 Seismic design parameters of the prototype. 139
Table A.2 Seismic response coefficient, reference frame. 140
Table A.3 Story drift check, reference frame. 141
Table A.4 Vertical load and story shear, reference frame. 143
Table B.1 Design of the column hoops. 144
Table B.2 Volumetric confinement ratio. 145
Table B.3 Mander confined-concrete parameters. 146
Table C.1 Plastic hinge assignment scheme. 147
Table C.2 Parameters of representative hinges, reference frame. 148
Table C.3 Hinge D/C evolution, reference frame. 148
Table D.1 Basis of the displacement modification coefficients. 149
Table D.2 Modal properties and target displacement. 150

CHAPTER 1 INTRODUCTION

1.1 Background

Earthquake-resistant design of building structures is founded on the acceptance that a structure need not remain elastic during the design-level earthquake. Instead, controlled inelastic deformation is permitted, provided the structural system possesses sufficient ductility and overstrength to prevent collapse. This philosophy reduces the design forces to a fraction of those corresponding to a fully elastic response, making construction economically feasible while maintaining life safety. The parameter that quantifies this force reduction is the response modification factor, denoted R in the ASCE 7 family of codes (*ASCE, 2016*), q (behavior factor) in Eurocode 8 (European Committee for Standardization, 2004), and R (response reduction factor) in the Indian standard IS 1893 (Bureau of Indian Standards, 2016).

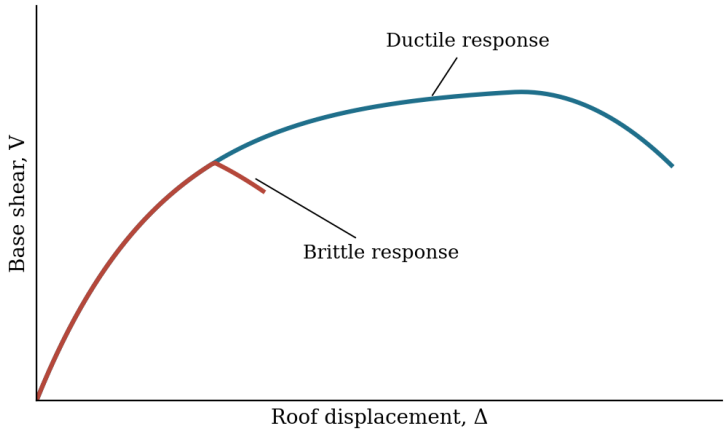

Figure 1.1 Ductile and brittle global response of a structure.

The conceptual basis of R was formalized by *Uang (1991)*, who decomposed the factor into two independent structural properties: the ductility reduction factor R_μ, which accounts for the energy dissipated through inelastic deformation, and the overstrength factor Ω, which accounts for the reserve strength of the structure above the code design level. The relationship is expressed as $R = R_\mu \times \Omega$. The ductility reduction factor depends on the fundamental period of the structure, following the relationships established by *Newmark and Hall (1982)*: $R_\mu = 1$ for very short periods, $R_\mu = \sqrt{(2\mu - 1)}$ for short-to-intermediate periods ($T < 0.5$ s, equal-energy range), and $R_\mu = \mu$ for long periods ($T > 0.5$ s, equal-displacement range), where μ is the displacement ductility ratio.

For special reinforced concrete moment-resisting frames (SMRFs), the current ASCE 7-16 Table 12.2-1 prescribes R = 8, a system overstrength factor $\Omega_0 = 3.0$, and a deflection amplification factor $C_d = 5.5$. These values trace their origin to the ATC 3-06 report (*ATC, 1978*), which introduced tabulated R-values for twenty-one seismic force-resisting systems on the basis of engineering judgment, observed building performance during past earthquakes, and qualitative estimates of system ductility and overstrength (*Charney, 2015*). Despite progressive expansion of the tabulated systems to eighty-five sets in ASCE 7-10 and the introduction of the FEMA P-695 performance-based procedure for validating new systems (*FEMA, 2009*), the R-values of established systems such as the SMRF have been assessed with collapse-based methods of that kind (*Haselton et al., 2011*) but have not been recalibrated. They remain empirically derived constants assigned to broad structural system categories, with no explicit dependence on building height, fundamental period, confinement detailing, or reinforcement ratio.

The special moment-resisting frame is distinguished from intermediate and ordinary frames by the stringent seismic detailing provisions of ACI 318-19 Chapter 18 (ACI, 2019). These provisions include mandatory confinement of potential plastic hinge zones through closely spaced transverse reinforcement, strong-column/weak-beam capacity ratios of at least 6/5, and joint shear stress limits. These requirements are intended to ensure that the frame develops a ductile mechanism under lateral loading, which is the physical basis for the high R-value of 8. Confinement raises the strength and the strain capacity of the concrete core (Mander et al., 1988), and in the assessment provisions of ASCE 41-17 it enters the plastic rotation capacity of a column through the transverse reinforcement ratio ρ_t.

Whether the prescribed R = 8 accurately represents the actual nonlinear behavior of SMRF buildings has been questioned by multiple researchers. Abdi et al. (2019) stated in a review that no uniform technique exists for determining R under different conditions and that the factor is affected by building height, and noted that the ratio of actual to nominal material strength affects its overstrength component. AlHamaydeh et al. (2011) evaluated SMRF buildings of 4, 16, and 32 stories in Dubai and found from nonlinear dynamic analysis that the 84th-percentile R demand under the ground motions with a 2 percent probability of exceedance in 50 years ranged from 4 to 7, below the code value in every case. Mondal et al. (2013) found that the R of ductile frames under the Indian standard depends on the performance level considered, falling below the code value at

the structural-stability level and exceeding it at the ultimate level. These studies indicate that a single R-value applied uniformly to all buildings of a given structural system may not represent every configuration, in a direction and by an amount that depend on the configuration.

1.2 Seismic Hazard of the Study Region

The West Bank of Palestine lies within the influence zone of the Dead Sea Transform (DST) fault system, a left-lateral strike-slip plate boundary extending approximately 1,000 km from the spreading center in the Gulf of Aqaba northward through the Jordan Valley, the Dead Sea, and the Sea of Galilee to southeastern Turkey. The DST accommodates the relative motion between the African and Arabian tectonic plates at a rate of approximately 4 to 6 mm per year (*Garfunkel, 2014*). The fault has produced several destructive earthquakes in the historical and instrumental records, including the 749 AD Galilee earthquake (estimated magnitude 7.0), the 1033 AD Jordan Valley earthquake (estimated magnitude 7.0), the 1202 AD earthquake (estimated magnitude 7.5), all documented by *Ambraseys (2009)*, and the 1927 Jericho earthquake (ML 6.25), which caused widespread damage to structures in Nablus, Jerusalem, and Jericho (Avni et al., 2002; Zohar and Marco, 2012).

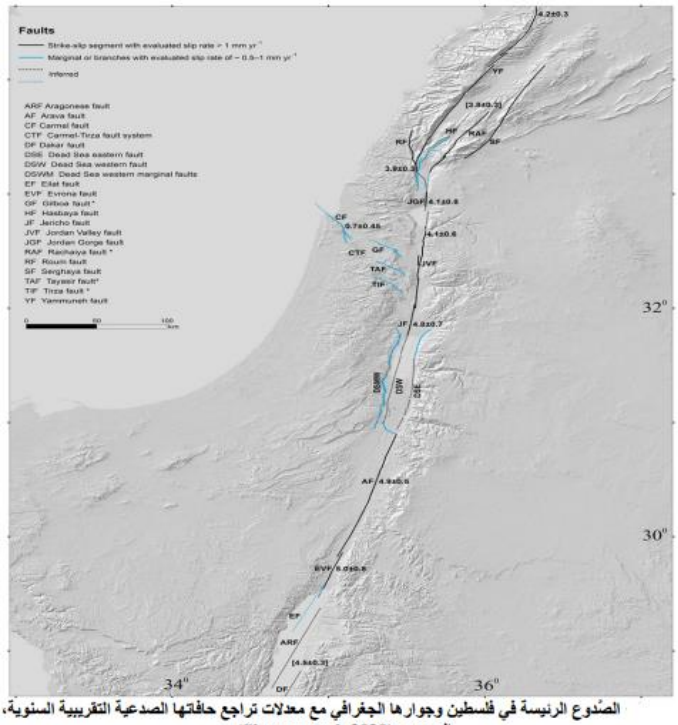

الصُدوع الرئيسة في فلسطين وجوارها الجغرافي مع معدلات تراجع حافاتها الصدعية التقريبية السنوية، المصدر: (Sharon et al.,2020).

Figure 1.2 Principal faults of Palestine and the surrounding region (Sharon et al., 2020).

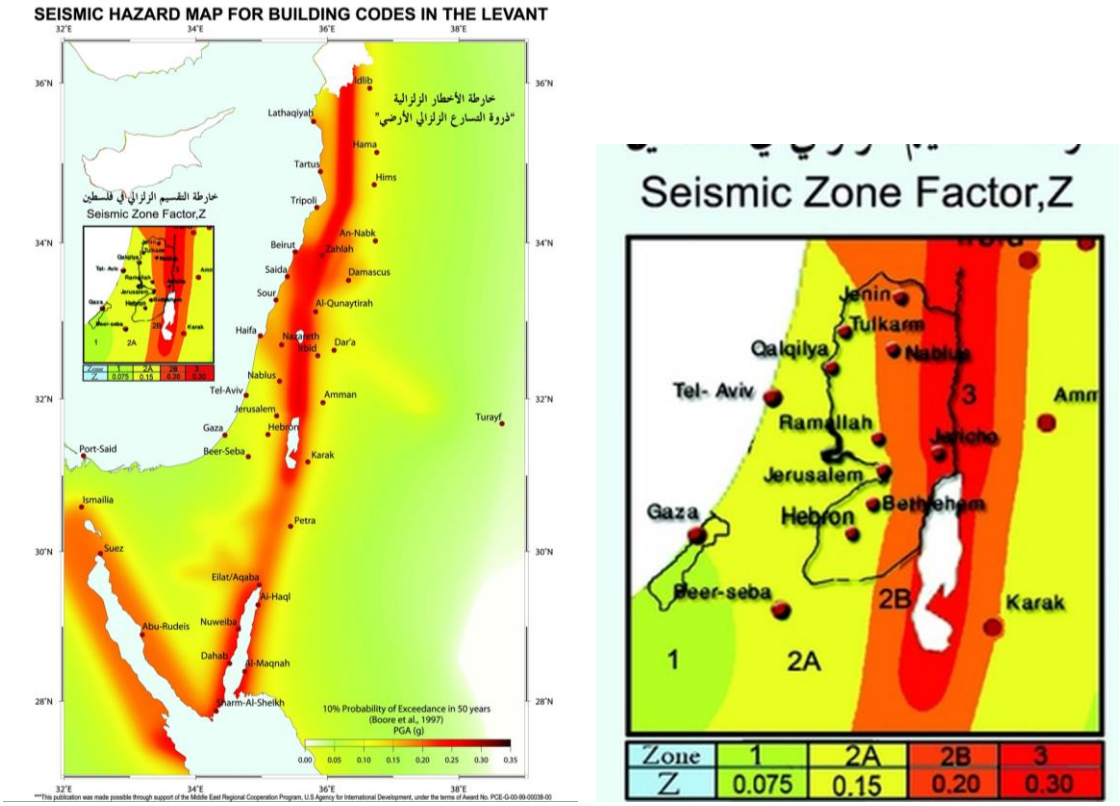

(a) (b)

Figure 1.3 Seismic hazard map of the Levant (An-Najah National University, n.d.).

Note. (a) Peak ground acceleration map; (b) seismic zone factor Z for Palestine. Peak ground acceleration for a 10% probability of exceedance in 50 years; the map cites Boore et al. (1997).

The proximity of population centers in the West Bank, including Nablus, Ramallah, Hebron, and Jericho, to the DST fault system, combined with the predominance of reinforced concrete frame construction and the limited application of modern seismic codes in local practice, creates a significant seismic vulnerability. Reinforced concrete frames with infill walls that were designed for gravity loads only are a common building type in the main cities of the West Bank (Al-Dabbeek and Al-Jawhari, 2002). A survey of buildings in seven West Bank cities assigned about one third of them to the most vulnerable class (Al-Dabbeek, 2007), and an assessment of RC frames in Ramallah found that most of them did not meet the life-safety performance level under the design earthquake (Safi and Karaki, 2024). The adoption of ASCE 7-16 and ACI 318-19 as the design basis for new construction, as assumed in this study, represents the target standard for earthquake-resistant design in the region.

The prototype is a hypothetical archetype and is not assigned to a particular town. It is given the seismic hazard of Zone 3 of the seismic zone map of Palestine (Figure 1.3), Z = 0.30, the highest zone of the map, which covers the Jordan Valley and the Dead Sea

margin and includes, for example, Jericho. Site Class A is adopted as an idealized rock-site assumption rather than a measured site classification; softer classes (C, D) are identified as future work.

1.3 Problem Statement

The R-factor prescribed by ASCE 7-16 for special reinforced concrete moment frames is a single constant (R = 8) applied uniformly to all SMRF buildings regardless of the number of stories, the fundamental period, the confinement level, or the longitudinal reinforcement ratio. Published research has identified three specific weaknesses in this approach.

First, the ductility reduction factor R_μ is fundamentally period-dependent, as established by *Newmark and Hall (1982)* and confirmed by *Miranda and Bertero (1994)*. The Newmark-Hall relationship separates an equal-energy branch below approximately 0.5 s from an equal-displacement branch above it, and the two branches return different values for the same ductility ratio. Most evaluation studies apply a single assumption to all heights without verifying which branch actually governs. The present study applies the branch selection explicitly and reports which branch governs each model.

Second, the influence of transverse reinforcement on the components of R has received limited attention in the published literature, even though confinement is the defining feature that distinguishes the special frame from the intermediate and ordinary frame classifications. In ASCE 41-17 the plastic rotation capacity of a column depends on its transverse reinforcement ratio and its axial load ratio (Table 10-8), so the confinement provided in design propagates to the displacement capacity of the frame and to the factor estimated from it.

Third, the definition of the maximum displacement used to extract R from the pushover capacity curve is not standardized. Different definitions yield different R-values for the same structure and the same pushover curve, and several studies use definitions that are not provisions of any code. The sensitivity of R to this definition has not been systematically quantified for SMRF buildings.

The research gap is therefore twofold. First, to the author's knowledge, no published study estimates R for a height family of special moment-resisting frames designed to ASCE 7-16 and detailed to ACI 318-19 for the seismic hazard of Palestine, with the governing branch of the R_μ-T relation identified for each frame. Second, the dependence

of R on the definition of the maximum displacement has not been quantified for such frames with definitions that are all taken from codes. This study addresses both: it estimates R for frames of 4, 6 and 15 stories under three code-based definitions of the maximum displacement, and it examines how hoop spacing combined with concrete strength, column reinforcement, and column section reduction change the result (Section 2.5).

1.4 Research Objectives

The primary objective of this study is to estimate and assess the response modification factor prescribed by ASCE 7-16 for special reinforced concrete moment-resisting frame buildings. The specific objectives are:

1. To estimate the ductility reduction factor (R_μ) for SMRF buildings of 4, 6, and 15 stories through nonlinear static pushover analysis, assigning the period-appropriate branch of the Newmark-Hall R_μ-T relationship to each model (equal-energy for $T < 0.5$ s, equal-displacement for $T > 0.5$ s).

2. To extract the overstrength factor (Ω) from the bilinear idealization of the pushover capacity curve, as the ratio of the effective yield strength (V_y) to the code design base shear (V_d).

3. To estimate the response modification factor as $R = R_\mu \times \Omega$ using three code-based definitions of the maximum displacement, and to compare the estimated values with the code-prescribed R = 8 on the basis of $R / I_e = 8 / 1.25 = 6.40$ for the Risk Category III prototype.

4. To investigate the combined effect of wider hoop spacing (100 mm in place of the design spacing of 70 to 75 mm) and a lower concrete strength in the nonlinear model (29 MPa in place of 35 MPa) on R and its components.

5. To investigate the effect of the longitudinal reinforcement ratio of the columns (about 1.0 percent against about 2.0 percent) on R and its components.

6. To investigate the effect of reducing the perimeter column cross-sections of stories 3 to 5 of the 15-story reference on R and its components.

7. To investigate the effect of reducing the column cross-sections of the upper stories (stories 13 to 15 of the 15-story reference) on R and its components.

1.5 Research Methodology

The study follows a four-stage methodology, consistent with the approach established in four previous master's theses at Palestine Polytechnic University under the same supervisor, which estimated the R-factor for intermediate moment frames (Abuznaid, 2023; Shrouf, 2025; Qubajeh, 2026) and for special moment and dual systems (Shaban, 2024). The present study focuses on the special moment frame system and introduces two methodological refinements over these works: the period-aware selection of the R_μ-T branch, and three code-based definitions of the maximum displacement.

Stage 1: Elastic design. A regular reinforced concrete prototype building with four bays of 6.0 m in the longitudinal direction and three bays of 6.0 m in the transverse direction is designed for the seismic parameters of the West Bank using the equivalent lateral force procedure of ASCE 7-16 Section 12.8. Members are detailed as special moment frames per ACI 318-19 Chapter 18. The elastic design, section sizing, and reinforcement detailing are performed in ETABS (Computers and Structures, Inc., 2022). Three building heights are modeled: 4, 6, and 15 stories, each with a story height of 3.0 m.

Stage 2: Validation. The nonlinear modeling procedure in SAP2000 is validated against three published experimental benchmarks: the Bresler and Scordelis (1963) single-span beam, the Duddeck-Mueller two-span continuous beam (Mueller, 1977), and the Xiao et al. (2006) one-story frame. The adequacy of the modelling approach for the subsequent analyses is assessed against the reported experimental capacities; the outcome of that assessment is presented in Chapter 4. It does not by itself validate cyclic degradation or collapse-level deformation capacity.

Stage 3: Pushover analysis. Nonlinear static pushover analysis is performed in SAP2000 (Computers and Structures, Inc., 2023) for each building model under a uniform and a first-mode lateral load pattern. The nonlinear models use expected material properties and the effective stiffness of ASCE 41-17 Table 10-5. Plastic hinges are assigned at beam and column ends, with modeling parameters and acceptance criteria from ASCE 41-17 Tables 10-7 and 10-8 (Section 5.3.1). P-Delta effects are included. The pushover capacity curve is idealized as a bilinear system by the equal-area procedure of FEMA 356 Section 3.3.3.2.4. Three definitions of the maximum displacement are applied, each taken from a code or standard:

Method A: The elastic roof displacement Δ_d from the ETABS model is amplified by the deflection amplification factor $C_d = 5.5$ and divided by the importance factor $I_e = 1.25$, $\Delta_{max} = C_d \Delta_d / I_e$, as in ASCE 7-16 Equation 12.8-15.

Method B: The target displacement δ_t is computed by the displacement coefficient method of FEMA 356 Equation 3-15, using the effective period of the nonlinear model and the spectral acceleration at that period.

Method C: The displacement capacity is the roof displacement at which the first component reaches its Collapse-Prevention acceptance criterion of ASCE 41-17 Tables 10-7 and 10-8, the condition of ASCE 41-17 Section 7.5.3.2.2, located by interpolation between the two analysis steps that bracket it.

Stage 4: Parametric studies. Four parametric studies are conducted: (a) the effect of building height (4, 6, and 15 stories); (b) the combined effect of wider hoop spacing and lower concrete strength (Model 4); (c) the effect of the longitudinal reinforcement ratio of the columns (Model 5); and (d) the effect of column cross-section, reduced at two locations of the 15-story reference: perimeter columns of stories 3 to 5 (Model 6) and all columns of stories 13 to 15 (Model 7). The three methods are applied to every model.

1.6 Scope and Limitations

This study is subject to the following limitations:

1. The analysis is limited to regular reinforced concrete special moment-resisting frame buildings without structural walls or any other supplementary lateral force-resisting system, and without plan irregularity.

2. The pushover analysis is performed on the full three-dimensional model loaded unidirectionally in the longitudinal (x) direction. Accidental torsion and bidirectional loading are not evaluated. Because the prototype is doubly symmetric in plan with a rigid diaphragm, inherent torsional response is not a feature of the model.

3. The nonlinear procedure is static pushover under two lateral load patterns. Nonlinear dynamic time-history analysis, which captures higher-mode effects, strength and stiffness degradation, and ground motion duration, is not performed.

4. The design uses $f'_c = 24$ MPa and Grade 60 reinforcement ($f_y = 420$ MPa). The nonlinear models use expected strengths of 35 MPa for concrete (29 MPa in Model 4)

and 455.05 MPa for the reinforcement, the latter below the value 1.25 f_y of ASCE 41-17 Table 10-1. The gravity load case of the nonlinear analysis is 1.0 D + 0.25 L rather than 1.1 (D + 0.25 L). Both are declared departures.

5. Site Class A (hard rock) is adopted for all models. The effect of softer site conditions (Classes C and D), which are common in parts of the West Bank, is not addressed.

6. Infill masonry walls, which are present in the majority of RC frame buildings in Palestine, are not modeled. Infill has been shown to significantly alter the overstrength and ductility of RC frames.

7. Soil-structure interaction effects are not considered.

8. The equivalent lateral force procedure of ASCE 7-16 Section 12.8 is applied to all three heights. Verification of the displacement demand under modal response spectrum analysis is identified as future work.

9. Model 4 changes the hoop spacing and the concrete strength together, so the effect of hoop spacing is not isolated.

10. The column Collapse-Prevention limits are evaluated with the axial load of the gravity load case, whereas ASCE 41-17 Table 10-8 defines that axial load including the effects of lateral forces. This is a declared departure (Section 6.10).

1.7 Research Significance

This study makes the following contributions to the field of earthquake engineering:

First, it provides a transparent pushover-based consistency assessment of the code-prescribed R = 8 for special moment frames designed to ASCE 7-16 and detailed to ACI 318-19, for a prototype located in a region of genuine seismic hazard. The assessment is a consistency check within the code framework rather than an independent probabilistic validation, which would require nonlinear response-history and collapse-margin analysis.

Second, the period-aware methodology assigns the Newmark-Hall R_μ-T branch to each model on the basis of its effective period, and the three definitions of the maximum displacement are each taken from a code or standard, so that the estimated factor rests on stated provisions rather than on conventions of the study.

Third, the three-method approach (Methods A, B, and C) exposes the dependence of R on the definition of the maximum displacement, and shows under which definitions the ductility of the frame enters the estimate at all. Reporting R under several definitions is more transparent than reporting a single value.

Fourth, the parametric investigation covers hoop spacing combined with concrete strength, longitudinal reinforcement and column section reduction, and identifies which component of R each of them changes and which members govern the Collapse-Prevention limit state.

Fifth, the study builds on previous master's theses at Palestine Polytechnic University, three on intermediate moment frames (Abuznaid, 2023; Shrouf, 2025; Qubajeh, 2026) and one on special and dual systems (Shaban, 2024). Those studies share the general pushover-based framework adopted here, but they differ in prototype geometry, site parameters, target-displacement definition and hinge formulation. The present results are therefore positioned against them rather than compared directly, and any numerical difference should be read as a difference in procedure and prototype as much as in structural system.

1.8 Thesis Organization

This thesis is organized into seven chapters.

Chapter 1 introduces the research background, the seismic hazard of the study region, the problem statement, the research objectives, the methodology, the scope and limitations, and the significance of the study.

Chapter 2 reviews the literature on the response modification factor, including its historical development, mathematical formulation, period dependence, and the published evaluation studies. The nonlinear analysis methods used to extract R are reviewed, and the research gap is identified.

Chapter 3 describes the prototype structure, the material properties, the gravity and seismic loading, the design framework per ASCE 7-16, and the parametric study framework.

Chapter 4 presents the validation of the SAP2000 nonlinear modeling procedure against three benchmark experiments (Bresler-Scordelis beam, Duddeck-Mueller beam, and Xiao frame).

Chapter 5 describes the SMRF modeling and nonlinear analysis, including the material properties of the nonlinear models, the ASCE 41-17 hinge parameters and acceptance criteria, the three definitions of the maximum displacement, the reinforcement detailing of all seven models, and the pushover analysis setup.

Chapter 6 presents the results and discussion of the R-factor estimation for all models, the parametric studies, the comparison of the two load patterns, the sensitivity of the results to the definition of the maximum displacement, and a discussion of the findings against the published literature.

Chapter 7 summarizes the conclusions drawn from the study, presents recommendations for practice, and identifies topics for future research.

CHAPTER 2 LITERATURE REVIEW

2.1 Introduction

This chapter reviews the body of research concerned with the response modification factor (R) of reinforced concrete (RC) moment-resisting frame buildings, with particular attention to special moment-resisting frames (SMRFs). The review is organized to answer three questions that the present study depends upon: how R is defined and decomposed, how it is estimated from nonlinear analysis, and what previous investigators have found regarding its magnitude and sensitivity. Section 2.2 introduces the concept of the factor, traces its code history, and defines its components. Section 2.3 examines the analysis procedures used to extract R, giving explicit attention to the way each study idealizes the capacity curve and, most importantly, to the source it adopts for the maximum (target) displacement, because this single choice governs the computed ductility and therefore the reported R. Section 2.4 presents a critical, theme-based synthesis of previous studies rather than a sequential list, and closes each theme by stating its implication for the present work. Section 2.5 draws the research gap directly from that synthesis, and Section 2.6 summarizes the chapter.

2.2 The Response Modification Factor: Concept, Formulation, and Components

2.2.1 Historical Development of the R-Factor

Seismic design codes permit a structure to be designed for lateral forces well below those associated with a fully elastic response, on the condition that the structure can dissipate the remaining energy through controlled inelastic deformation. The parameter that governs this force reduction is the response modification factor, denoted R in the ASCE 7 family of standards, q (behavior factor) in Eurocode 8, and R (response reduction factor) in the Indian standard IS 1893. The concept was first codified in the ATC 3-06 report (ATC, 1978), which tabulated R-values for twenty-one seismic force-resisting systems. The values tabulated in that report were not obtained from analysis of individual structures; they were assigned by committee consensus on the basis of observed building performance in past earthquakes and qualitative estimates of overstrength, ductility, and damping (Uang, 1991). Analytical formulations for R followed (Uang, 1991). The tabulated systems expanded through successive NEHRP and IBC editions, reaching eighty-five system entries in ASCE 7-10 (Charney, 2015). The system overstrength factor did not appear explicitly until ASCE 7-98, and the current ASCE 7-16 Table 12.2-1

assigns R = 8, the overstrength factor of 3.0, and a deflection amplification factor C_d = 5.5 to special reinforced concrete moment frames.

A more rigorous, performance-based procedure for quantifying R was later established by FEMA P-695 (FEMA, 2009). In that methodology, archetype models are designed for a trial R, then subjected to incremental dynamic analysis using twenty-two far-field ground-motion pairs scaled to increasing intensity until collapse. The trial value is accepted only when two conditions are met: the probability of collapse under the Maximum Considered Earthquake is less than twenty percent for each individual archetype, and less than ten percent on average for each performance group. The assessment is made through an adjusted collapse margin ratio that accounts for uncertainty in the modelling, the design requirements, the system test data, and the ground-motion records (FEMA, 2009). Sadeghian et al. (2023), in a critical review comparing of the Canadian and American approaches, observed that force modification factors in the National Building Code of Canada were originally set by engineering judgment, and recommended a standardized rational procedure comparable to FEMA P-695. Despite these advances, the R-values in ASCE 7-16 remain, in practice, empirically calibrated constants assigned to broad system categories rather than to individual buildings. That observation is the central motivation for the present study, which estimates R analytically for a specific SMRF configuration and compares it with the code value.

2.2.2 Mathematical Formulation

Uang (1991) provided the foundational analytical derivation of R, relating it to two independent structural properties, the ductility reduction factor R_μ and the overstrength factor Ω:

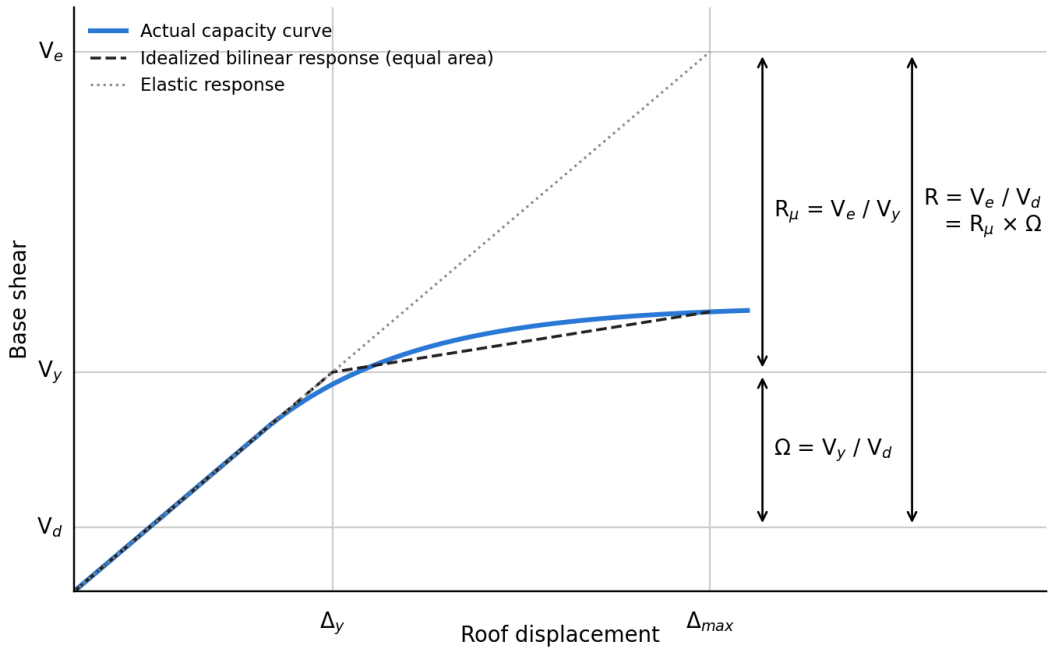

Figure 2.1 Decomposition of the response modification factor on the capacity curve.

$$R = R_\mu \times \Omega \tag{2.1}$$

Here R_μ is the ratio of the elastic strength demand to the yield strength of an equivalent elasto-plastic system, and Ω is the ratio of the actual yield strength (V_y) to the code design base shear (V_d). Uang also showed that R, C_d, and Ω are interdependent. Several investigators (for example Attia et al., 2020; Patel and Parikh, 2022) adopt an extended form that carries a redundancy term:

$$R = R_\mu \times \Omega \times R_\rho \tag{2.2}$$

where R_ρ accounts for additional lateral resistance provided by structural redundancy. ASCE 7-16 Section 12.3.4, however, defines the redundancy factor ρ as a demand amplifier (values of 1.0 or 1.3) applied to the seismic force, not as a capacity-side multiplier. Including ρ in Equation 2.2 while also applying it on the demand side would count its effect twice. The present study therefore adopts Equation 2.1 and treats ρ exclusively as a demand amplifier, consistent with the ATC-19 formulation (ATC, 1995) and with the procedure used in Chapters 5 and 6.

2.2.3 The Ductility Reduction Factor and Its Period Dependence

The ductility reduction factor R_μ quantifies the reduction in elastic strength demand permitted by the inelastic deformation capacity of the structure. Its value depends fundamentally on the fundamental period. Newmark and Hall (1982) established the classical period-dependent relationships:

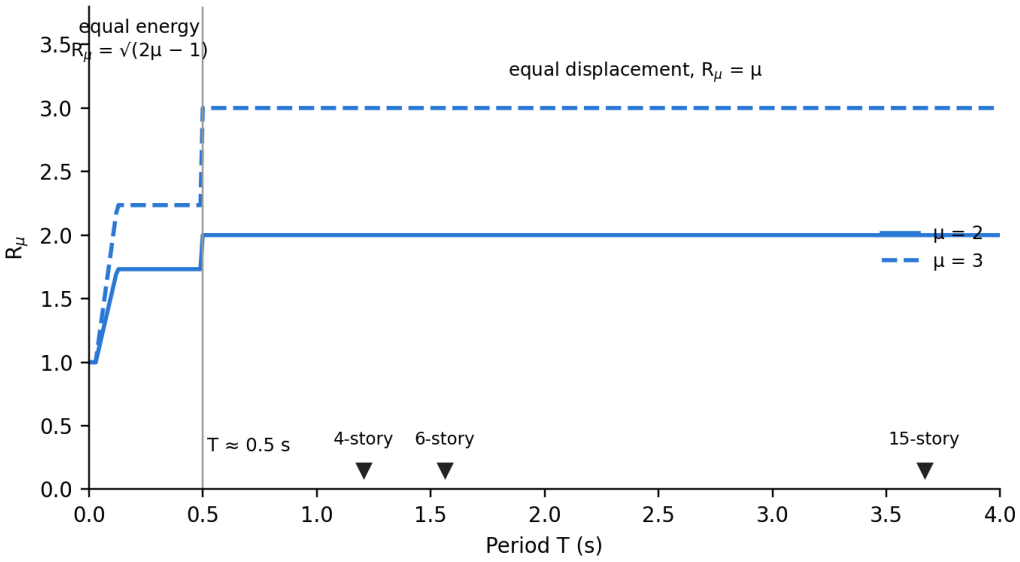

Figure 2.2 Newmark-Hall ductility reduction factor against period.

Note. μ = 2 and 3. The markers show the effective periods of the three frames of this study.

$$R_\mu = 1 \qquad (T \to 0) \qquad (2.3a)$$

$$R_\mu = \sqrt{(2\mu - 1)} \qquad \text{(short-to-intermediate T)} \qquad (2.3b)$$

$$R_\mu = \mu \qquad (T \geq \sim 0.5 \text{ s}) \qquad (2.3c)$$

where μ is the displacement ductility ratio (Δ_u/Δ_y). Equation 2.3b is the equal-energy range, in which the areas under the elastic and inelastic force-displacement curves are set equal; Equation 2.3c is the equal-displacement range, in which the peak inelastic displacement equals the elastic one. Miranda and Bertero (1994) evaluated six representative R_μ-T relationships against mean values from 124 ground motions on rock, alluvium, and soft soil, and confirmed that the equal-displacement approximation holds well above roughly 0.5 s but underestimates R_μ for short-period structures on soft soil. Vidic et al. (1994) proposed parametric R_μ expressions depending on period, ductility, hysteretic model, and damping that were later embedded in the N2 method of Eurocode 8, and Borzi and Elnashai (2000) found R_μ to be only weakly sensitive to the hysteretic model.

These relationships are, by construction, idealizations for elasto-plastic single-degree-of-freedom systems, and it is important to acknowledge their limits. Modern displacement-based procedures move beyond them. FEMA 440 (FEMA, 2005) refined the equal-displacement assumption through the coefficient method, in which the inelastic displacement is obtained from the elastic value multiplied by coefficients C_1 and C_2 that

account for the difference between inelastic and elastic peak response, for the effect of pinched hysteresis, cyclic stiffness degradation, and strength loss, and for the influence of the post-yield stiffness ratio. FEMA P-695 (FEMA, 2009) goes further and replaces a closed-form R_μ altogether with a collapse-margin assessment that captures P-Delta driven negative stiffness and in-cycle strength degradation through incremental dynamic analysis. The present study retains the Newmark-Hall branches because they remain the transparent and widely reported basis for pushover-based R extraction, but it applies them in a period-aware manner (Section 2.3) rather than through a single blanket assumption, and it interprets the resulting R against this fuller understanding of their idealized origin.

2.2.4 The Overstrength Factor

Following Uang (1991) and ATC-19 (ATC, 1995), the overstrength factor Ω is defined as the ratio of the actual lateral yield strength of the structure to the code design base shear. It arises from material overstrength, load-factor and strength-reduction combinations, member oversizing driven by drift limits or gravity design, and force redistribution after first yield. Humar and Rahgozar (2000) examined these sources systematically and showed that overstrength is often the dominant contributor to the total force reduction in code-designed frames, especially at low periods. Mitchell and Paultre (1994) demonstrated through nonlinear analyses that overstrength significantly affects the capacity of RC structures to resist lateral load without collapse, and criticized codes for not clearly separating ductility from overstrength. Elnashai and Mwafy (2002) analyzed twelve buildings spanning a range of contemporary RC construction using both pushover and time-history collapse analyses, and introduced the inherent overstrength ratio (Ω/R) as a more meaningful measure of reserve strength. Kim et al. (2016), studying small-size RC moment frames sized by prescriptive rules, reported moderate overstrength and ductility, with mean values of about 2.1 each, and suggested that a slightly higher response modification factor may be used for such buildings. In assessment practice the material contribution is made explicit through expected material strengths, which ASCE 41-17 Table 10-1 relates to the specified strengths; the present study uses expected strengths in its nonlinear models (Section 5.3). Throughout the present study the code system overstrength factor (a prescribed constant of 3.0 for SMRF) is kept distinct from the analytically estimated Ω read from the pushover capacity curve.

2.2.5 The Redundancy Factor

Redundancy rewards structures with multiple lines of vertical seismic framing. Tsopelas and Husain (2004) studied the effect of element ductility, beam flexibility, column slenderness, and gravity level on the redundancy of plane frames with three, five, and seven stories and one to six bays, and estimated a reliability-based redundancy response modification factor. ASCE 7-16 Section 12.3.4 sets the redundancy factor ρ to 1.0 or 1.3, and Section 12.3.4.2 states the conditions under which $\rho = 1.0$ is permitted for structures in Seismic Design Categories D to F. In the present study $\rho = 1.3$ is used in the strength load combinations. This is conservative for member design, since it amplifies the seismic load effect and therefore the required member capacity, and it does not enter the estimation of the response modification factor, which is based on the design base shear rather than on the amplified load effect.

2.3 Methods of Estimating R from Nonlinear Analysis

Because the reported value of R depends as much on the extraction procedure as on the structure itself, this section reviews the analysis methods and, in particular, isolates the one modeling choice that most strongly controls the outcome: the definition of the maximum (target) displacement.

2.3.1 Nonlinear Static (Pushover) Analysis

Pushover analysis subjects the model to a monotonically increasing lateral load or displacement pattern while accounting for material and geometric nonlinearity, producing a capacity curve of base shear against roof displacement. The method was standardized in FEMA 356 (Federal Emergency Management Agency [FEMA], 2000), ASCE 41-17 (American Society of Civil Engineers [ASCE], 2017), and, for the capacity-spectrum variant, ATC-40 (ATC, 1996). It is efficient, requiring one analysis per load pattern rather than a suite of records. A single lateral load pattern, however, cannot represent the change of the story-shear distribution as the higher modes participate, FEMA 356 Section 3.3.3.2.3 therefore required at least two vertical distributions of lateral load, one modal and one uniform. ASCE 41-17 Section 7.4.3.2.3 instead prescribes a single distribution proportional to the fundamental mode shape, and its commentary notes that multiple patterns do little to improve the accuracy of the procedure. ASCE 41-17 Section 7.3.2.1 also defines when higher-mode effects are significant: when the story shear from a modal response spectrum analysis with ninety percent mass participation exceeds 130 percent

of the corresponding story shear from the first mode alone, in which case the nonlinear static procedure must be supplemented by a linear dynamic procedure (ASCE, 2017). Zameeruddin and Sangle (2021), pushing fifteen moment frames under three load patterns, found that the uniform pattern gives the upper bound of the response modification factor and the first-mode pattern a median value, and Karanja Kuria and Kegyes-Brassai (2023) reviewed its evolution and documented its now-standard role in R-factor evaluation. The present study analyzes every model under a uniform and a first-mode pattern; for the fifteen-story frames, with an effective period of about 3.7 s, the higher-mode limitation is stated with the results.

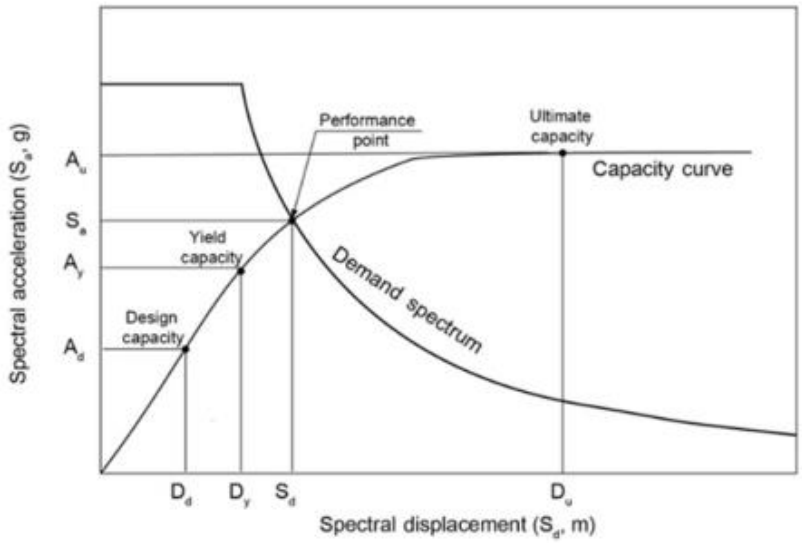

Figure 2.3 Capacity-spectrum method (after ATC-40, 1996).

2.3.2 Bilinear Idealization and Extraction of the R-Components

The factor and its components are read from a bilinear idealization of the capacity curve, from which the yield point (V_y, Δ_y) and the ultimate point (V_u, Δ_u) are obtained. Two idealization conventions recur in the literature: the equal-area (equal-energy) rule of Paulay and Priestley (1992), and the initial-stiffness construction. Once the bilinear form is fixed, three families of estimation appear across the studies reviewed here. In the first, the overstrength is taken as $\Omega = V_y/V_d$, the ductility as $\mu = \Delta_u/\Delta_y$, R_μ is evaluated from a period-dependent Newmark-Hall expression, and $R = R_\mu \times \Omega$ (for example Chaulagain et al., 2014; Fayed et al., 2018). In the second, the ductility reduction factor is taken directly as the ratio of the elastic strength demand to the yield strength, $R_\mu = V_e/V_y$, and multiplied by Ω (Zafar, 2009). In the third, favored in the Indian literature, R is expanded into four

explicit multipliers, $R = R_\mu \times R_s \times RR \times R\xi$, where the strength factor $R_s = V_y/V_d$, $R_\mu = V_e/V_y$, and $RR = V_u/V_y$ carry overstrength, ductility, and redundancy separately (Patel and Parikh, 2022). The three families are algebraically related, but they diverge numerically because they rely on different definitions of the displacement at which V_u and Δ_u are read, which is the subject of Section 2.3.4.

The present study uses the equal-area rule in the form of FEMA 356 Section 3.3.3.2.4, with the effective stiffness taken as the secant to 0.6 V_y, for all seven models, and the first of the three families of estimation, $R = R_\mu \times \Omega$.

2.3.3 Nonlinear Dynamic and Incremental Dynamic Analysis

Nonlinear dynamic analysis solves the equation of motion for a suite of records, capturing hysteretic response, higher-mode participation, stiffness and strength degradation, and duration effects. Incremental dynamic analysis, formalized by Vamvatsikos and Cornell (2002), scales each record to increasing intensity and traces the response from elasticity through collapse; it underlies the FEMA P-695 validation of R. Studies that compare the two procedures do not agree on the direction of the difference. Oggu et al. (2021) obtained higher R-values from incremental dynamic analysis than from pushover analysis, whereas Abou-Elfath and Elhout (2018) obtained lower values from time-history analysis (5.43 to 8.43) than from pushover analysis (6.18 to 9.85). Attia et al. (2020), for an elevated metro station structure, found pushover values based on the Newmark-Hall relations close to time-history values. The present study applies the Newmark-Hall relations within the pushover procedure and does not perform dynamic analysis (Section 6.10).

2.3.4 The Maximum-Displacement Problem

The single most consequential choice in R extraction is the displacement at which the structure is considered to have reached its usable limit, because it fixes Δ_u and therefore μ. The reviewed studies resolve it in four distinct ways, and the differences explain much of the scatter reported in Section 2.4. The first is the equal-displacement rule, which sets the inelastic peak equal to the elastic spectral demand and is appropriate for longer-period structures (Chaulagain et al., 2014; Zafar, 2009). The second is the equal-energy rule, applied in the short-to-intermediate range. The third is a code-defined target displacement: Al-Ahmar and Al-Samara (2015) took the FEMA 356 target displacement as the monitored maximum, while others adopt the ASCE 41 coefficient

method. The fourth is a fixed global drift limit taken as a proxy for the performance limit state, for example a roof or inter-story drift of four percent used by Zafar (2009), Oggu et al. (2021), and Ariyanto et al. (2026). A structure evaluated under the equal-displacement rule and the same structure evaluated at a four percent drift cap can yield materially different R-values, even though nothing in the model has changed. This sensitivity is rarely made explicit in the studies reviewed, and addressing it directly, by applying more than one definition and reporting the result as a bracket, is one of the methodological contributions of the present study.

2.4 Critical Review of Previous Studies

Rather than list each study in turn, this section groups the findings by theme, states where the evidence agrees and where it conflicts, explains the mechanism behind each trend, and ends each theme by connecting it to the present work. Table 2.1 then consolidates the studies with their systems, codes, methods, estimation and target-displacement choices, R-values relative to code, and principal conclusions.

2.4.1 Effect of Building Height and Period

The clearest and most consistent finding in the literature is that R changes systematically with building height, although the reported direction of that change depends on how R is extracted. Studies that fix the maximum displacement through a code target or a drift cap generally report that R decreases as height increases. Al-Ahmar and Al-Samara (2015), using pushover analysis of twenty-five SMRF models designed to UBC 97, found R falling across the three-to-fifteen-story range and concluded that a fixed value of 8.5 is unsafe for tall frames and uneconomic for low-rise ones. AlHamaydeh et al. (2011) reached the same conclusion for SMRFs of 4, 16, and 32 stories in Dubai using nonlinear dynamic analysis in IDARC-2D, reporting 84th-percentile values of R between 4 and 7 under the 2/50 ground motions, below the code value of 8 in every case, and recommending period-dependent R and C_d factors. Abou-Elfath and Elhout (2018) confirmed the decline for nine RC frames under both pushover (R = 6.18 to 9.85) and time-history analysis (R = 5.43 to 8.43), with the dynamic values consistently lower. Balendra et al. (1999) showed the mechanism most starkly: for three-bay frames of 3, 6, and 10 stories designed to BS 8110, the overstrength fell from 7.5 to 2.2 as height increased while ductility stayed near 2, so R collapsed from 18.0 to 4.7. Kumar et al. (2017) reported the same decreasing trend for SMRF and OMRF frames of 2 to 12 stories,

and Cui et al. (2021) found the global drift capacity of fifteen frames diminishing with story count.

A minority of studies report the opposite direction: Nishanth et al. (2017) found R to increase slightly with the period of the frame, and Attia et al. (2020) found it to decrease as the height decreases. The contradiction is instructive rather than genuine. When the maximum displacement is governed by the equal-displacement rule, the longer period of a taller frame admits a larger inelastic displacement, so the computed ductility, and with-it R, tends to rise with height. This is the behavior that produces the increasing trend, and it is the same physics that the present study encounters for its taller models. The apparent conflict in the literature therefore reduces to the maximum-displacement choice discussed in Section 2.3.4, not to a disagreement about the structures themselves. For the present study, which spans a height family of four, six, and fifteen stories (the one-story frame in Chapter 4 is a validation benchmark only), this reconciliation is central. The period-appropriate Newmark-Hall branch is selected for each model from its computed fundamental period rather than assumed in advance. Because all three heights return a fundamental period greater than 0.5 s, the equal-displacement branch ($R\mu = \mu$) governs the entire family, so no frame in the study is penalized by an energy rule intended for stiff, short-period systems, and the branch selection is a verified outcome of the period calculation rather than a modeling assumption.

2.4.2 Effect of Bay Configuration and Global Geometry

Across studies that varied the number and span of bays independently of height, the effect on R was consistently secondary. Al-Ahmar and Al-Samara (2015) found the number and length of bays to have an insignificant effect compared with the number of stories, and Abou-Elfath and Elhout (2018) reported that the number and span of bays had a minor effect on R while frame height dominated; in their frames R also decreased as the story height increased. Ariyanto et al. (2026), varying the story height of three 30 m SMRF models, found that it changed the period, the base-shear capacity and the drift; their study does not estimate R. This body of evidence supports a modeling decision in the present study: the prototype plan is held constant across the three heights, so that bay geometry does not enter the comparison. The member sizes and reinforcement follow the design of each height, so the height family compares code-designed archetypes rather than frames that differ in height alone.

2.4.3 Effect of Reinforcement Detailing and Confinement

Detailing is the feature that formally separates the special frame from intermediate and ordinary frames, yet quantitative studies of its effect on R within the SMRF class remain comparatively few. The available evidence is nonetheless consistent in mechanism. Ferraioli (2021), evaluating the behavior factor of ductile code-designed RC frames through combined pushover and dynamic analyses, showed that the local ductility of the columns governs the global behaviour factor; while the pushover results make the code value appear conservative, the refined dynamic analysis indicates it may be slightly nonconservative for middle-to-high-rise frames, and improvements to the local-ductility detailing of the columns were proposed. Oggu et al. (2021) found that adding masonry infill, which stiffens and strengthens the frame, raised both the overstrength and the ductility factors, so the overall factor increased. The small-size frames of Kim et al. (2016), detailed by prescription rather than analysis, displayed moderate overstrength and ductility, each near 2.1, and the authors suggested that a slightly higher factor may be used. Rationalizing the factor further, Goud and Pradeep Kumar (2014) reported that closer shear reinforcement, through ductile detailing, raised the displacement capacity and ductility and therefore the attainable factor, although the maximum base shear did not increase. That study evaluated a five-story frame under the Indian standard, and the direction it reports is not necessarily transferable to a taller code-detailed SMRF in which the limit state is located by component acceptance criteria; the present study therefore treats the direction of the confinement effect as an open question rather than an expectation. Chaulagain et al. (2014) provided the design-level counterpart: frames with a complete load path that satisfied a column-to-beam capacity ratio above 1.1 reached R = 4.0, whereas those violating it fell to 2.16, a direct link between capacity-design detailing and the realized factor. These findings frame a parametric question of the present study, namely how hoop spacing and the longitudinal reinforcement ratio of the columns (about 1.0 percent against about 2.0 percent) propagate into R_μ, Ω, and R, an interaction that the reviewed studies motivate but do not resolve for a code-detailed SMRF. In the present study confinement enters the column hinges through the transverse reinforcement ratio ρ_t of ASCE 41-17 Table 10-8.

2.4.4 Effect of Vertical Irregularity and Redundancy

Irregularity reduces R, and redundancy raises it, both through the extent to which a favorable inelastic mechanism can develop. Ahmed et al. (2021) found that setback and

soft-story configurations both lower R, and recommended reducing it by about 15 percent for a single and 25 percent for a combined vertical irregularity. Magar Patil (2017) concluded that a single value for all buildings of a given framing type, regardless of plan and vertical geometry, cannot be justified. On the redundancy side, Keerthi and Vivek Philip (2017) showed R rising from 3.09 for a single-bay ten-story (G+9) SMRF to 5.44 for a five-bay one, exceeding the code value only for the most redundant configuration. Because the present prototype is regular in plan and elevation and possesses three-to-four-bay redundancy, these studies justify treating irregularity as outside the present scope while retaining redundancy on the demand side.

2.4.5 Influence of the Estimation Method and Target-Displacement Definition

Several studies isolate the extraction procedure itself as a source of variation in R, reinforcing Section 2.3.4. Mondal et al. (2013), in a performance-based evaluation of ductile RC frames of two to twelve stories, computed R component-wise at two performance limits. At the first, based on the drift and member-rotation limits of ATC-40, R was 4.23 to 4.96, below the Indian code value of 5, and they concluded that the code overestimates R; at an ultimate limit based on member plastic-rotation capacity it was 5.46 to 8.48. The dependence of the reported R on the chosen performance level is itself the finding. Damayanti and Muin (2023) showed that the R adopted in design feeds back onto the demand, since a lower R increases the story drift and the required longitudinal reinforcement, so the factor and the structure it produces are coupled. Attia et al. (2020) reported that, for the elevated metro station they studied, pushover estimates of R based on the Newmark-Hall relations were close to time-history estimates. Taken together, these studies establish that a defensible R cannot be reported as a single number divorced from its extraction assumptions, which is the reasoning behind the present study reporting R as a bracket produced by three target-displacement definitions.

2.4.6 Code Comparison and the Developing-Country Context

A recurring conclusion is that code R-values are frequently higher than the values buildings actually achieve, with consequences that are sharper where construction and design practice diverge from the code's originating context. Zafar (2009), using incremental dynamic analysis in OpenSees for frames representative of Pakistani practice, found R sensitive to both geometry and material strength and argued for locally calibrated factors. Layas et al. (2026) showed for an existing 1980s six-story RC building

in Istanbul that adopting R = 8 produced demand estimates falsely indicating adequate performance, whereas a reduced R = 3 matched the observed earthquake damage. Fayed et al. (2018) found R varying with story count, seismic zone, and spectrum type under the Egyptian code, and Nishanth et al. (2017) estimated an R-period-zone relationship in which the code value sat on the high side across the combinations examined. This literature bears directly on the present study, which adopts the hazard of seismic Zone 3 of Palestine on a hypothetical Site Class A rock condition (SDC D) and examines whether the pushover estimates for a code-detailed SMRF in that specific setting are consistent with the adopted R = 8, rather than assuming its transferability.

2.4.7 Collapse-Risk and Post-Earthquake Functionality Approaches

A more recent strand embeds R in a probabilistic or resilience framework instead of a single deterministic estimation. Cui et al. (2021) applied the demand-capacity-factor method to fifteen frames and found that both a conservative R near 3 and a higher R near 6 met the expected collapse-safety goals, implying room to raise the factor. Banerjee et al. (2023) estimated design factors for RC-SMRF buildings within a seismic-risk framework using the FEMA P-695 ground-motion suite across occupancy classes. Prasanth and Ghosh (2022) and Prasanth et al. (2023) introduced post-earthquake functionality as a criterion, reporting that the highest R for which a high-rise RC building retained roughly half its resilience without exceeding Collapse Prevention was about 6, falling to 4 under bi-directional loading. These studies point toward the collapse-based validation that the present study identifies as future work, while confirming that a static pushover estimation remains a necessary and interpretable first step.

Table 2.1 Representative studies on the R-factor of RC moment frames.

Study (Author, Year)	System / Code	Stories (Bays)	Method	R Estimation & Target Displacement	R vs Code	Key Parameters	Main Conclusion
AlHamaydeh et al. (2011)	SMRF / IBC 2009	4, 16, 32	NLTHA (IDARC-2D)	Ω_0=Vmax/V; R from record demand-to-yield	R=4–7 < 8	Height; motion 10/50 vs 2/50	R decreases with height; period-dependent R, C_d urged
Al-Ahmar and Al-Samara (2015)	SMRF / UBC 97	3–15 (2–5)	Pushover	$R=R_\mu\times\Omega$; $\mu=\Delta_u/\Delta_y$; FEMA 356 target displ.	R=5–12 vs 8.5	Stories; bay count & span	Fixed R unsafe for tall, uneconomic for low-rise
Mondal et al. (2013)	Ductile RC / IS 1893	2, 4, 8, 12	Pushover (perf. -based)	Component-wise; ATC-40 drift/rotation limit and ultimate rotation limit	4.23–4.96 (SS); 5.46–8.48 (ult.)	Height; performance level	Code overestimates R at the first limit; R exceeds code only at the ultimate limit
Abou-Elfath and Elhout (2018)	RC MRF / ECP-201	4, 8, 12 (3, 5)	Pushover + THA	$R=R_\mu\times\Omega$; monitored roof displ.	6.18–9.85 (pushover); 5.43–8.43 (THA)	Height; bays; story height	R decreases with height; bays minor; dynamic < static
Balendra et al. (1999)	RC MRF / BS 8110	3, 6, 10	Pushover	$\Omega=V_u/V_d$; $\mu\approx 2$; equal-displacement	R=18.0→4.7	Height; gravity design	Ω falls sharply with height, driving R down
Chaulagain et al. (2014)	RC (irregular) / IS	avg. set	Pushover	$\Omega=V_u/V_d=\Omega o\times RR$; equal-displacement	R = 1.54–4.66 < 5	Column/beam ratio; load path	SCWB>1.1 gives R≈4; violation drops R to 2.16
Zafar (2009)	RC MRF / developing	varied	IDA (OpenSees)	$R=R_\mu\times\Omega$; $R_\mu=V_e/V_y$; 4% target drift	geometry-dependent	Geometry; material strength	Local calibration of R needed, not code transfer
Oggu et al. (2021)	RC MRF (±infill) / IS	8 configs	NSA + IDA	IDR=4% collapse; first-mode $S_a(T1)$	pushover R < IDA R	Infill; open ground story	Infill raises Ω and Rμ; IDA R > pushover R
Patel and Parikh (2022)	SMRF/OMRF / IS 1893	4, 12	NLTHA (SAP2000)	$R=R_\mu\times R_s\times RR\times R\xi$; $R_s=V_y/V_d$	SMRF R = 3.08–4.45 < 5	Height; zone; plan	R falls up to 25% with height; also falls with zone
Attia et al. (2020)	Elevated metro station / ECP, ASCE 7	special structure	Pushover + NLTHA (ABAQUS)	$\mu=\Delta_u/\Delta_y$; Newmark-Hall R_μ	pushover ≈ NLTHA (R)	Configuration; cladding	Pushover R (Newmark-Hall) close to NLTHA
Ahmed et al. (2021)	RC (irregular) / code	moderate-rise	Pushover	$R=R_\mu\times\Omega$; bilinear idealization	R reduced by irregularity	Setback; soft story	R to be reduced about 15% (single) and 25% (combined irregularity)
Keerthi and Vivek Philip (2017)	SMRF / IS	10 (1–5 bays)	Pushover (SAP2000)	$R=R_\mu\times\Omega$; redundancy focus	R=3.09→5.44	Bay count (redundancy)	Few-bay frames overestimated by code R

Study (Author, Year)	System / Code	Stories (Bays)	Method	R Estimation & Target Displacement	R vs Code	Key Parameters	Main Conclusion
Fayed et al. (2018)	RC MRF / ECP-201	3, 6, 9	Pushover (3D, SAP2000)	$R=R_\mu \times \Omega$; $R_\mu=1+(\mu-1)\ T/0.7$	varies with stories/zone	Height; zone; spectrum	R decreases with story count
Nishanth et al. (2017)	SMRF/OMRF / IS	varied	Pushover	$R=R_\mu \times \Omega$; R-T-Z relation	code R on high side	Zone; period	R decreases with zone; increases slightly with period
Kim et al. (2016)	Small-size RC / KBC	low-rise	Pushover	Ω and μ from bilinear curve	moderate Ω and μ ($\approx$2.1)	Prescriptive member sizing	Moderate Ω and μ; slightly higher R may be used
Cui et al. (2021)	RC / Chinese code	3–12	DCFM (probabilistic)	Drift capacity vs demand distribution	R$\approx$3 conservative vs 6	Height; PGA level	Both R$\approx$3 and R$\approx$6 meet collapse safety
Ferraioli (2021)	Ductile RC / EC8	varied heights	Pushover + dynamic	Behavior factor from capacity + IDA	q consistent with design	Ductility class; height	Local ductility (confinement) governs global q
Ariyanto et al. (2026)	SMRF / SNI 1726:2019	3 models, 30 m	Pushover	Target max displ. = 4% of height	drift-based	Vertical geometry	Story height changes period, capacity and drift; R not estimated
Damayanti and Muin (2023)	SMRF vs OMRF / SNI 1726:2019	case study	Pushover	R from capacity curve; drift check	lower R $\rightarrow$ more reinf.	Detailing compliance	R and demand are coupled through drift
Layas et al. (2026)	Existing RC / TBEC	6	Pushover	$R=R_\mu \times \Omega$; damage-calibrated	R=8 false; R=3 real	Substandard existing frame	Reduced R matches observed damage

2.5 Research Gap and Positioning of the Present Study

The synthesis above establishes four points on which the literature agrees: code R-values are assigned by committee consensus, informed by observed performance rather than estimated for the individual structure, and they often exceed the values structures achieve; R depends strongly on period, height, and the analysis method; the ductility, overstrength, and redundancy components must be evaluated separately; and the reported magnitude of R is inseparable from the definition of the maximum displacement used to extract it. From these, two specific gaps define the contribution of the present study.

First, few studies evaluate a pure special moment-resisting frame designed and detailed to ACI 318-19 Chapter 18 while applying the period-dependent R_μ-T framework consistently across a height family and confirming which branch governs each height, rather than assuming a single branch without justification. As Section 2.2.3 showed, the Newmark-Hall branches return different values of R_μ for the same ductility ratio, and the equal-displacement approximation holds well only above about 0.5 s, so the branch must be selected for each frame from its period. A period-aware estimation applied consistently to a family of SMRFs of four, six, and fifteen stories (the one-story frame in Chapter 4 is a validation benchmark only) has not been reported.

Second, and closely related, the sensitivity of R to the definition of the maximum displacement is widely implied by the scatter in the literature but rarely confronted directly, and several of the definitions in use are conventions of the individual studies rather than provisions of a code. The present study addresses it by estimating R under three definitions, each taken from a code or standard: the code-amplified displacement of ASCE 7-16, the target displacement of FEMA 356, and the displacement at which the first component reaches its Collapse-Prevention acceptance criterion of ASCE 41-17. Within this framework the study also examines the effect of hoop spacing combined with concrete strength, of the longitudinal reinforcement ratio and of column section reduction on each component of R, the question that Section 2.4.3 identified as motivated but unresolved for a code-detailed SMRF. Addressing these two gaps provides a more rational basis for judging whether the code value of R = 8 represents the actual nonlinear behavior of special reinforced concrete moment frames.

2.6 Summary

This chapter defined the response modification factor, traced its evolution from the consensus tables of ATC 3-06 to the collapse-based validation of FEMA P-695, and decomposed it into its ductility, overstrength, and redundancy components. It reviewed the nonlinear static and dynamic procedures used to extract the factor and singled out the definition of the maximum displacement as the choice that most strongly governs the reported value. A theme-based critical synthesis of previous studies showed that R decreases with height under code and drift-limited target displacements but can increase under the equal-displacement rule, that bay geometry is secondary, that detailing and confinement act through the ductility and overstrength components, and that code values generally exceed achieved values, most sharply outside their originating context. From this synthesis two gaps were identified, a period-aware estimation across a family of SMRFs and an explicit treatment of the sensitivity to the definition of the maximum displacement, together with the effect of confinement and other design variables, which the following chapters address.

CHAPTER 3 STUDY DESCRIPTION

3.1 Introduction

This chapter describes the prototype reinforced concrete building, its material properties, the gravity and seismic loading, and the design framework adopted to evaluate the response modification factor (R) of Special Moment-Resisting Frame (SMRF) systems. The prototype geometry follows a regular multi-story configuration so that the influence of building height and of selected design parameters on the R-factor can be examined without the effects of plan irregularity. All members are designed and detailed as a special moment frame in accordance with ACI 318-19 (American Concrete Institute [ACI], 2019), and the seismic design parameters are established in accordance with ASCE 7-16 (ASCE, 2016). The nonlinear modeling procedure, the plastic hinge definitions, and the pushover setup are presented separately in Chapter 5.

3.2 Prototype Structure Description

The prototype is a regular reinforced concrete framed building intended for educational occupancy. In plan, the structure comprises four bays of 6.0 m in the longitudinal (x) direction and three bays of 6.0 m in the transverse (y) direction, giving overall plan dimensions of 24 m × 18 m. Each story is 3.0 m high and is supported on twenty columns arranged on a regular 5 × 4 grid, together with primary beams along every gridline and a two-way solid slab of 250 mm thickness.

Three models with different heights are developed to investigate the dependence of the R-factor on building height: 4-story, 6-story, and 15-story configurations. The plan layout, bay spacing, story height, and nominal material properties are the same in all models. Member sizes, reinforcement, and confinement detailing follow the design requirements of each height, so the height comparison is a comparison between code-designed archetypes rather than between identical frames scaled only in height. This is taken into account when the height trend is interpreted in Chapter 6. The 15-story model represents the mid-to-high-rise range for which special moment frames are commonly specified, and it is designated as the reference model for the parametric study of Section 3.8.

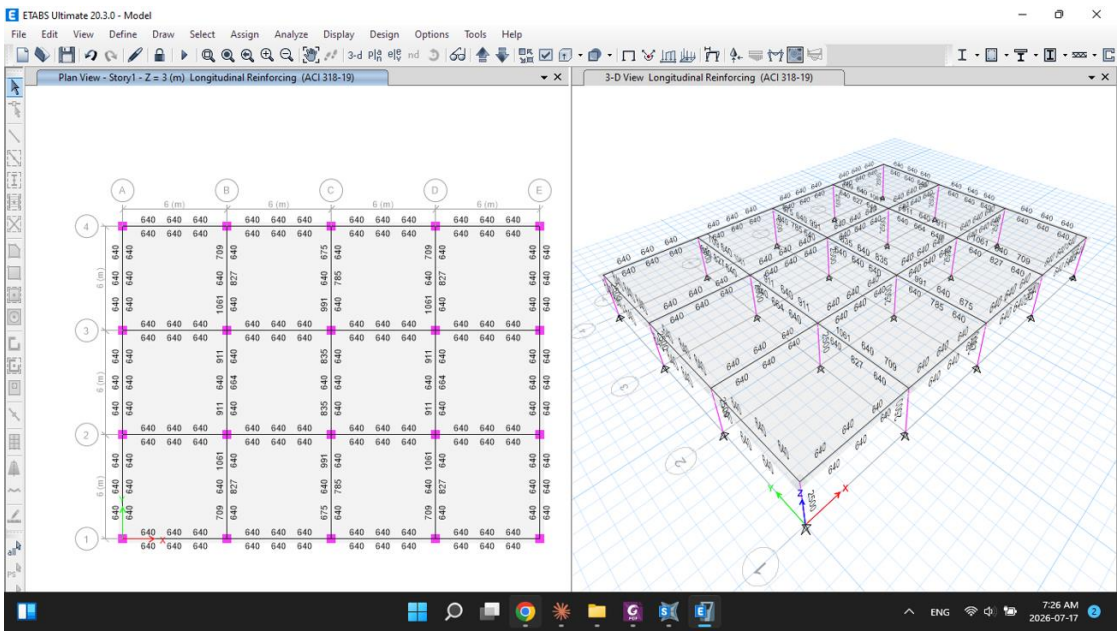

Figure 3.1 Plan and three-dimensional views of the prototype structure.

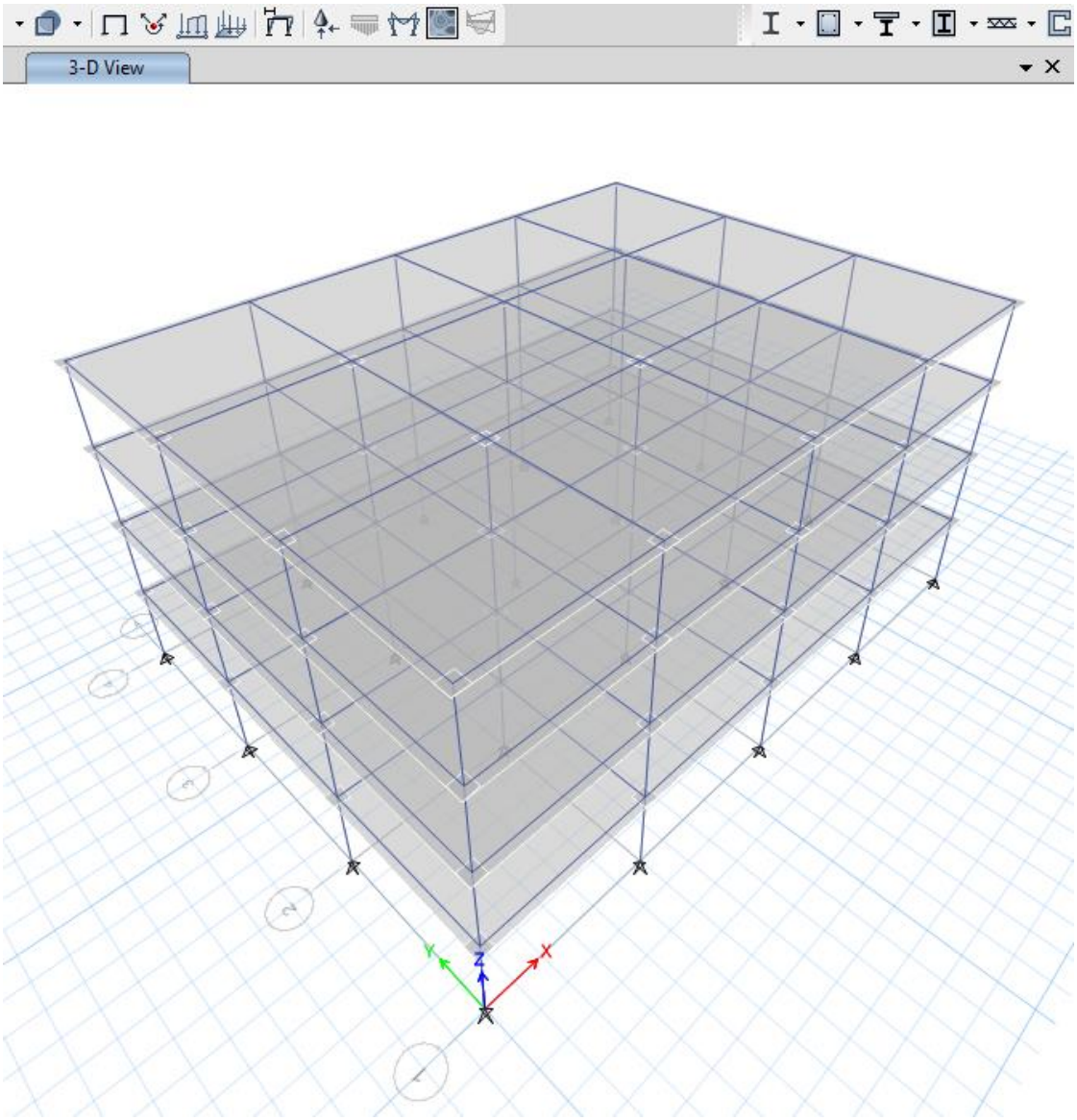

Figure 3.2 Four-story frame (ETABS).

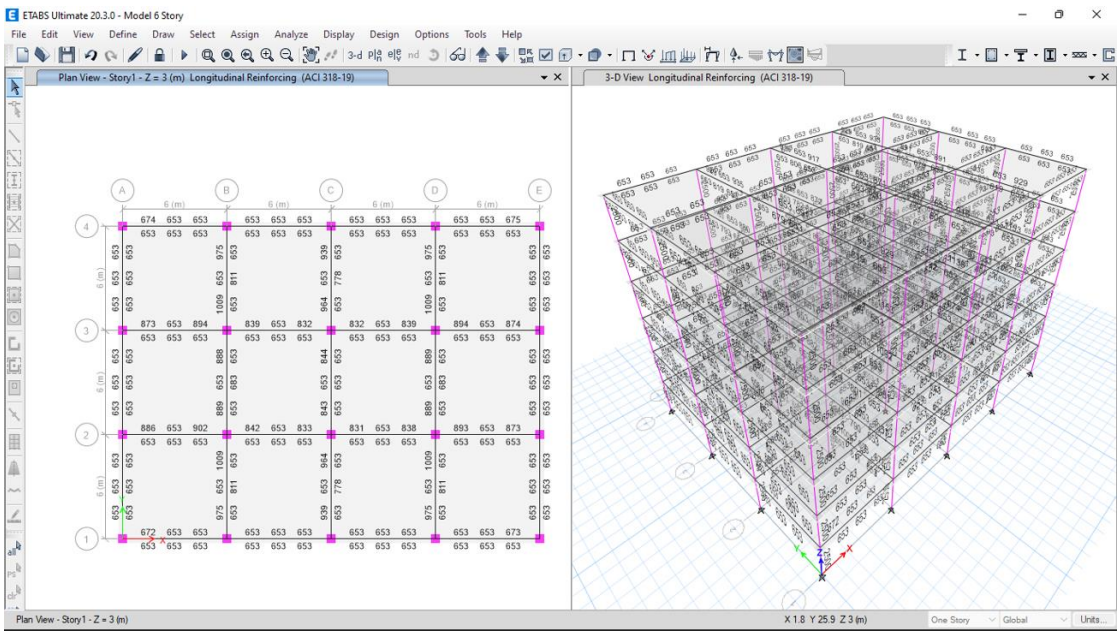

Figure 3.3 Six-story frame (ETABS).

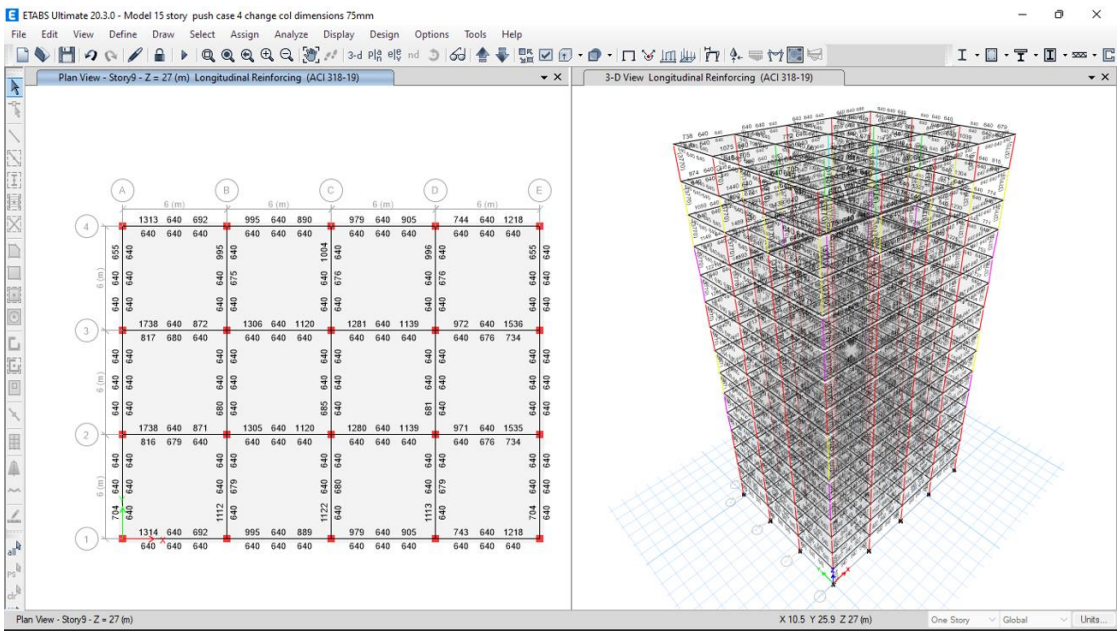

Figure 3.4 Fifteen-story reference frame (ETABS).

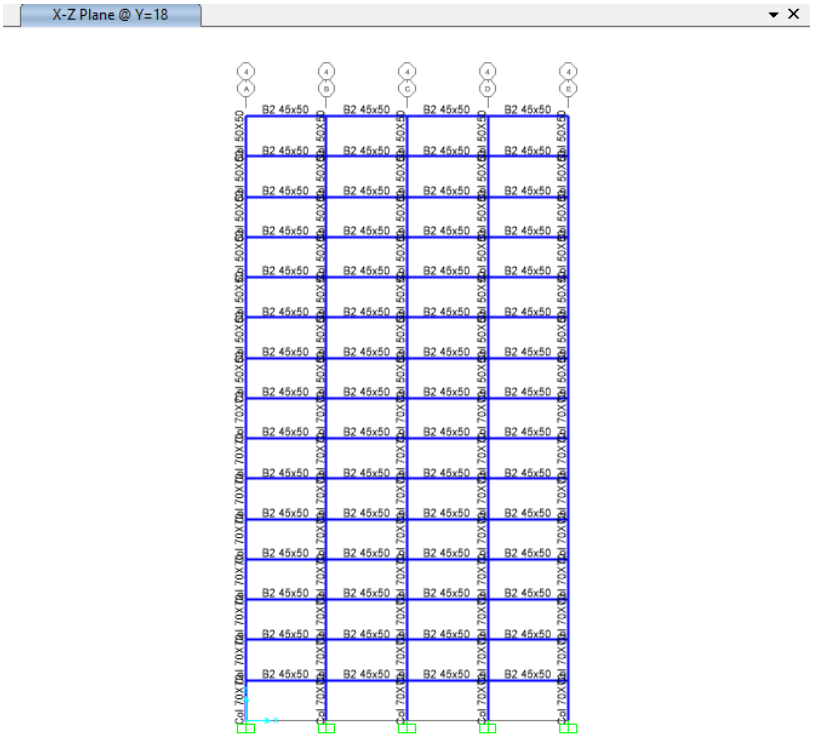

Figure 3.5 Elevation of the fifteen-story reference frame (SAP2000).

In the fifteen-story reference model the columns follow a graded schedule that reduces the section with height: at the ground story the six interior columns are 1000 × 1000 mm and the fourteen perimeter columns 800 × 800 mm, and the sections step down over the height to 500 × 500 mm in the top three stories. The sections were sized so that the axial-flexural demand-capacity ratio remains below unity at every level, the governing value being 0.99. The four-story frame uses 500 × 500 mm columns throughout. The six-story frame uses 600 × 600 mm interior columns in the lower three stories and 500 × 500 mm columns elsewhere. The beams are 500 × 450 mm (width × depth) in the four- and fifteen-story frames and 500 × 550 mm in the six-story frame. The column hoops are Ø10 at 70 mm in the four-story frame, Ø12 at 75 mm in the six-story frame, and Ø10 at 70 or 75 mm in the fifteen-story frame, with the number of legs set for each section. The complete column and beam schedules are given in Section 5.6. The principal geometric and material parameters of the prototype are summarized in Table 3.1.

Table 3.1 Geometric and material properties of the prototype.

Structural system	**Special moment-resisting RC frame (SMRF)**
Plan dimensions	24 m (4 bays) × 18 m (3 bays)
Bay span (both directions)	6.0 m (center to center)
Story height	3.0 m
Number of stories	4, 6, and 15
Slab	Two-way solid slab, 250 mm
Columns, four-story frame	500 × 500 mm throughout
Columns, six-story frame	600 × 600 mm interior (stories 1 to 3); 500 × 500 mm elsewhere
Columns, fifteen-story reference frame	1000 × 1000 mm interior and 800 × 800 mm perimeter at the ground story, stepping down to 500 × 500 mm in the top three stories (Table 5.4)
Beams (width × depth)	500 × 450 mm (four- and fifteen-story frames); 500 × 550 mm (six-story frame)
Concrete compressive strength, f'_c (design)	24 MPa
Reinforcement, specified yield strength, f_y (design)	ASTM A615 Grade 60, 420 MPa
Concrete unit weight	25 kN/m³
Superimposed dead load (excl. self-weight)	5.0 kN/m²
Live load	3.0 kN/m²

3.3 Material Properties

The specified compressive strength of concrete is taken as f'c = 24 MPa, and the reinforcement is ASTM A615 Grade 60 with a specified yield strength f_y = 420 MPa. The modulus of elasticity of concrete is computed in accordance with ACI 318-19 Section 19.2.2 (ACI, 2019) as $E_c = 4700 \sqrt{f'c}$ (MPa), which gives E_c = 23,025 MPa; the ETABS design models use 23,270 MPa, 1.1 percent higher. The Poisson's ratio for concrete is taken as 0.20, and the modulus of elasticity of the reinforcement is E_s = 200,000 MPa. These nominal properties are used in the elastic design models in ETABS. The nonlinear models in SAP2000 use expected material properties, which are defined in Section 5.3.

3.4 Gravity Loading

A superimposed dead load of 5.0 kN/m² (excluding the self-weight of the structural members, which is generated automatically by the software) and a live load of 3.0 kN/m² are applied at each floor level. The self-weight of the columns, beams, and slab is computed internally from the member geometry and the concrete unit weight of 25 kN/m³.

These gravity loads are combined with the seismic actions through the load combinations defined in Section 3.7.

The seismic mass is defined from the dead load pattern alone, with element self-mass excluded so that the self-weight of the members is not counted twice. The live load is not included in the seismic mass, in accordance with ASCE 7-16 Section 12.7.2 (ASCE, 2016). All models are analyzed with fixed bases, and the same boundary condition is applied in the elastic design model and in the nonlinear model so that the two are directly comparable.

3.5 Seismic Design Parameters

The prototype is a hypothetical archetype with the seismic hazard of Zone 3 of the seismic zone map of Palestine, Z = 0.30 (Figure 1.3). The mapped spectral accelerations are obtained from the zone factor as $S_s = 2.5\ Z = 0.75$ g and $S_1 = 1.25\ Z = 0.375$ g, the conversion used in previous studies at this institution (Shrouf, 2025). With Site Class A they give $S_{DS} = 0.40$ g and $S_{D1} = 0.20$ g and place the structure in Seismic Design Category D. Site Class A is an idealized rock-site assumption rather than a measured site classification. It was chosen so that the estimated factor reflects the structural system without the amplification of a particular soil profile; it gives the lowest site coefficients of ASCE 7-16 ($F_a = F_v = 0.8$), and the sensitivity of the results to softer classes is identified as future work. The long-period transition period is taken as $T_L = 4$ s; it does not affect the design, since the design periods of the three frames (0.654 to 2.150 s) are below it. The corresponding average shear-wave velocity in the upper 30 m exceeds 1500 m/s, satisfying the Site Class A requirement of ASCE 7-16 (ASCE, 2016, Table 20.3-1). The design spectral parameters are derived in accordance with ASCE 7-16 and are summarized in Table 3.2.

Table 3.2 Seismic design parameters.

Parameter	Symbol	Value	Reference (ASCE 7-16)
Mapped short-period spectral acceleration	S_s	0.75	2.5 Z, Z = 0.30 (Section 3.5)
Mapped 1-s spectral acceleration	S_1	0.375	1.25 Z, Z = 0.30 (Section 3.5)
Site class	—	A (hard rock)	Chapter 20
Short-period site coefficient	F_a	0.8	Table 11.4-1
Long-period site coefficient	F_v	0.8	Table 11.4-2
MCE_R short-period acceleration	$S_{MS} = F_a \cdot S_s$	0.60	Eq. 11.4-1
MCE_R 1-s acceleration	$S_{M1} = F_v \cdot S_1$	0.30	Eq. 11.4-2
Design short-period acceleration	$S_{DS} = (2/3) \cdot S_{MS}$	0.40	Eq. 11.4-3
Design 1-s acceleration	$S_{D1} = (2/3) \cdot S_{M1}$	0.20	Eq. 11.4-4
Long-period transition period	T_L	4 s	Adopted value (Section 3.5)
Risk category / Importance factor	III / I_e	1.25	Tables 1.5-1, 1.5-2
Seismic design category	SDC	D	Tables 11.6-1, 11.6-2

Based on S_{DS} = 0.40 and S_{D1} = 0.20 combined with Risk Category III, the structure is assigned to Seismic Design Category D, for which a special moment-resisting frame is a permitted and appropriate seismic force-resisting system per ASCE 7-16 Table 12.2-1.

3.6 Seismic Force-Resisting System and Design Coefficients

The lateral force-resisting system is a special moment-resisting reinforced concrete frame. The corresponding seismic design coefficients are taken from ASCE 7-16 Table 12.2-1 (ASCE, 2016) and listed in Table 3.3. A clear distinction is maintained throughout this study between the code system overstrength factor Ω_0, which is a prescribed amplification factor used in the design of force-controlled elements, and the overstrength factor Ω computed analytically from the pushover capacity curve. Ω is one of the components of the response modification factor evaluated in this research.

Table 3.3 Seismic design coefficients of the SMRF system.

Seismic design coefficient	Value	Reference
Response modification coefficient, R	8	ASCE 7-16, Table 12.2-1
System overstrength factor, Ω_0	3.0	ASCE 7-16, Table 12.2-1
Deflection amplification factor, C_d	5.5	ASCE 7-16, Table 12.2-1

3.7 Design Base Shear and Load Combinations

The seismic design forces are determined using the Equivalent Lateral Force (ELF) procedure of ASCE 7-16 Section 12.8 (ASCE, 2016). The seismic base shear is computed as $V = C_s \cdot W$, where C_s is the seismic response coefficient obtained from the design spectral accelerations, the importance factor, and the response modification coefficient R, and W is the effective seismic weight of the structure. The structural members are then designed in ETABS for the most critical of the following strength load combinations, in which the seismic vertical effect is incorporated through the $0.2 \cdot S_{DS} \cdot D$ term and ρ is the redundancy factor, retained as 1.3 for member design although 1.0 is permitted for this structure (Appendix A.3):

- 1.4D
- 1.2D + 1.6L
- (1.2 + 0.2SDS) D + ρQE + L → 1.28D + 1.3QE + L
- (0.9 − 0.2SDS) D + ρQE → 0.82D + 1.3QE

Table 3.4 Design base shear of the three frames.

Quantity	Basis	Four-story	Six-story	Fifteen-story
Approximate period, $C_u T_a$ (s)	ASCE 7-16 Section 12.8.2	0.654	0.943	2.150
$C_s = S_{DS} I_e / R$	ASCE 7-16 Eq. 12.8-2	0.0625	0.0625	0.0625
$C_s = S_{D1} I_e / (T R)$	ASCE 7-16 Eq. 12.8-3	0.0478	0.0332	0.0145
$C_{s,min} = 0.044 S_{DS} I_e$	ASCE 7-16 Eq. 12.8-5	0.0220	0.0220	0.0220
Governing C_s		0.0478 (Eq. 12.8-3)	0.0332 (Eq. 12.8-3)	0.0220 (Eq. 12.8-5)
Effective seismic weight, W (kN)	ETABS	25,545	39,747.8	100,171.9
Design base shear, $V_d = C_s W$ (kN)	ASCE 7-16 Eq. 12.8-1	1,219.8	1,317.7	2,203.8

For the four- and six-story frames the computed fundamental periods exceed $C_u T_a$, so the design period is the capped value $C_u T_a$, and the period-dependent coefficient of Equation 12.8-3 governs. For the fifteen-story frame the minimum coefficient of Equation 12.8-5 governs: it exceeds the value of Equation 12.8-3 by the factor $0.044 S_{DS} T R / S_{D1}$, which is greater than unity whenever T exceeds $S_{D1} / (0.044 S_{DS} R) = 1.42$ s. The importance factor cancels from both sides of that comparison. The design base shears of

the fifteen-story variants with reduced column sections (Section 3.8) are 2,199.1 kN (stories 3 to 5) and 2,199.7 kN (stories 13 to 15), from their own ETABS models.

The beams, columns, and beam-column joints are subsequently detailed to satisfy the special moment frame requirements of ACI 318-19 Chapter 18 (ACI, 2019). The detailing provisions distinguish the special moment frame from intermediate and ordinary frame classifications and govern the ductility capacity available for R-factor estimation. The specific detailing requirements applied to the reference model and the parametric variants are presented in Chapter 5.

The structural height of the fifteen-story frame is 45.0 m, below the 160 ft (48.8 m) threshold of ASCE 7-16 Table 12.6-1, and the prototype has no structural irregularities. The equivalent lateral force procedure of Section 12.8 is therefore permitted for this structure without a period limitation; the 3.5Ts criterion of that table applies only to structures exceeding 160 ft in height. The commentary explains the basis of that criterion: higher modes become more dominant in taller buildings, so that the procedure may underestimate the seismic base shear and may not correctly predict the vertical distribution of seismic forces (ASCE, 2016, C12.6). Verification of the displacement demand under modal response spectrum analysis is identified as future work.

3.8 Parametric Study Framework

The parametric study evaluates how selected design variables influence the response modification factor. Four families are examined: building height; hoop spacing combined with concrete strength; longitudinal reinforcement ratio of the columns; and column cross-section reduction at two locations over the height. The variants are identified in this thesis as Models 4 to 7 of the fifteen-story family, the reference frame being the base model.

The first family varies the building height while keeping the plan layout constant. Three heights are analyzed: 4-story, 6-story, and 15-story. Because member sizes, reinforcement, and periods change with height, the comparison is made between code-designed archetypes rather than between frames that differ in height only. The effective periods of the three nonlinear models, between 1.21 and 3.67 s, all exceed $T_s = S_{D1} / S_{DS} = 0.50$ s, so the same branch of the ductility reduction relation of Newmark and Hall (1982) applies to all three (Chapter 6).

The second family (Model 4) widens the hoop spacing of the fifteen-story frame and lowers its concrete strength. The hoop spacing of every column is increased from the design value of 70 or 75 mm to 100 mm, with the same hoop diameter and the same number of legs, which lowers the transverse reinforcement ratio ρ_t of each column section by 25 to 30 percent. In the nonlinear model this variant also carries a concrete strength of 29 MPa in place of the expected strength of 35 MPa used in the other models (Section 5.3). Two parameters therefore change together, and the comparison with the reference frame measures the combined effect of wider hoop spacing and lower concrete strength rather than the effect of hoop spacing alone. The 100 mm spacing does not satisfy the confinement requirements of ACI 318-19 Section 18.7.5; it is a deliberate parametric departure from the code-compliant design.

The third family (Model 5) raises the longitudinal reinforcement ratio of the columns of the fifteen-story frame from about 1.0 to 1.1 percent in the reference design to about 2.0 percent in most column sections; the 650, 700, and 750 mm sections keep their reference reinforcement. The section dimensions, the beams, and the nominal material properties are unchanged. The complete schedule is given in Table 5.5.

The fourth family varies the column cross-section at two locations of the fifteen-story frame. In Model 6 the perimeter columns of stories 3 to 5 are reduced by 50 mm (800 to 750 mm, 750 to 700 mm, and 700 to 650 mm). In Model 7 all columns of stories 13 to 15 are reduced to 450 × 450 mm. The two locations were chosen away from the first story, where the axial load is highest and the base hinges of the columns were expected to control the Collapse-Prevention limit state: one in the lower third of the height and one at the top, where designers commonly reduce column sections. Comparing the two variants shows whether a section reduction away from the expected critical region, and its location over the height, affects the estimated factor. The outcome is reported in Section 6.9.4.

For every model the design procedure of Sections 3.5 to 3.7 is applied with R = 8, as prescribed by ASCE 7-16 Table 12.2-1 for special reinforced concrete moment frames. The pushover analysis then estimates the R-factor from the capacity curve, and the estimated value is compared with the code value on a declared basis (Chapter 6). The results of the parametric study are presented and discussed in Chapter 6.

CHAPTER 4 VALIDATION OF THE NONLINEAR MODELING PROCEDURE

4.1 Introduction

This chapter validates the nonlinear static analysis procedure used later in this thesis to estimate the response modification factor of the Special Moment Resisting Frame (SMRF) prototypes. Before the pushover response of the prototypes can be treated as reliable, the modeling assumptions embedded in SAP2000 must be tested against independently measured structural responses reported in the literature. This step separates the software's inherent capability from the specific design choices made in later chapters.

Three reinforced concrete specimens serve as validation benchmarks. The first is a slender single-span beam with a shear span-to-depth ratio close to seven, in which flexure-compression governs the failure mode. The second is a two-span continuous beam that develops extensive plastic redistribution before collapse. The third is a one-story frame that couples axial-flexure interaction in columns with flexural yielding in beams. Each benchmark examines a different aspect of the software's numerical performance.

The Bresler and Scordelis (1963) beam evaluates how the model reproduces the elastic-to-cracked transition and the flexural collapse load of a slender member. Because the formulation adopted here uses lumped flexural plastic hinges, shear-controlled failure is outside its representational capability and is not claimed to be validated. The Duddeck-Mueller beam (*Mueller, 1977*) tests numerical stability under progressive yielding of both concrete and steel across multiple plastic hinge locations. The Xiao et al. (2006) frame provides the closest analog to the SMRF study because it captures the same combination of gravity axial load and lateral flexural demand present in the 15-story prototype.

Good agreement between the numerical predictions and the reported experimental data across the three cases supports the lumped-plasticity pushover procedure used for the prototypes. The validation also produces practical guidelines for nonlinear modeling in SAP2000, which are applied in Chapter 5.

4.2 Nonlinear Analysis Framework in SAP2000

4.2.1 Solution Strategy

Nonlinear structural analysis in SAP2000 relies on iterative solution algorithms that update stiffness and internal force distributions after each load increment. The

displacement-based method dominates commercial implementations because nodal displacements act as the natural unknowns of finite element formulations (*Bathe, 1996*). Under this method, the tangent stiffness matrix is reassembled whenever a material or geometric nonlinearity is triggered, and equilibrium is restored through the modified Newton-Raphson procedure. The main drawback is error accumulation across steps, especially near yield transitions where the tangent stiffness changes abruptly.

An alternative approach uses internal element forces as the primary unknowns. Force-based formulations are more efficient for members that develop distributed plasticity along their length, but they require careful integration of nonlinear section responses. SAP2000 supports both formulations through the lumped-plasticity hinge option and the distributed-plasticity fiber section, respectively. The validation cases in this chapter use lumped plasticity, which is also the formulation of the prototype frames.

4.2.2 Material Constitutive Models

Concrete under cyclic loading behaves as a strongly nonlinear material. Two idealizations are commonly used to represent concrete in nonlinear frame analysis: the elastic-perfectly plastic model and the bilinear model with linear strain hardening. The validation cases in this chapter use neither in isolation: their hinge backbones are generated from a Mander confined-concrete stress-strain curve built from the measured properties of each specimen, as described in Section 4.2.3. Figure 4.1 illustrates both responses. The elastic-perfectly plastic model idealizes concrete as elastic up to its ultimate compressive strength, after which it deforms at constant stress. The bilinear model extends this by allowing a positive post-yield slope fitted to experimental data.

When realistic capacity assessment is the goal, the bilinear model provides a closer match to observed cyclic degradation because it captures the residual strength that concrete retains after cracking (*Priestley et al., 1996*). Steel reinforcement enters the model through similar bilinear or multilinear representations of its stress-strain diagram. The validation cases in Sections 4.3, 4.4, and 4.5 use experimentally measured properties for both concrete and steel so that no material property is fitted to the test result.

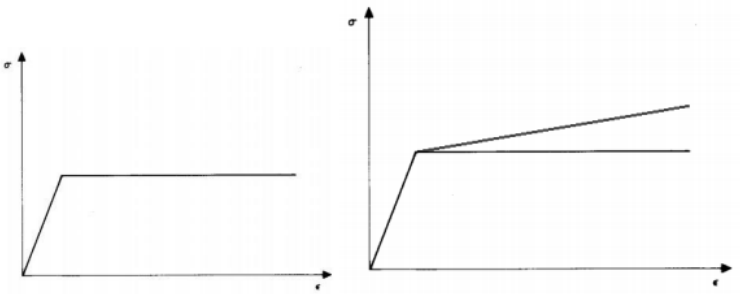

Figure 4.1 a. Elastic-Perfectly Plastic Stress-Strain Curve. b. Elasto-Plastic With Linear Hardening Stress-Strain Curve.

Figure 4.1 Elastic-perfectly plastic and linear-hardening stress-strain curves.

4.2.3 Plastic Hinge Definitions

SAP2000 offers two methods to introduce plastic hinges into frame elements. The Auto Hinge option generates a moment-rotation or force-displacement backbone automatically from the assigned section and material. When the section is assigned a default material, the backbone follows the acceptance criteria published in FEMA 356 and ATC-40, which scale the plastic rotation limits with axial load ratio, longitudinal reinforcement ratio, and shear stress. When the section is assigned a user-defined material stress-strain curve, the same automatic hinge derives its backbone from that curve instead. The User Defined Hinge option, by contrast, requires the analyst to input the entire backbone manually. The validation cases of this chapter use automatic hinges whose backbone is driven by a user-defined Mander confined-concrete stress-strain curve.

The automatic hinge generator keeps the modeling reproducible and traceable, while the user-defined Mander material curve reflects the confinement of the specimens in the hinge response (Mander et al., 1988). The validation cases in Sections 4.3 through 4.5 apply this combination, each with a Mander curve built from the measured material properties of the corresponding specimen. The prototype frames of Chapters 5 and 6 use the same lumped-plasticity pushover procedure in SAP2000, but their hinge parameters and acceptance criteria are taken from ASCE 41-17 Tables 10-7 and 10-8 (Section 5.3.1). The validation therefore supports the analysis procedure, not the specific hinge parameters of the prototypes.

4.3 Validation Case 1: Single-Span Beam (Bresler and Scordelis, 1963)

4.3.1 Geometry and Test Configuration

The first benchmark is a simply supported reinforced concrete beam tested by Bresler and Scordelis *(1963)* under a single concentrated load applied at midspan. The specimen was designed to fail in a brittle flexure-compression mode, which occurred at a shear span-to-effective-depth ratio close to seven. This test is widely cited as a reference case for numerical models that aim to represent brittle, deformation-limited failure in reinforced concrete members.

The elevation, cross section, and reinforcement layout are shown in Figure 4.2. Longitudinal reinforcement consists of two #4 bars in the compression zone and six #9 bars in the tension zone. The concrete cross section was discretized into ten horizontal layers, and reinforcement was represented as smeared steel layers within the section.

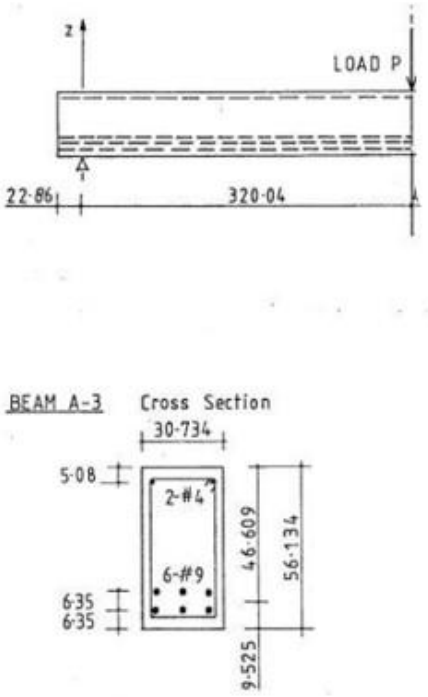

Figure 4.2 Single-span beam of Bresler and Scordelis (1963).

4.3.2 Material Properties

Table 4.1 summarizes the material properties adopted in the numerical model. The concrete Young's modulus, the ultimate compressive strength, and the peak compressive

strain were taken from the experimental report. Tensile strength and the tensile stiffness coefficients were assumed from typical values.

Table 4.1 Material properties of the single-span beam.

Concrete Property	Value	Steel Property	Value
E_c (MPa)	29,800	E_s (#9) (MPa)	205,300
Poisson's ratio, ν	0.15	f_y (#9) (MPa)	552
f'c (MPa)	35.0	E_s (#4) (MPa)	201,200
f't (MPa)	4.3	f_y (#4) (MPa)	345.2
Ultimate compressive strain, ε_c	0.003	Post-yield modulus (#4)	0

4.3.3 Numerical Model Setup and Results

The beam was discretized in SAP2000 using frame elements with automatic plastic hinges at the anticipated critical section beneath the applied load. The hinge backbone was derived from a Mander stress-strain curve constructed from the measured concrete and steel properties of the specimen.

The numerical simulation predicts a collapse load close to 480 kN, which matches the ACI 318 section analysis solution and slightly exceeds the experimental collapse value of approximately 467 kN. The response also exhibits a stiffer initial branch than that observed in the test. This behavior is a known outcome of the initial stiffness formulation adopted by SAP2000, which does not degrade uncracked concrete stiffness gradually with cracking progression. The overestimation remains within acceptable engineering bounds and does not compromise the reliability of the model in the yielding range that governs the pushover assessment of the SMRF prototype.

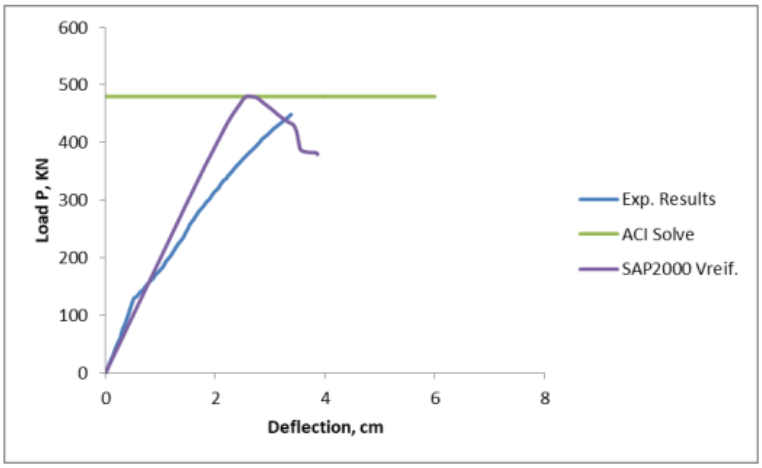

Figure 4.5: Load-Deflection Curve for Single Span Beam.

Figure 4.3 Load-deflection curve of the single-span beam.

4.4 Validation Case 2: Two-Span Continuous Beam (Duddeck-Mueller)

4.4.1 Geometry and Test Configuration

The second benchmark is a two-span continuous reinforced concrete beam. The specimen was tested experimentally and reported in detail by Mueller (1977). In contrast with the single-span beam of the first benchmark, this specimen develops a pronounced nonlinear response before failure. Extensive concrete cracking and yielding are accompanied by significant nonlinear behavior of the steel reinforcement. These features make the beam an appropriate case for testing the numerical stability of the solution algorithm when multiple plastic hinges form and interact.

The cross-section measures 60 × 80 mm with eight Φ4 longitudinal bars distributed between the compression and tension regions. Because of the geometric and load symmetry, only half of the beam was modeled. The half span was discretized into seven equal frame elements as shown in Figure 4.4(a). For the cross-section idealization, the beam was divided into eight equal horizontal concrete layers plus two smeared layers representing the reinforcing steel, as illustrated in Figure 4.4(b). Each steel layer was assigned a thickness of 0.084 cm. Transverse reinforcement was omitted from the model because shear did not govern the response.

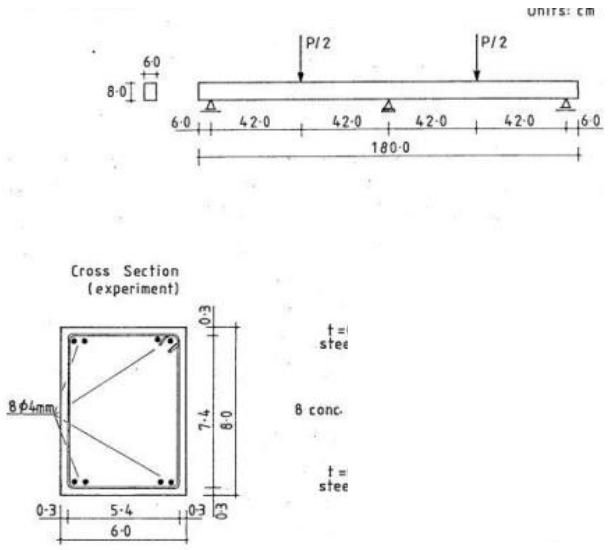

Figure 4.4 Cross section of the two-span beam.

4.4.2 Material Properties

Concrete properties for this specimen were obtained from the original experimental report. Steel properties were treated using a multilinear representation with linear hardening. Table 4.2 lists the values employed in the numerical model.

Table 4.2 Material properties of the two-span beam.

Concrete Property	Value	Steel Property	Value
E_c (MPa)	16,660	E_s (MPa)	196,000
Poisson's ratio, ν	0.0	Post-yield modulus, E_s' (MPa)	28,000
f'c (MPa)	32.0	Second post-yield modulus, E_s'' (MPa)	5,000
f't (MPa)	3.2	f_y (MPa)	490
Ultimate compressive strain, εu	0.004	Ultimate yield stress, f_y' (MPa)	574
Tensile stiffness coefficient, α	0.5	Compressive strain at peak, ε_c	0.0027

4.4.3 Numerical Model Setup and Results

Figure 4.5 shows the load-deflection response predicted by the numerical model together with the experimental data. The two curves match closely throughout the elastic and early yielding ranges. The predicted ultimate load reaches approximately 32.4 kN, exceeding the experimental limit load of 32.0 kN by 1.3 percent and the ACI 318 plastic hinge solution of 31.3 kN by 3.5 percent. Table 4.4 reports the comparison against the

experimental value. The plastic hinge solution provides a lower-bound estimate based on section analysis according to the ACI 318 provisions.

As in the first validation case, the numerical curve exhibits a slightly stiffer initial slope than that measured experimentally. This deviation traces back to the initial stiffness assumption in SAP2000 and does not affect the ultimate strength or the location of the primary yielding events. The ability of the numerical model to reproduce the ultimate capacity within a narrow band supports the use of the lumped-plasticity procedure for the pushover analysis of the prototypes.

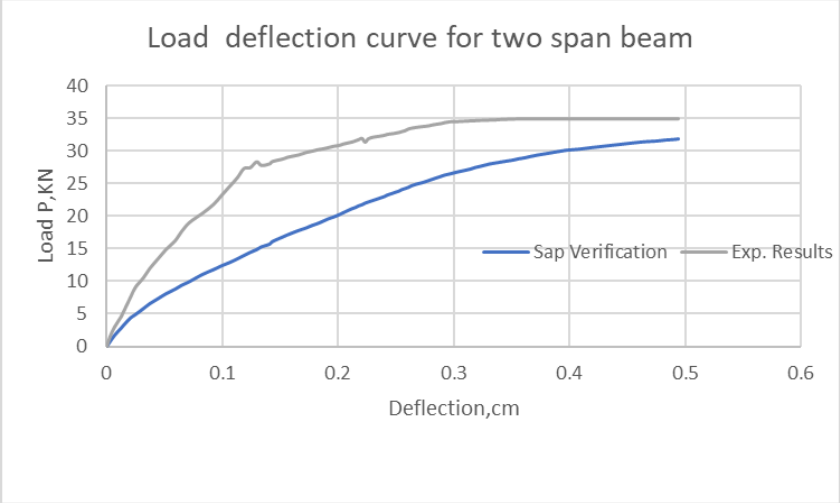

Figure 4.5 Load-deflection curve of the two-span beam.

4.5 Validation Case 3: One-Story Reinforced Concrete Frame (Xiao et al., 2006)

4.5.1 Geometry and Test Configuration

The third benchmark is one of four one-story, one-bay reinforced concrete frame specimens tested at 1:2 scale by Xiao et al. (2006) under a low-frequency cyclic lateral load with constant vertical actions. The four specimens are identical in geometry and reinforcement and differ only in the recycled coarse aggregate replacement percentage of the concrete, which is 0, 30, 50 and 100 percent. The specimen adopted here is FRAC-0, for which the replacement percentage is zero and the concrete is conventional natural-aggregate concrete; the authors identify it as the reference specimen for comparison. The frame spans 3.0 m between column centerlines and the lateral load is applied 1,725 mm above the base. The specimen consists of two columns and one beam; the columns are 150 × 250 mm and the beam 150 × 180 mm in cross section. Each member carries four Φ14 longitudinal bars distributed between the compression and tension regions.

Transverse reinforcement uses Φ6 stirrups. Stirrup spacing is 60 mm in the confinement zones near member ends and 120 mm in the middle regions. The concrete cover to the longitudinal reinforcement is 20 mm. This benchmark is the most representative of the SMRF prototype because it captures the same combination of gravity axial load in the columns and flexural demand transferred through the beam under lateral loading.

Two vertical point loads of 150 kN were applied at the top of each column to represent gravity forces. Two additional point loads of 12 kN each were applied on the beam at the one-third and two-thirds points measured from the left end. Lateral loading was then imposed at the roof level to induce the pushover response. Figure 4.6 shows the geometry, the reinforcement layout, and the loading configuration.

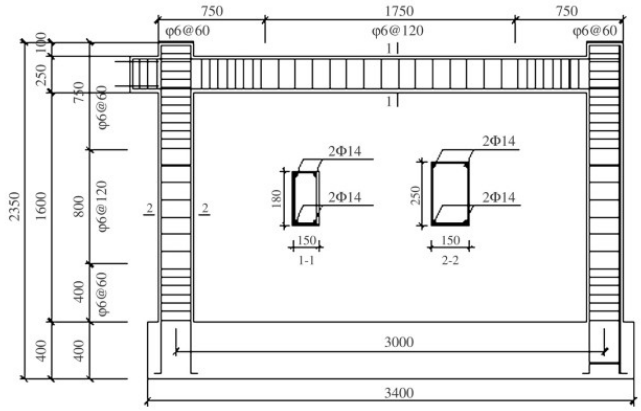

Figure 4.6 One-story frame tested by Xiao et al. (2006).

4.5.2 Material Properties

The concrete of specimen FRAC-0 reached a measured prism compressive strength of 27.0 MPa and a cube compressive strength of 35.6 MPa, with an elastic modulus of 33.0 GPa. The longitudinal reinforcement is HRB335 ribbed bar of 14 mm diameter with a measured yield strength of 448 MPa, and the transverse reinforcement is HPB235 plain bar of 6 mm diameter with a measured yield strength of 433 MPa (Xiao et al., 2006). The elastic modulus of the reinforcement was 200 GPa. Table 4.3 collects these properties for reference.

Table 4.3 Material properties of the one-story frame.

Concrete Property	Value	Steel Property	Value
E_c (GPa)	33	E_s (GPa)	200
f'c at 28 days (MPa)	27	f_y longitudinal (MPa)	448
Concrete cover (mm)	20	fyt stirrups (MPa)	433

4.5.3 Numerical Model Setup and Results

The frame was modeled in SAP2000 with frame elements assigned automatic plastic hinges whose backbone was derived from a Mander stress-strain curve built from the measured material properties of the specimen.

Up to the cracking load the numerical response agrees with the published cracking point of the specimen: for FRAC-0 the measured crack load is P_{cr} = 20.5 kN at a top displacement of 1.48 mm, and the model reaches that load at about 1.4 mm. The digitised experimental branch of Figure 4.7 is more flexible in this range (about 2.1 mm at 20 kN). In the same source, the yield load is Py = 81.7 kN at 14.61 mm, and the maximum load is Pmax = 95.2 kN at 39.40 mm (Xiao et al., 2006). Beyond cracking the model is stiffer than the test, because the lumped-plasticity formulation does not degrade the uncracked concrete stiffness as cracking progresses. At the last computed step, the model reaches 91.8 kN, that is 3.6 percent below the reported maximum load, and it is still on a rising branch. This deviation is again attributed to the initial stiffness formulation, which does not degrade the concrete contribution as cracking progresses. Because the pushover analysis of the SMRF prototype targets the yielding and post-yield ranges rather than the initial branch, the observed deviation does not compromise the reliability of the model for the objectives of this thesis.

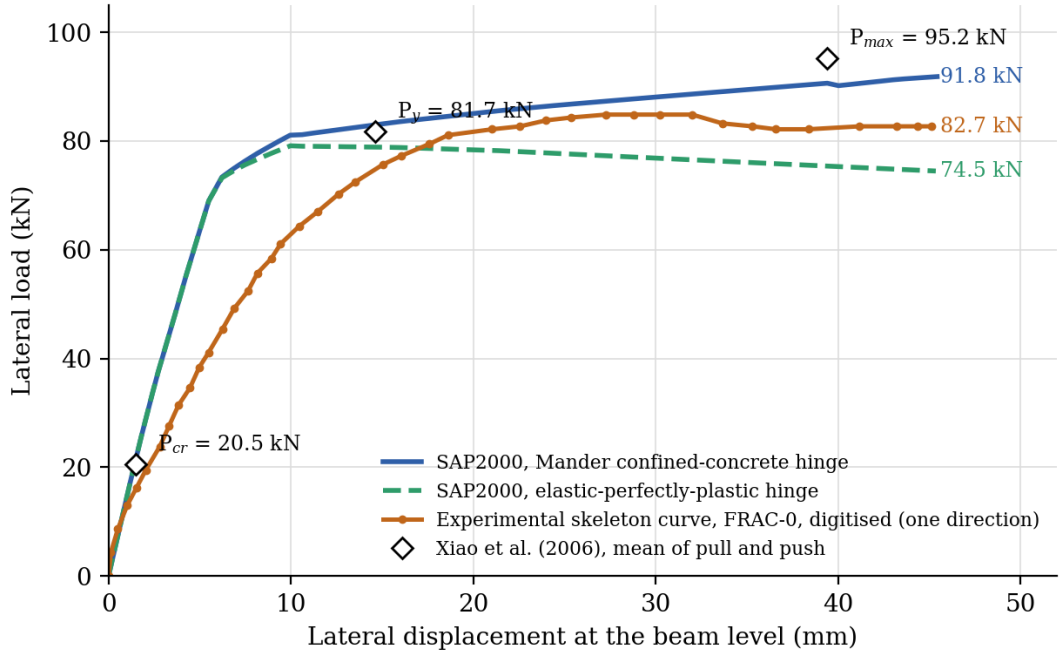

Figure 4.7 Load-deflection response of the one-story frame.

Note. Experimental skeleton curve digitized from Xiao et al. (2006), one loading direction. The published characteristic loads are the mean of the pull and push results and therefore lie above the digitized branch.

4.6 Consolidated Assessment of Modeling Accuracy

The three validation cases produce a consistent picture of the numerical performance offered by SAP2000. Table 4.4 states, for each validation case, the quantity compared, the reported experimental value, the value obtained from the numerical model, and the deviation between them.

Table 4.4 Numerical and experimental capacities.

Validation case	Quantity compared	Experimental	SAP2000	Deviation
Bresler-Scordelis single-span beam	Ultimate load	467 kN	480 kN	+2.8%
Duddeck-Mueller two-span beam	Ultimate load	32.0 kN	32.4 kN	+1.3%
Xiao one-story frame, specimen FRAC-0	Maximum lateral load	95.2 kN	91.8 kN	−3.6%

Three observations emerge from this consolidated view. First, the capacity predicted by SAP2000 is within 3.6 percent of the reported experimental value in all three specimens. This level of agreement is acceptable for capacity assessment purposes. Second, the numerical models systematically overestimate the initial stiffness. This trend is consistent across all three benchmarks and stems from the initial-stiffness formulation

of the plastic hinges. Third, the plastic hinges form in the model at the locations at which each specimen was reported to fail; the sequence in which they form is not compared against the test records and is not claimed here.

These findings have direct implications for the SMRF study. The pushover analysis of the prototypes targets the yielding branch, the post-yield stiffness, and the ultimate capacity of the frame, which SAP2000 captures with acceptable accuracy according to the validation results. The overestimation of the initial stiffness observed in the benchmarks would, if present in the prototypes, raise the effective stiffness K_e and lower the yield displacement $\Delta_y = V_y / K_e$. The stiffness of the prototype models is, however, set explicitly by the effective-stiffness factors of ASCE 41-17 Table 10-5 (Section 5.7.1), so the bias identified here is confined to the pre-yield branch and is not quantified for the prototypes; it is retained as a limitation on the precision of the reported values.

4.7 Chapter Summary

This chapter established the numerical credibility of the SAP2000 pushover framework adopted throughout the thesis. Three independent experimental benchmarks were reproduced: the single-span beam of Bresler and Scordelis, which fails in a brittle flexure-compression mode, the two-span continuous beam of Duddeck and Mueller, and the one-story reinforced concrete frame of Xiao et al. The two beam benchmarks produced ultimate load predictions within three percent of the experimental values. For the one-story frame the numerical and measured responses agree up to a lateral load of approximately 20 kN, which the source identifies as the cracking load of the specimen rather than as first yielding. Beyond cracking the model is stiffer than the test, yet at the last computed step it reaches 91.8 kN against the reported maximum load of 95.2 kN, a difference of 3.6 percent. The frame benchmark therefore supports the pre-cracking stiffness and the maximum capacity, and does not support the stiffness of the cracked range.

The validation exercise supports the lumped-plasticity formulation and the displacement-controlled solution scheme in SAP2000 for the pushover analysis presented in the following chapters.

The first two benchmarks are monotonic tests. The third is a low-frequency cyclic test, and the comparison in Section 4.5.3 is made against its skeleton curve. The three benchmarks therefore compare monotonic or backbone load-deflection response and the

associated cracking, yield and maximum capacities. They do not address the phenomena that a cyclic protocol is required to reproduce: the progressive loss of strength and stiffness under repeated cycles at a given deformation, low-cycle fatigue of the longitudinal reinforcement, and shear-controlled failure, which the lumped flexural hinge formulation adopted here cannot represent in any case. In particular they do not validate the plastic rotation capacities on which the Collapse-Prevention criterion of Method C rests, because ASCE 41-17 Section 7.6.1 requires the modelling parameters and acceptance criteria of a component to be established from cyclic loading protocols and permits monotonic tests only to supplement them (ASCE, 2017). The validation therefore supports the use of the model for deterministic pushover assessment of strength and global response; the deformation-capacity limits that govern the Collapse-Prevention criterion are taken from the adopted acceptance framework rather than validated experimentally here, and independent verification of those limits is identified as future work.

Chapter 5 builds on these findings by defining the material properties, the effective stiffness and the ASCE 41-17 hinge parameters of the prototypes, the analytical framework for the ductility factor and the overstrength factor, and the nonlinear models used to estimate the response modification factor.

CHAPTER 5 SPECIAL MOMENT RESISTING FRAME MODELING AND NONLINEAR ANALYSIS

5.1 Introduction

This chapter presents the analytical framework and the numerical modeling procedure used to estimate the response modification factor of the prototype Special Moment Resisting Frames. Chapter 4 showed that the lumped-plasticity pushover procedure in SAP2000 reproduces the measured nonlinear response of reinforced concrete members with acceptable accuracy. This chapter applies that procedure to the prototypes described in Chapter 3. It defines the material properties of the nonlinear models and the plastic hinge acceptance criteria, the components of the response modification factor and the three definitions of the maximum displacement, the bilinear idealization and the effective stiffness, the reinforcement detailing of all models, and the modeling decisions adopted for the nonlinear static analysis.

5.2 Prototype Geometry

Three prototype frames of four, six, and fifteen stories share the same plan and differ in height and member sizing. The plan has four 6.0 m bays in one direction and three 6.0 m bays in the other, giving overall plan dimensions of 24 m by 18 m. The beams are 500 mm wide and 450 mm deep in the four- and fifteen-story frames and 500 mm wide and 550 mm deep in the six-story frame. The columns range from 500 mm square in the low-rise frames to 1000 mm square at the base of the fifteen-story frame. Four variants of the fifteen-story frame (Models 4 to 7, Section 3.8) complete the family of seven models. The three-dimensional model of the reference frame is shown in Figure 5.1.

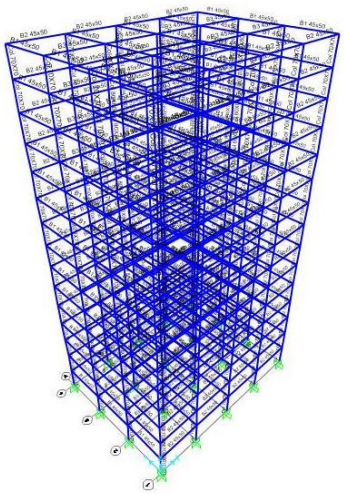

Figure 5.1 Fifteen-story reference model (SAP2000).

5.3 Material Properties of the Nonlinear Model

The nonlinear models in SAP2000 use expected material properties, as ASCE 41-17 Section 10.2 provides for nonlinear assessment (ASCE, 2017), whereas the ETABS design models use the nominal properties of Section 3.3. Table 5.2 lists the two sets together.

The expected compressive strength of the concrete is 35 MPa, slightly below the value $1.50 \times 24 = 36$ MPa given by ASCE 41-17 Table 10-1. The expected yield strength of the reinforcement is $f_{yE} = 455.05$ MPa, the value assigned to ASTM A615 Grade 60 bars in the material library of ETABS and SAP2000. It is lower than $1.25\, f_y$ of Table 10-1 and is a declared departure; its effect is a lower yield base shear and therefore a lower, conservative overstrength factor (inference, not quantified). The same values are used in every model.

Confinement enters the column hinges through the transverse reinforcement ratio ρ_t of ASCE 41-17 Table 10-8 (Section 5.3.1); confined concrete is not modeled as a separate material in the hinges. The confined-concrete model of Mander, Priestley and Park (1988) is used only to define the concrete strength of Model 4. In that model the compressive stress of confined concrete is (Mander et al., 1988)

$$f_c = f'_{cc}\, x\, r / (r - 1 + x^r) \tag{5.1}$$

where f'_{cc} is the confined strength, $x = \varepsilon_c / \varepsilon_{cc}$ is the strain normalized by the strain at peak stress, and $r = E_c / (E_c - E_{sec})$ (Mander et al., 1988). The SAP2000 parametric Mander material returns, for a representative column, a confined strength of 35 MPa at 75 mm hoop spacing and 29 MPa at 100 mm (Table 5.1, Figure 5.2; derivation in Appendix B). The second value is the concrete strength of Model 4, which therefore differs from the reference frame in two parameters at once, ρ_t and the concrete strength, and its result is interpreted as their combined effect (Section 3.8).

Table 5.1 Confined-concrete parameters of a representative column.

Parameter	75 mm	100 mm	Change
Confined strength, f'cc (MPa)	35.0	29.0	−17.1%
Confinement ratio, f'cc/f'c	1.458	1.208	—
Peak strain, ε_{cc}	0.00658	0.00408	−38.0%
Ultimate strain, ε_{cu}	0.01738	0.01611	−7.3%

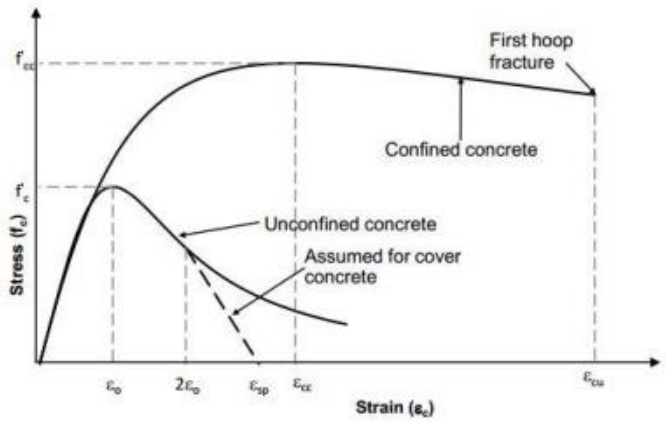

Figure 5.2 Confined and unconfined concrete (after Mander et al., 1988).

Table 5.2 Material properties of the design and nonlinear models.

Property	**Design models (ETABS)**	**Nonlinear models (SAP2000)**	**Source**
Concrete strength	f'_c = 24 MPa	f'_{cE} = 35 MPa (29 MPa in Model 4)	Section 3.3; ASCE 41-17 Table 10-1 (1.50 f'_c = 36 MPa)
Concrete modulus, E_c	23,270 MPa	23,025 MPa	ACI 318-19 Section 19.2.2 (4700 √24 = 23,025 MPa)
Reinforcement yield strength	f_y = 420 MPa	f_{yE} = 455.05 MPa	Program library, A615 Grade 60; ASCE 41-17 Table 10-1 gives 1.25 f_y
Reinforcement modulus, E_s	200,000 MPa	200,000 MPa	
Section stiffness	ACI 318-19 Section 6.6.3.1	ASCE 41-17 Table 10-5	Section 5.7.1

5.3.1 Acceptance criteria for plastic hinges

The three performance levels used in this study, Immediate Occupancy, Life Safety and Collapse Prevention, are those of ASCE 41-17 (ASCE, 2017). The modeling parameters and the acceptance criteria of the plastic hinges are those of ASCE 41-17 Table 10-7 for beams and Table 10-8 for columns.

ASCE 41-17 describes every plastic hinge by the generalized backbone of its Figure 10-1, reproduced in Figure 5.3. The hinge is elastic up to the effective yield point B; it then hardens slightly up to the peak C, loses strength suddenly to D, carries a residual strength up to E, and fails beyond E. The three modeling parameters are plastic rotations and a strength ratio: a is the plastic rotation from B to C, b is the plastic rotation from B

to E, and c is the residual strength ratio. Tables 10-7 and 10-8 give a, b and c, and the acceptance criteria IO, LS and CP, for each component.

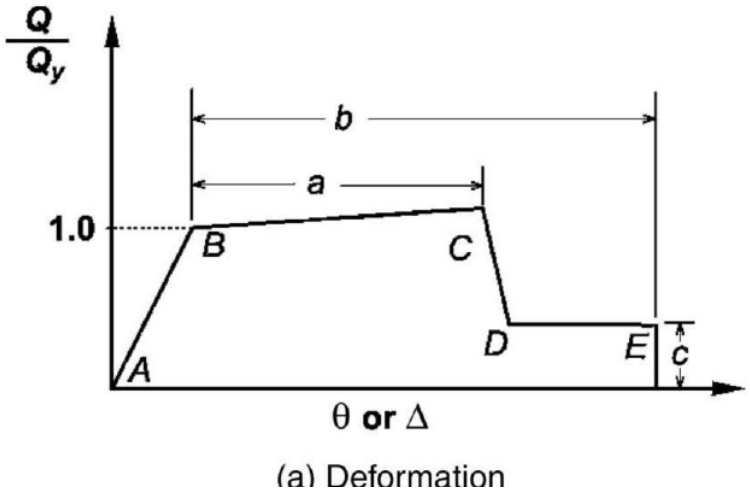

Figure 5.3 Generalized force-deformation relation (ASCE 41-17, Figure 10-1a).

For the beams, Table 10-7 is divided into four conditions according to what controls the failure of the beam: Condition i, flexure; ii, shear; iii, inadequate development or splicing; iv, inadequate embedment into the joint. The beams of this study fall under Condition i: they are flexure-controlled, their stirrups are conforming ($s \leq d/3$, and the stirrups resist at least three quarters of the design shear), and the shear stress ratio $V / (b_w\, d\, \sqrt{f'_{cE}})$ is between 0.12 and 0.16, below the limit of 0.25 that separates the rows of the table. Within Condition i, a, b and the Collapse-Prevention rotation depend on the ratio $(\rho - \rho') / \rho_{bal}$, which is computed for each beam section and each sign of moment with $\rho_{bal} = 0.0297$ from the expected material properties, and interpolated linearly between the rows $(\rho - \rho') / \rho_{bal} \leq 0$ and ≥ 0.5 of the table. For a beam in the first row, a = 0.025 rad, b = 0.05 rad and CP = 0.05 rad. The Collapse-Prevention rotations of the beams of this study lie between 0.047 and 0.050 rad (Table 5.6).

For the columns, Table 10-8 (Figure 5.6d) defines the modeling parameter b in terms of the axial load ratio and the transverse reinforcement ratio, for columns not controlled by inadequate development or splicing:

$$b = 0.5 / [\, 5 + (N_{UD} / (0.8\, A_g\, f'_{cE}))\, (1 / \rho_t)\, (f'_{cE} / f_{ytE})\,] - 0.01 \qquad (5.2)$$

where N_{UD} is the axial force of the column, A_g the gross area of the section, and $\rho_t = A_v / (b\, s)$ the transverse reinforcement ratio of the section (ASCE 41-17, Table 10-8). The axial load ratio is taken as not less than 0.1 (Table 10-8, note b), and the Collapse-Prevention plastic rotation of a column hinge is 0.7 b. Table 10-8 defines N_{UD} as the

maximum compressive axial load including the effects of lateral forces; this study uses the axial load of the gravity load case of Section 5.7.3, which is a declared departure (Section 6.10). Because ρ_t and N_{UD} differ from section to section and from story to story, every column hinge carries its own limit; the ρ_t values of all sections are listed in Tables 5.3 to 5.5.

The plastic rotation demand of each hinge is compared with its own Collapse-Prevention limit at every saved step of the pushover analysis. For a column hinge the demand is the resultant of the plastic rotations about the two principal axes, $\sqrt{(\theta_{p2}^2 + \theta_{p3}^2)}$; for a beam hinge it is the plastic rotation θ_{p3}, compared with the limit of the corresponding sign of moment. The ratio of demand to limit is the demand-capacity ratio D/C of the hinge, which is used to define Method C in Section 5.4.3.

5.4 Components of the Response Modification Factor

Following ATC-19 (ATC, 1995) and Uang (1991), R is the product of the ductility reduction factor and the overstrength factor, $R = R\mu \times \Omega$.

5.4.1 Ductility and ductility reduction factor

The displacement ductility is $\mu = \Delta u/\Delta y$. The ductility reduction factor follows Newmark and Hall *(1982)*: for T > 0.5 s, the equal-displacement rule gives $R\mu = \mu$; for T ≤ 0.5 s, the equal-energy rule gives $R\mu = \sqrt{(2\mu - 1)}$. No frame analyzed in this study falls on the equal-energy branch; all of them use the equal-displacement rule. The displacement ductility and its reduction factor are illustrated in Figure 5.4.

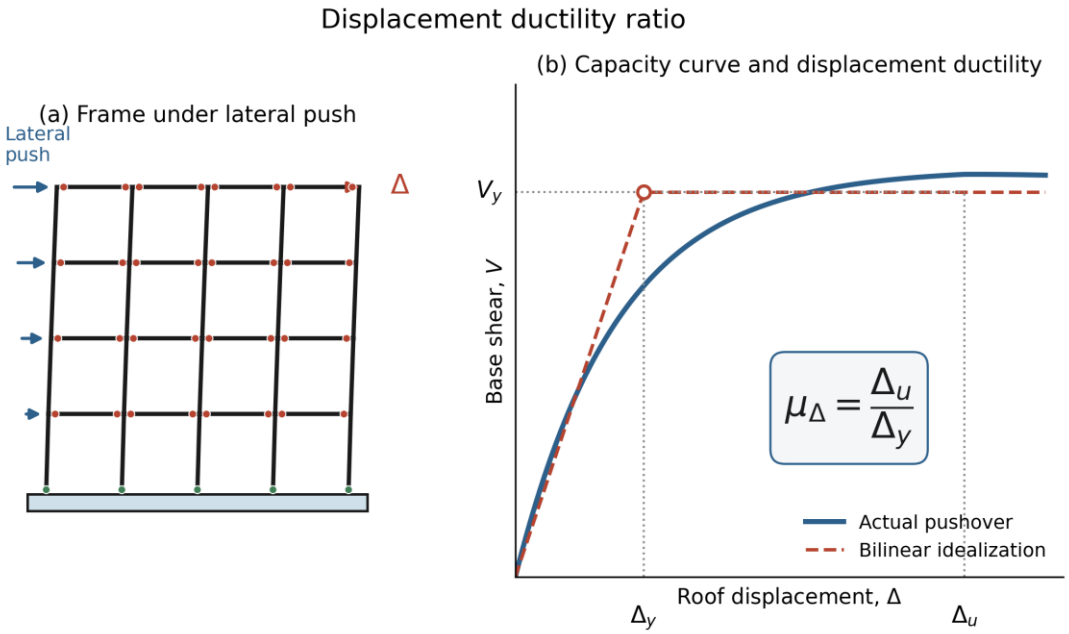

Figure 5.4 Displacement ductility ratio.

5.4.2 Overstrength factor

The overstrength factor is $\Omega = V_y / V_d$, the ratio of the effective yield base shear of the bilinear idealization to the design base shear. Its margin above unity reflects the combined effect of member sizing for drift and for the strong-column weak-beam requirement, the minimum reinforcement and detailing required for special moment frames by ACI 318-19, the strength reduction factors of design, and the expected material strengths of Section 5.3, without any single source being isolated in this study. Because V_y is obtained by the equal-area construction up to the maximum displacement of Method C (Section 5.5), the value of Ω depends on that anchor displacement. The decomposition of the overstrength factor is shown in Figure 5.5.

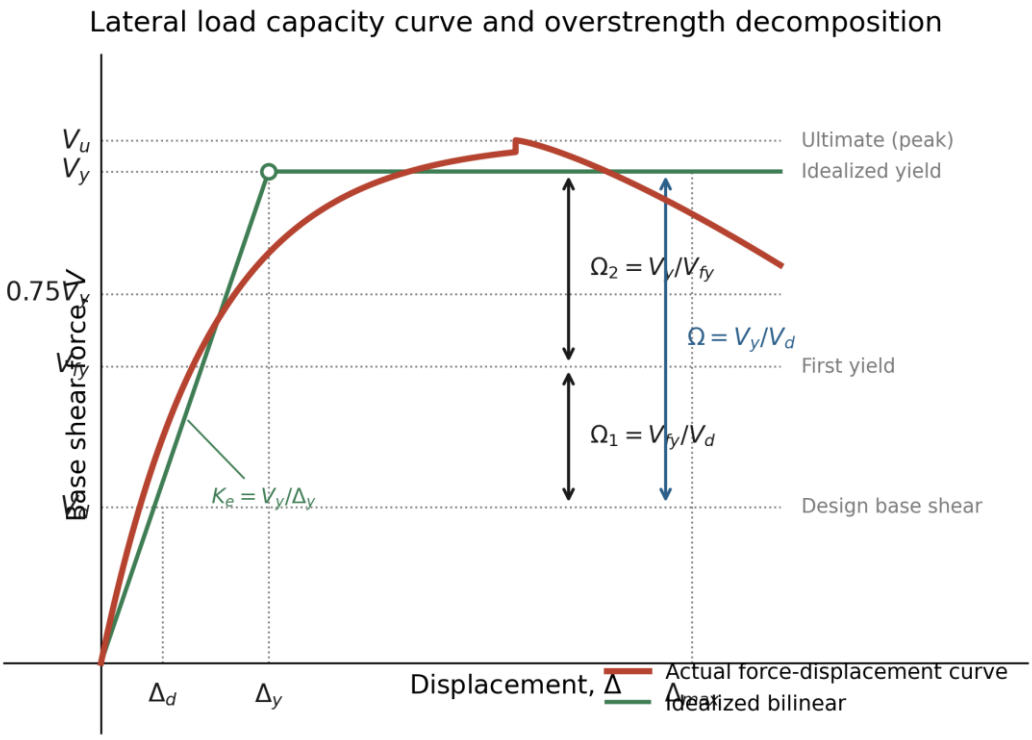

Figure 5.5 Overstrength factor on the capacity curve.

5.4.3 Definition of the Maximum Displacement: Three Methods

The two quantities R_μ and Ω are common to every estimation in this study. The three methods differ only in how the maximum displacement Δ_{max}, and therefore the ductility ratio $\mu = \Delta_{max} / \Delta_y$, is defined. Each definition is taken from a code or standard and is stated below together with its source. Methods A and B define the maximum displacement as a displacement demand, and Method C defines it as a displacement capacity.

Method A: code-amplified displacement (ASCE 7-16). The maximum displacement is the design-level elastic roof displacement amplified by the deflection amplification factor of the code. ASCE 7-16 Section 12.8.6, Equation 12.8-15, defines the amplified displacement as

$$\delta_x = C_d \, \delta_{xe} / I_e \qquad (12.8\text{-}15)$$

where C_d is the deflection amplification factor of Table 12.2-1, δ_{xe} is the elastic displacement from the analysis, and I_e is the importance factor of Section 11.5.1. For a special reinforced concrete moment frame Table 12.2-1 gives $C_d = 5.5$, and the prototype uses $I_e = 1.25$. The maximum displacement is therefore $\Delta_{max,A} = C_d \, \Delta_d / I_e$, where Δ_d is the elastic roof displacement of the ETABS design model under the design lateral forces.

The importance factor appears in both the design base shear and the elastic displacement, which is proportional to that shear; the division by I_e in Equation 12.8-15 removes it from the displacement, consistently with the strength side of the estimation. This follows the deflection-amplification concept that Uang (1991) established together with the R factor.

For structures assigned to Seismic Design Category C, D, E, or F that have horizontal irregularity Type 1a or 1b of Table 12.3-1, the design story drift, Δ, shall be computed as the largest difference of the deflections of vertically aligned points at the top and bottom of the story under consideration along any of the edges of the structure.

The deflection at level x (δ_x) (in. or mm) used to compute the design story drift, Δ, shall be determined in accordance with the following equation:

$$\delta_x = \frac{C_d \delta_{xe}}{I_e} \qquad (12.8\text{-}15)$$

where

C_d = deflection amplification factor in Table 12.2-1;
δ_{xe} = deflection at the location required by this section determined by an elastic analysis; and
I_e = Importance Factor determined in accordance with Section 11.5.1.

Figure 5.6a ASCE 7-16 Equation 12.8-15 (Method A).

Method B: FEMA 356 target displacement. The maximum displacement is the target roof displacement of the nonlinear static procedure. FEMA 356 Section 3.3.3.3.2, Equation 3-15, defines the target displacement as

$$\delta_t = C_0 \, C_1 \, C_2 \, C_3 \, S_a \, (T_e^2 / 4\pi^2) \, g \qquad (3\text{-}15)$$

in which C_0 relates the spectral displacement of the equivalent single-degree-of-freedom system to the roof displacement of the building, C_1 relates the expected inelastic displacement to the elastic displacement, C_2 accounts for pinched hysteresis and stiffness and strength degradation, C_3 accounts for P-Δ effects, S_a is the spectral acceleration at the effective period T_e, and g is the acceleration of gravity. The ductility is computed as $\mu = \delta_t / \Delta_y$. The values of the coefficients are set out in Chapter 6 and Appendix D.

3.3.3.3.2 Target Displacement

The target displacement, δ_t, at each floor level shall be calculated in accordance with Equation (3-15) and as specified in Section 3.3.3.3.1.

$$\delta_t = C_0 C_1 C_2 C_3 S_a \frac{T_e^2}{4\pi^2} g \qquad (3\text{-}15)$$

Figure 5.6b FEMA 356 Equation 3-15 (Method B).

Method C: Collapse-Prevention displacement capacity (ASCE 41-17). The maximum displacement is a displacement capacity rather than a demand. ASCE 41-17 Section 7.5.3.2.2 requires, for the nonlinear static procedure, that the deformation demands of deformation-controlled actions do not exceed the acceptance criteria of the selected performance level. The building therefore satisfies the Collapse-Prevention level up to the roof displacement at which the first deformation-controlled component reaches its Collapse-Prevention acceptance criterion, and no longer beyond it. That roof displacement is taken as the maximum displacement of Method C:

$$\Delta_{max,C} = \text{roof displacement at which max (D/C) over all hinges} = 1.0 \qquad (5.3)$$

where D/C is the demand-capacity ratio of each hinge defined in Section 5.3.1. Since the pushover output is available at discrete steps, $\Delta_{max,C}$ is obtained by linear interpolation of the maximum D/C between the last step below unity and the first step at or above it. The Collapse-Prevention limits are those of ASCE 41-17 Table 10-7 for beams and Table 10-8 for columns, so the definition contains no parameter chosen by this study. The sensitivity of the result to a global criterion based on a fraction of the hinge population, as used in parts of the literature, is examined in Chapter 6.

Table 10-7. Modeling Parameters and Numerical Acceptance Criteria for Nonlinear Procedures—Reinforced Concrete Beams

			Modeling Parameters[a]			Acceptance Criteria[a]		
						Plastic Rotation Angle (radians)		
			Plastic Rotation Angle (radians)		Residual Strength Ratio	Performance Level		
Conditions			*a*	*b*	*c*	IO	LS	CP
Condition i. Beams controlled by flexure[b]								
$\frac{\rho - \rho'}{\rho_{bal}}$	Transverse reinforcement[c]	$\frac{V^d}{b_w d\sqrt{f'_{ce}}}$						
≤0.0	C	≤3 (0.25)	0.025	0.05	0.2	0.010	0.025	0.05
≤0.0	C	≥6 (0.5)	0.02	0.04	0.2	0.005	0.02	0.04
≥0.5	C	≤3 (0.25)	0.02	0.03	0.2	0.005	0.02	0.03
≥0.5	C	≥6 (0.5)	0.015	0.02	0.2	0.005	0.015	0.02
≤0.0	NC	≤3 (0.25)	0.02	0.03	0.2	0.005	0.02	0.03
≤0.0	NC	≥6 (0.5)	0.01	0.015	0.2	0.0015	0.01	0.015
≥0.5	NC	≤3 (0.25)	0.01	0.015	0.2	0.005	0.01	0.015
≥0.5	NC	≥6 (0.5)	0.005	0.01	0.2	0.0015	0.005	0.01
Condition ii. Beams controlled by shear[b]								
Stirrup spacing ≤ *d*/2			0.0030	0.02	0.2	0.0015	0.01	0.02
Stirrup spacing > *d*/2			0.0030	0.01	0.2	0.0015	0.005	0.01
Condition iii. Beams controlled by inadequate development or splicing along the span[b]								
Stirrup spacing ≤ *d*/2			0.0030	0.02	0.0	0.0015	0.01	0.02
Stirrup spacing > *d*/2			0.0030	0.01	0.0	0.0015	0.005	0.01
Condition iv. Beams controlled by inadequate embedment into beam–column joint[b]			0.015	0.03	0.2	0.01	0.02	0.03

Note: f'_{ce} in lb/in.^{2} (MPa) units.
[a] Values between those listed in the table should be determined by linear interpolation.
[b] Where more than one of conditions i, ii, iii, and iv occur for a given component, use the minimum appropriate numerical value from the table.
[c] "C" and "NC" are abbreviations for conforming and nonconforming transverse reinforcement, respectively. Transverse reinforcement is conforming if, within the flexural plastic hinge region, hoops are spaced at ≤ *d*/3, and if, for components of moderate and high ductility demand, the strength provided by the hoops (V_s) is at least 3/4 of the design shear. Otherwise, the transverse reinforcement is considered nonconforming.
[d] *V* is the design shear force from NSP or NDP.

STANDARD ASCE/SEI 41-17

Figure 5.6c ASCE 41-17 Table 10-7, beams (Method C).

Table 10-8. Modeling Parameters and Numerical Acceptance Criteria for Nonlinear Procedures—Reinforced Concrete Columns Other Than Circular with Spiral Reinforcement or Seismic Hoops as Defined in ACI 318

Modeling Parameters	Acceptance Criteria		
	Plastic Rotation Angle (radians)		
	Performance Level		
Plastic Rotation Angles, *a* and *b* (radians) Residual Strength Ratio, *c*	IO	LS	CP
Columns not controlled by inadequate development or splicing along the clear height[a]			
$a = \left(0.042 - 0.043\frac{N_{UD}}{A_g f'_{cE}} + 0.63\rho_t - 0.023\frac{V_{yE}}{V_{ColOE}}\right) \geq 0.0$	0.15 *a* ≤ 0.005	0.5 b^b	0.7 b^b
$For\ \frac{N_{UD}}{A_g f'_{cE}} \leq 0.5\left\{ b = \frac{0.5}{5 + \frac{N_{UD}}{0.8A_g f'_{cE}}\frac{1}{\rho_t}\frac{f'_{cE}}{f_{ytE}}} - 0.01 \geq a^a \right.$			
$c = 0.24 - 0.4\frac{N_{UD}}{A_g f'_{cE}} \geq 0.0$			
Columns controlled by inadequate development or splicing along the clear height[c]			
$a = \left(\frac{1}{8}\frac{\rho_t f_{ytE}}{\rho_t f_{ytE}}\right) \geq 0.0$ $\leq 0.025^d$	0.0	0.5 *b*	0.7 *b*
$b = \left(0.012 - 0.085\frac{N_{UD}}{A_g f'_{cE}} + 12\rho_t{}^e\right) \geq 0.0$ $\geq a$ ≤ 0.06			
$c = 0.15 + 36\rho_t \leq 0.4$			

Figure 5.6d ASCE 41-17 Table 10-8, columns (Method C).

Reporting R under the three definitions tests the sensitivity of the result to the choice of maximum displacement. Because Methods A and B evaluate μ against a displacement demand, they give a demand-consistent R, whereas Method C gives a capacity-based value. The three results are compared model by model in Chapter 6.

The distinction carries a further implication. In its equivalent lateral force procedure, ASCE 7-16 estimates the maximum inelastic displacement by amplifying the elastic displacement through Equation 12.8-15 (ASCE, 2016), and it uses that amplified

displacement to verify the story-drift limits of Section 12.12.1 and the P-Δ provisions of Section 12.8.7. The code does not employ pushover analysis for design. Pushover analysis is a nonlinear assessment procedure defined in ASCE 41-17 and FEMA 356 (ASCE, 2017; FEMA, 2000). Method A therefore reproduces the code's own design displacement, obtained from a linear-elastic model, whereas Methods B and C draw on the nonlinear static procedure for the displacement demand and the displacement capacity, respectively.

5.5 Performance Levels and Bilinear Idealization

The capacity curve is interpreted through the ASCE 41-17 performance levels of Immediate Occupancy, Life Safety, and Collapse Prevention. The curve is idealized as a bilinear system by the equal-area procedure of FEMA 356 Section 3.3.3.2.4 (FEMA, 2000), up to the anchor point (Δ_u, V_u), where Δ_u is the maximum displacement of the method considered (Section 5.4.3) and V_u is the base shear of the actual curve at that displacement. The elastic branch has the effective stiffness K_e of Section 5.5.1, the post-yield branch passes through the anchor point, and the yield point is located so that the areas under the actual curve and under the bilinear curve are equal up to Δ_u. The construction is not elastic-perfectly-plastic: the post-yield branch carries the slope between the yield point and the anchor point. The secant-stiffness and equal-area idealizations are shown in Figures 5.7 and 5.8, respectively; Figure 5.8 is drawn on the actual curve of the four-story frame.

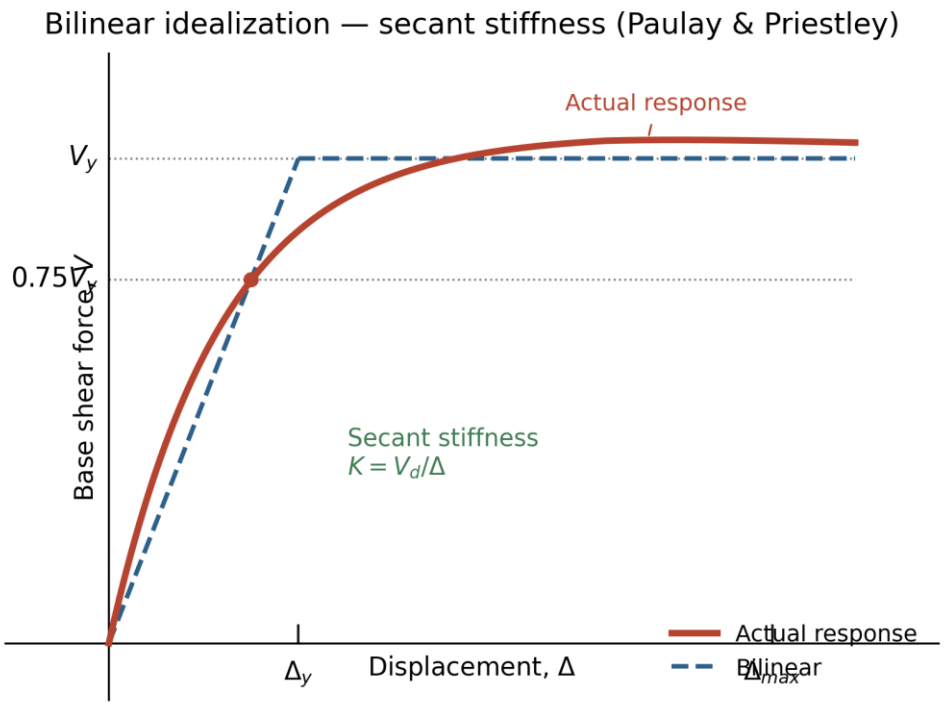

Figure 5.7 Secant-stiffness bilinear idealization (Paulay and Priestley, 1992).

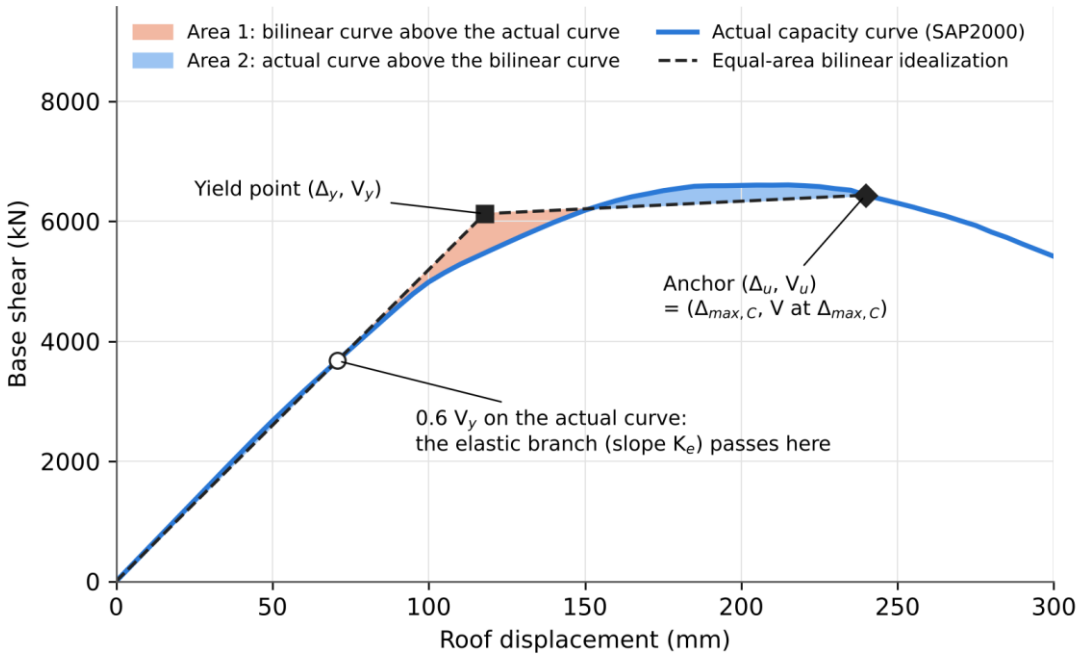

Figure 5.8 Equal-area rule on the capacity curve of the four-story frame.

Note. Area 1 = Area 2 = 20,466 kN·mm.

The construction requires that the anchor displacement lie beyond the yield displacement, $\Delta_y < \Delta_u$. This condition is checked for every model in Chapter 6 and is satisfied in all of them.

5.5.1 Effective Stiffness K_e

The yield displacement common to all three methods is $\Delta_y = V_y / K_e$, where K_e is the effective lateral stiffness. Following FEMA 356 Section 3.3.3.2.4 and Figure 3-1 (FEMA, 2000), K_e is the secant stiffness from the origin to the point on the actual capacity curve at a base shear of 0.6 V_y. Since V_y depends on K_e through the equal-area condition, the two are found together by iteration until K_e no longer changes. The same definition is used for all seven models. The construction is illustrated in Figure 5.9.

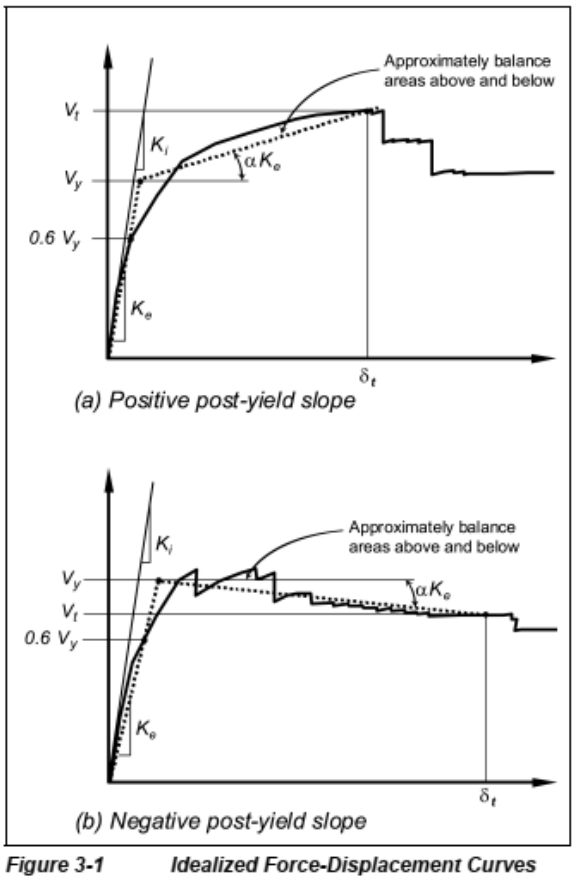

Figure 5.9 Effective stiffness and bilinear idealization (FEMA 356, Figure 3-1).

5.6 Reinforcement Detailing of the Prototype Models

This section documents the column and beam reinforcement of all seven models, as designed in ETABS to ACI 318-19 and transferred to SAP2000. The column hoops satisfy ACI 318-19 Section 18.7.5. Where $P_u > 0.3\ A_g\ f'_c$, Section 18.7.5.2(f) requires every longitudinal bar around the perimeter to be laterally supported by a corner of a hoop or a crosstie, so the number of hoop legs in each direction equals the number of bars on that face. The hoop diameter is Ø10, with Ø12 in the six-story frame, and the spacing is

70 or 75 mm, set for each section so that the area required by Table 18.7.5.4 is provided. The clear cover is 40 mm. The transverse reinforcement ratio of each section, $\rho_t = A_v / (b\,s)$, with A_v taken in the direction with fewer legs, enters the column hinges through Table 10-8. The beam stirrups are two-leg Ø10 at 90 mm in the four-story frame and at 75 mm in the six- and fifteen-story frames within the hinge regions, satisfying ACI 318-19 Section 18.6.4. Strong-column weak-beam ratios were checked with the provided reinforcement; the upper-story columns of the four- and six-story frames and the roof columns of the fifteen-story frames were reinforced beyond the strength demand for that reason (Tables 5.3 to 5.5).

5.6.1 Four-story and six-story models

Table 5.3 Reinforcement of the four- and six-story frames.

Model	Member	Location	Size (mm)	Longitudinal bars	Hoops / stirrups	ρ_t
Four-story	Column	Stories 1 to 3	500 × 500	12Ø18 (1.22%)	Ø10, 4 × 4 legs @ 70	0.00898
	Column	Story 4	500 × 500	12Ø25 (2.36%)	Ø10, 4 × 4 legs @ 70	0.00898
	Beam B1	All stories	500 × 450	5Ø18 top / 4Ø18 bottom	Ø10, 2 legs @ 90	
	Beam B2	All stories	500 × 450	4Ø16 top / 4Ø16 bottom	Ø10, 2 legs @ 90	
	Beam B2+	Stories 1 and 2	500 × 450	5Ø16 top / 4Ø16 bottom	Ø10, 2 legs @ 90	
Six-story	Column, interior	Stories 1 to 3	600 × 600	12Ø25 (1.64%)	Ø12, 4 × 4 legs @ 75	0.01005
	Column, perimeter	Stories 1 to 3	500 × 500	10Ø18 (1.02%)	Ø12, 4 × 3 legs @ 75	0.00905
	Column	Stories 4 and 5	500 × 500	12Ø20 (1.51%)	Ø12, 4 × 4 legs @ 75	0.01206
	Column	Story 6	500 × 500	12Ø25 (2.36%)	Ø12, 4 × 4 legs @ 75	0.01206
	Beam B1R	Stories 1 to 5	500 × 550	5Ø20 top / 5Ø18 bottom	Ø10, 2 legs @ 75	
	Beam B2R	Stories 1 to 5	500 × 550	5Ø18 top / 5Ø16 bottom	Ø10, 2 legs @ 75	
	Beam BR	Story 6	500 × 550	5Ø16 top / 5Ø16 bottom	Ø10, 2 legs @ 75	

Note. In the six-story frame the interior columns of story 3 are 600 × 600 mm at four of the six interior positions. Bar percentages are $\rho = A_s / A_g$.

5.6.2 Fifteen-story reference model

The reference frame uses a graded column schedule that steps the section down with height. The six interior columns are 1000 × 1000 mm at the first story and reduce in fifty-millimetre increments to 500 × 500 mm over the top three stories; the fourteen perimeter columns follow a parallel schedule from 800 × 800 mm at the base. The axial-flexural demand-capacity ratio stays below unity at every level, the governing value being 0.99, and the longitudinal reinforcement ratio is close to one percent, the minimum permitted for special moment-frame columns by ACI 318-19 Section 18.7.4.1 (ACI, 2019). The roof columns carry 14Ø18 instead of 14Ø16 to satisfy the strong-column weak-beam ratio at the roof joints. The beams are 500 × 450 mm and are detailed in five reinforcement types; their schedule is given in Table 5.6, and the sections are shown in Figures 5.10 and 5.11.

Table 5.4 Column schedule of the fifteen-story reference frame.

Story	Interior (6)	Bars	Hoops Ø10	ρ_t	Perimeter (14)	Bars	Hoops Ø10	ρ_t
1	1000	22Ø25	7 × 6 @ 70	0.00673	800	22Ø20	6 × 7 @ 75	0.00785
2 to 3	950	20Ø25	6 × 6 @ 70	0.00709	800	22Ø20	6 × 7 @ 75	0.00785
4	900	26Ø20	7 × 8 @ 75	0.00814	750	18Ø20	6 × 5 @ 70	0.00748
5	850	24Ø20	7 × 7 @ 75	0.00862	700	20Ø18	6 × 6 @ 75	0.00898
6	800	22Ø20	6 × 7 @ 75	0.00785	650	18Ø18	6 × 5 @ 75	0.00806
7 to 8	750	18Ø20	6 × 5 @ 70	0.00748	650	18Ø18	6 × 5 @ 75	0.00806
9	700	20Ø18	6 × 6 @ 75	0.00898	600	16Ø18	5 × 5 @ 75	0.00873
10	650	18Ø18	6 × 5 @ 75	0.00806	550	16Ø16	5 × 5 @ 75	0.00952
11	600	16Ø18	5 × 5 @ 75	0.00873	550	16Ø16	5 × 5 @ 75	0.00952
12	550	16Ø16	5 × 5 @ 75	0.00952	500	14Ø16	4 × 5 @ 75	0.00838
13 to 14	500	14Ø16	4 × 5 @ 75	0.00838	500	14Ø16	4 × 5 @ 75	0.00838
15	500	14Ø18	4 × 5 @ 75	0.00838	500	14Ø18	4 × 5 @ 75	0.00838

Note. Square sections, side in mm. Hoop legs are given as the numbers in the two principal directions; ρ_t is computed with the smaller number.

5.6.3 Parametric variants of the fifteen-story frame

Table 5.5 lists the column sections of Models 4 to 7 that differ from the reference schedule; all other members are identical to the reference frame.

Table 5.5 Column sections of the parametric variants.

Model	Section (location)	Size (mm)	Bars	Hoops Ø10	ρ_t
4 (100 mm hoops, 29 MPa concrete)	All column sections	as reference	as reference	as reference, @ 100	0.00471 to 0.00714
5 (about 2% longitudinal)	Interior, story 1	1000	20Ø36 (2.04%)	6 × 6 @ 65	0.00725
	Interior, stories 2 to 3	950	24Ø32 (2.14%)	7 × 7 @ 75	0.00772
	Interior, story 4	900	20Ø32 (1.99%)	6 × 6 @ 75	0.00698
	Interior, story 5	850	18Ø32 (2.00%)	5 × 6 @ 65	0.00711
	Interior story 6; perimeter stories 1 to 3	800	16Ø32 (2.01%)	5 × 5 @ 65	0.00755
	Interior, story 11; perimeter, story 9	600	16Ø25 (2.18%)	5 × 5 @ 75	0.00873
	Interior, story 12; perimeter, stories 10 to 11	550	12Ø25 (1.95%)	4 × 4 @ 75	0.00762
	Stories 13 to 15; perimeter, story 12	500	16Ø20 (2.01%)	5 × 5 @ 75	0.01047
6 (stories 3 to 5 reduced)	Perimeter, story 3	750	20Ø20 (1.12%)	6 × 6 @ 75	0.00838
	Perimeter, story 4	700	20Ø18 (1.04%)	6 × 6 @ 75	0.00898
	Perimeter, story 5	650	18Ø18 (1.08%)	5 × 6 @ 75	0.00806
7 (stories 13 to 15 reduced)	All, stories 13 to 14	450	12Ø16 (1.19%)	4 × 4 @ 75	0.00931
	All, story 15	450	12Ø25 (2.91%)	4 × 4 @ 75	0.00931

Note. In Model 5 the 650, 700 and 750 mm sections keep their reference reinforcement.

Table 5.6 Beam schedule of the fifteen-story frames.

Type	Top	Bottom	Number of beams	M_y^+ / M_y^- (kN·m)	CP, positive moment (rad)	CP, negative moment (rad)
B1	5Ø14	5Ø14	151	132.5 / 132.5	0.0500	0.0500
B1+	5Ø16	5Ø14	74	132.5 / 171.3	0.0500	0.0492
B2	5Ø18	5Ø14	112	132.5 / 215.0	0.0500	0.0483
B2+	5Ø20	5Ø14	8	132.5 / 261.6	0.0500	0.0472
B3	6Ø20	5Ø16	120	171.3 / 309.7	0.0500	0.0470

Note. Yield moments from the SAP2000 section analysis with the expected material properties of Section 5.3 (reference frame; about 1 percent lower in Model 4). Stirrups two-leg Ø10 at 75 mm in the hinge regions. Every beam type satisfies $M_n^+ \geq 0.5\, M_n^-$ at the joint face (ACI 318-19 Section 18.6.3.2).

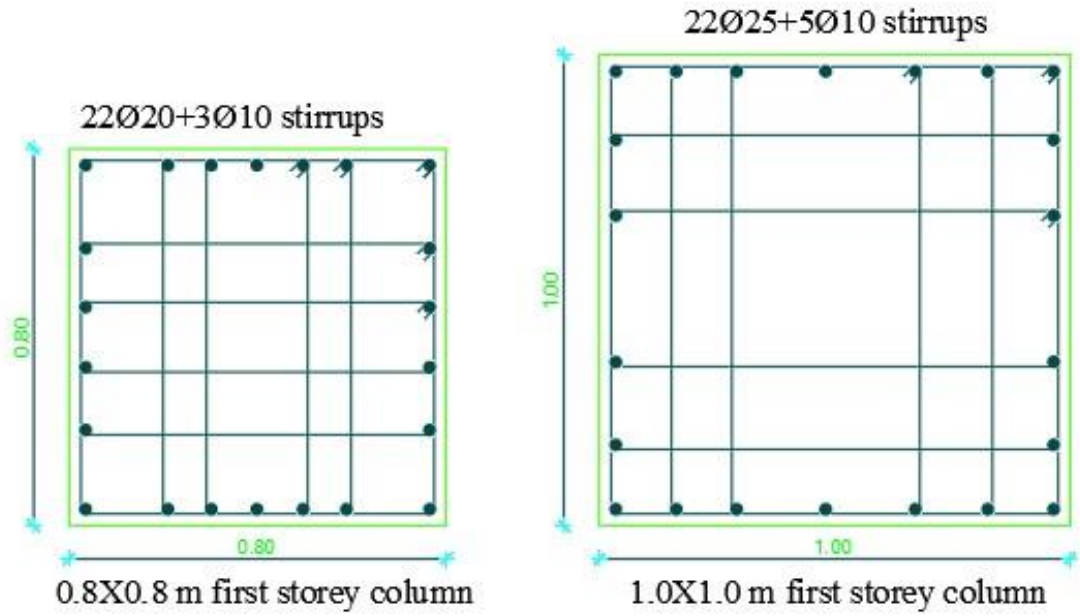

Figure 5.10 First-story column sections of the fifteen-story reference frame.

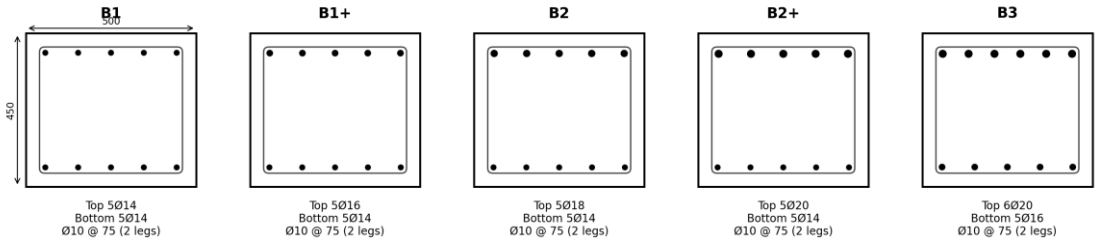

Figure 5.11 Beam sections of the fifteen-story frames.

5.7 Numerical Modeling

5.7.1 Analysis platform and design transfer

The elastic design was performed in ETABS to ACI 318-19 and ASCE 7-16, and the designed members were transferred to SAP2000 for the nonlinear static analysis. This separates the code-based design from the performance assessment. The two models differ in stiffness. The ETABS design models apply the cracked-section modifiers of ACI 318-19 Section 6.6.3.1 (0.35 I_g for beams and 0.70 I_g for columns). The SAP2000 nonlinear models apply the effective-stiffness values of ASCE 41-17 Table 10-5: 0.3 E_cI_g for beams; for columns, 0.3 E_cI_g at an axial load ratio of 0.1 or less, rising linearly to 0.7 E_cI_g at 0.5 (0.30 to 0.47 in these models); 0.4 E_cA_w for shear; and 0.25 for the flexural stiffness of the slab. The effective fundamental periods of the nonlinear models in the loading direction are 1.205 s, 1.561 s, and 3.667 s for the four-, six-, and fifteen-story frames, and between 3.667 and 3.676 s for the fifteen-story variants. As a consequence, the effective

stiffness K_e of the pushover curve is lower than the design stiffness $K_d = V_d / \Delta_d$ of the ETABS model, with K_e / K_d between 0.72 and 0.94 (Chapter 6). This difference enters Methods A and B and is discussed with the results.

5.7.2 Plastic hinge formulation

Plastic hinges are concentrated at both ends of every beam and column. The beam hinges are user-defined moment-rotation (M3) hinges, one definition for each beam section. Their yield moments M_y^+ and M_y^- are read from the SAP2000 section analysis with the expected material properties (Table 5.6), the peak point C is taken at 1.1 M_y, an assumption of this study that lies within the range of capping-to-yield moment ratios reported for reinforced concrete members by Haselton et al. (2007) and below the value of 1.2 adopted by Sattar (2018) in ASCE 41-17 assessments of reinforced concrete moment frames, and the modeling parameters a = 0.025, b = 0.05 and c = 0.2 are those of ASCE 41-17 Table 10-7 row i. The backbone is symmetric in rotation; the sign-dependent Collapse-Prevention limits of Section 5.3.1, which differ from the symmetric value by at most 6 percent, are applied when the hinge states are evaluated. The column hinges are interacting P-M2-M3 hinges generated automatically by SAP2000 to ASCE 41-17 Table 10-8, with the axial load taken from the gravity load case and the transverse reinforcement ratio ρ_t of each section; the peak point is likewise at 1.1 M_y. In the SAP2000 hinge model each backbone is defined by the five points A to E, where A is the origin, B is effective yield, C is the peak strength, D marks the onset of residual strength, and E is the final point. The base columns develop hinges as part of the expected mechanism of the frame. The hinge state at an intermediate pushover step is illustrated in Figure 5.12.

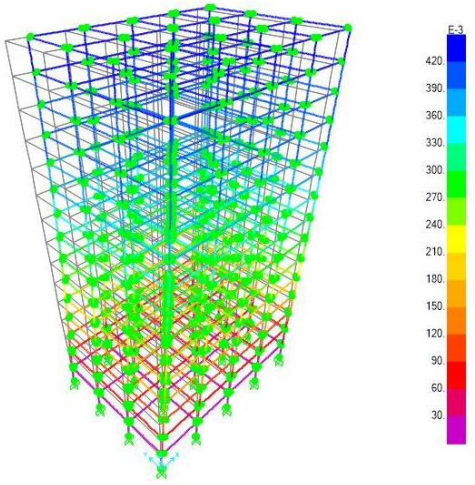

Figure 5.12 Deformed shape and plastic hinge state (SAP2000).

5.7.3 Loading protocol and second-order effects

Gravity loads were applied first as a nonlinear static case, 1.0 D + 0.25 L, to set the column axial forces; ASCE 41-17 Equation 7-1 gives 1.1 (D + 0.25 L) for the upper bound of gravity action, and the factor 1.0 is a declared simplification. The lateral load was then applied under displacement control from the end of the gravity case, with the roof displacement monitored at the center of mass of the top floor. Two lateral load patterns were analyzed for every model. The uniform pattern, with lateral forces proportional to the mass of each floor, is the second of the two patterns required by FEMA 356 Section 3.3.3.2.3 (Figure 5.14) and is the primary basis of the results. The first-mode pattern, with forces proportional to the mass times the fundamental mode shape, is the single pattern prescribed by ASCE 41-17 Section 7.4.3.2.3 (Figure 5.13), and its results are reported in Section 6.8.2. The conclusions are also stated for the lower of the two patterns in each model. Second-order (P-Δ) effects were included. The four- and six-story models were solved with the event-to-event strategy. The fifteen-story models were solved with the iterative strategy, a target roof displacement of 2.0 m and up to 100 null steps; a comparison of the two strategies on the reference frame showed base shears that agree within 0.9 to 1.4 percent over the common range of displacement. Between 100 and 200 steps were saved for each analysis.

7.4.3.2.3 Lateral Load Distribution for NSP. Lateral loads shall be applied to the mathematical model in proportion to the distribution of mass in the plane of each floor diaphragm. The vertical distribution of these forces shall be proportional to the shape of the fundamental mode in the direction under consideration.

Figure 5.13 Lateral load distribution of ASCE 41-17 Section 7.4.3.2.3.

3.3.3.2.3 Lateral Load Distribution

Lateral loads shall be applied to the mathematical model in proportion to the distribution of inertia forces in the plane of each floor diaphragm. For all analyses, at least two vertical distributions of lateral load shall be applied. One pattern shall be selected from each of the following two groups:

1. A modal pattern selected from one of the following:
   - 1.1. A vertical distribution proportional to the values of C_{vx} given in Equation (3-12). Use of this distribution shall be permitted only when more than 75% of the total mass participates in the fundamental mode in the direction under consideration, and the uniform distribution is also used.
   - 1.2. A vertical distribution proportional to the shape of the fundamental mode in the direction under consideration. Use of this distribution shall be permitted only when more than 75% of the total mass participates in this mode.
   - 1.3. A vertical distribution proportional to the story shear distribution calculated by combining modal responses from a response spectrum analysis of the building, including sufficient modes to capture at least 90% of the total building mass, and using the appropriate ground motion spectrum.This distribution shall be used when the period of the fundamental mode exceeds 1.0 second.
2. A second pattern selected from one of the following:
   - 2.1. A uniform distribution consisting of lateral forces at each level proportional to the total mass at each level.
   - 2.2. An adaptive load distribution that changes as the structure is displaced. The adaptive load distribution shall be modified from the original load distribution using a procedure that considers the properties of the yielded structure.

Figure 5.14 Lateral load distribution of FEMA 356 Section 3.3.3.2.3.

5.8 Chapter Summary

This chapter presented the analytical and numerical framework for estimating the response modification factor of the seven models. The nonlinear models use expected material properties and the effective stiffness of ASCE 41-17, with plastic hinges whose modeling parameters and Collapse-Prevention limits follow ASCE 41-17 Tables 10-7 and

10-8. The factor is decomposed into ductility and overstrength, and the maximum displacement is defined in three ways: the code-amplified displacement of ASCE 7-16, the target displacement of FEMA 356, and the Collapse-Prevention displacement capacity of ASCE 41-17. The yield point follows from the equal-area idealization with the effective stiffness of FEMA 356. The column and beam reinforcement of all models was documented in full schedules. The estimated factors and the parametric investigation follow in Chapter 6.

CHAPTER 6 ESTIMATION OF THE RESPONSE MODIFICATION FACTOR

6.1 Introduction and Decomposition Framework

This chapter estimates the response modification factor of the seven analyzed frames from their nonlinear static response and compares the estimated values with the code value of ASCE 7-16. The modeling on which it rests is described in Chapter 5, and the conclusions drawn from it are consolidated in Chapter 7. All results in Sections 6.2 to 6.6 are for the uniform lateral load pattern; the first-mode pattern is compared in Section 6.8.2.

Every quantity used in this chapter comes from one of three origins: a clause of a design or assessment standard, an output of the analysis software, or a published reference. Table 6.1 lists the notation and states that origin for each symbol.

Table 6.1 Notation and origin of each quantity.

Symbol	Meaning	Unit	Origin of the quantity
R	Response modification factor	—	ASCE 7-16 Table 12.2-1; estimated in this chapter
R_μ	Ductility reduction factor	—	Newmark and Hall (1982); Uang (1991)
Ω	Overstrength factor, V_y / V_d	—	Uang (1991); ATC-19
μ	Displacement ductility ratio, Δ_{max} / Δ_y	—	Uang (1991)
V_d	Design base shear	kN	ASCE 7-16 Section 12.8.1; ETABS output
V_y	Effective yield base shear	kN	Equal-area idealization, Equation (6.9)
V_u	Base shear at the anchor displacement	kN	SAP2000 capacity curve
Δ_d	Elastic roof displacement of the design model	mm	ETABS output, load case EQX
Δ_y	Effective yield displacement, V_y / K_e	mm	Derived
Δ_{max}	Maximum displacement, three definitions	mm	Equations (6.11), (6.12), (6.14)
Δ_u	Anchor displacement of the bilinear idealization	mm	Maximum displacement of the method considered (Section 6.3.3)
K_e	Effective lateral stiffness	kN/mm	FEMA 356 Section 3.3.3.2.4
K_d	Elastic design stiffness, V_d / Δ_d	kN/mm	Calculated from two ETABS outputs (Section 6.2)
A	Area under the actual capacity curve up to Δ_u	kN·mm	Numerical integration of the SAP2000 curve
C_d	Deflection amplification factor	—	ASCE 7-16 Table 12.2-1
I_e	Seismic importance factor	—	ASCE 7-16 Table 1.5-2
T_e	Effective fundamental period	s	SAP2000 modal analysis of the nonlinear model
$C_0 \dots C_3$	Modification coefficients of the target displacement	—	FEMA 356 Section 3.3.3.3.2
δ_t	Target displacement	mm	FEMA 356 Equation 3-15
θ_{CP}	Collapse-Prevention plastic rotation of a hinge	rad	ASCE 41-17 Tables 10-7 and 10-8
D/C	Demand-capacity ratio of a hinge, θ_p / θ_{CP}	—	Derived from SAP2000 hinge output
N	Total number of plastic hinges in the model	—	SAP2000 model

Following Uang (1991) and ATC-19, the response modification factor is decomposed into a ductility reduction factor and an overstrength factor:

$$R = R_\mu \times \Omega \tag{6.1}$$

The overstrength factor is the ratio of the effective yield base shear developed by the frame to the design base shear used in its design:

$$\Omega = Vy / V_d \tag{6.2}$$

The displacement ductility ratio and the yield displacement follow from the bilinear idealization of the capacity curve, which is constructed in Section 6.3:

$$\mu = \Delta_{max} / \Delta_y, \qquad \Delta_y = V_y / K_e \tag{6.3}$$

The ductility reduction factor is obtained from the Newmark-Hall relations (Newmark and Hall, 1982), selected on the basis of the fundamental period:

$$R_\mu = 1 \qquad \text{if } \mu \leq 1 \tag{6.4a}$$

$$R_\mu = \sqrt{(2\mu - 1)} \qquad \text{if } \mu > 1 \text{ and } T \leq 0.5 \text{ s} \tag{6.4b}$$

$$R_\mu = \mu \qquad \text{if } \mu > 1 \text{ and } T > 0.5 \text{ s} \tag{6.4c}$$

Equation (6.4a) places a floor of unity on the ductility reduction factor. A reduction factor below unity would mean that inelastic response requires greater strength than elastic response, which has no physical meaning. Where the maximum displacement falls below the yield displacement the frame does not yield under the displacement considered, the ductility contribution vanishes, and the response modification factor reduces to the overstrength factor alone. The effective period of every frame analyzed in this study exceeds $T_s = S_{D1} / S_{DS} = 0.50$ s, so Equation (6.4b) is never activated; it is stated for completeness.

6.1.1 The reduced identity and the condition for its use

Where the frame has yielded under the maximum displacement considered, the yield base shear cancels between the two factors of Equation (6.1). Substituting Equations (6.2) and (6.3) with $R_\mu = \mu$:

$$R = \mu\,\Omega = (\Delta_{max} / \Delta_y)(V_y / V_d) = (\Delta_{max}\, K_e / V_y)(V_y / V_d) = \Delta_{max}\, K_e / V_d \tag{6.5}$$

Equation (6.5) is an algebraic rearrangement of Equation (6.1) and holds only when $\mu > 1$. In this study $\mu > 1$ in every model under all three methods (Sections 6.4 to 6.6), so Equation (6.5) applies throughout and is used in this chapter as an arithmetic check. For Method A, substituting $\Delta_{max,A} = C_d\, \Delta_d / I_e$ and $K_d = V_d / \Delta_d$ gives the factor in terms of the two stiffnesses:

$$R_A = (C_d / I_e)(K_e / K_d) \tag{6.6}$$

Equation (6.6) shows what Method A measures: the code ratio $C_d / I_e = 4.40$, scaled by the ratio of the effective stiffness of the nonlinear model to the elastic stiffness of the design model. The strength of the frame does not appear in it. Since K_e / K_d is below unity in every model, R_A cannot exceed 4.40 on the basis of R / I_e, whatever the capacity of the frame. The values are given for every model in Table 6.4.

6.1.2 Source of the three definitions of the maximum displacement

Equation (6.3) requires a maximum displacement. Each of the three definitions used in this chapter is taken from a code or standard, and the clause is stated here so that no step of the derivation rests on an undeclared choice.

Method A takes the maximum displacement from the design standard. ASCE 7-16 Equation 12.8-15 defines the amplified deflection $\delta_x = C_d \delta_{xe} / I_e$ as the code estimate of the inelastic deflection at the design earthquake, and Section 12.9.1.2 applies the same factor C_d / I_e to modal response spectrum results. The same relation is stated by Ahmad et al. (2021) in their study of the seismic response parameters of reinforced concrete moment frames: the elastic deformation demand obtained under the reduced design forces is modified by the deflection amplification factor C_d to obtain the inelastic deflection demand. In their study C_d is an output, obtained from response-history analysis, whereas in Method A it is an input taken from the code; the citation supports the relation, not the method.

Method B takes the maximum displacement from an assessment standard. FEMA 356 Section 3.3.3.3.2 and Equation 3-15 define the target displacement of the nonlinear static procedure, and its modification coefficients are fixed by explicit conditions of that standard rather than chosen here (Table 6.6).

Method C takes the maximum displacement from the acceptance criteria of ASCE 41-17. Tables 10-7 and 10-8 define the plastic rotation at which a reinforced concrete beam or column reaches the Collapse-Prevention level, and Section 7.5.3.2.2 requires, for the nonlinear static procedure, that the deformation demands of deformation-controlled actions do not exceed those criteria. The roof displacement at which the first component reaches its criterion is therefore the largest displacement at which the frame satisfies Collapse Prevention under the standard. The choice of the Collapse-Prevention level is consistent with the proposal of Foutch and Wilcoski (2005), who recommend that R be

set so that buildings satisfy the Collapse-Prevention performance objective with 90 percent confidence at the 2,475-year earthquake. Their procedure is probabilistic and measures demand and capacity by story drift from response-history analysis, so the agreement with Method C is in the performance level, not in the method.

6.2 Elastic Design Quantities

The elastic design quantities were extracted from the ETABS design models with fixed bases and with the mass source defined by the dead load pattern alone, in accordance with ASCE 7-16 Section 12.7.2. Table 6.2 summarizes them for the seven models. Models 4 and 5 share the elastic design model of the reference frame, because the confinement and the longitudinal reinforcement do not change the cracked-section stiffness or the mass of the design model; Models 6 and 7 have their own design models. The derivation of the design base shear is given in Table 3.4 and Appendix A.

Table 6.2 Elastic design quantities of the seven models.

Model	**W (kN)**	**V_d (kN)**	**Δ_d (mm)**	**$K_d = V_d / \Delta_d$ (kN/mm)**	**Governing C_s**
Four-story	25,545.0	1,219.82	16.990	71.80	0.0478 (Eq. 12.8-3)
Six-story	39,747.8	1,317.71	25.555	51.56	0.0332 (Eq. 12.8-3)
Fifteen-story reference	100,171.9	2,203.78	92.554	23.81	0.0220 (Eq. 12.8-5)
Model 4	100,171.9	2,203.78	92.554	23.81	0.0220 (Eq. 12.8-5)
Model 5	100,171.9	2,203.78	92.554	23.81	0.0220 (Eq. 12.8-5)
Model 6	99,959.5	2,199.11	93.044	23.64	0.0220 (Eq. 12.8-5)
Model 7	99,984.3	2,199.65	93.502	23.53	0.0220 (Eq. 12.8-5)

The elastic design stiffness K_d in the fifth column is not read directly from ETABS. It is calculated from two ETABS outputs, the design base shear V_d and the elastic roof displacement Δ_d that this base shear produces, and it is used in Equation (6.6). For the fifteen-story models the effective seismic weight is V_d / C_s with C_s = 0.044 S_{DS} I_e = 0.0220, since the minimum coefficient governs their design (Section 3.7).

6.3 Bilinear Idealization of the Capacity Curve

The decomposition of Equation (6.1) requires a yield point, and a pushover curve of a reinforced concrete frame has no single point that is unambiguously the yield point. An idealization is therefore required. This study adopts the equal-area rule in the form given in FEMA 356 Section 3.3.3.2.4 and Figure 3-1 (FEMA, 2000): the bilinear idealization is the two-segment curve whose enclosed area equals the area under the actual capacity curve, both taken up to the same anchor displacement, with the elastic branch passing through the actual curve at 0.6 V_y.

6.3.1 The area A, and how it is obtained

The quantity A is the area under the actual capacity curve from the origin to the anchor displacement Δ_u. Its unit is kN·mm, that is, an energy: it is the work done by the lateral load on the structure in reaching that displacement. The capacity curve produced by SAP2000 is a list of analysis steps, each giving a roof displacement and the corresponding base shear. The area is obtained by summing trapezoids between consecutive steps, the final trapezoid being partial because the anchor displacement generally falls between two steps:

$$A = \Sigma\ 0.5\ (V_i + V_{i+1})(\Delta_{i+1} - \Delta_i) \tag{6.7}$$

The construction is illustrated here with Method C for the four-story frame, for which $\Delta_u = \Delta_{max,C} = 239.77$ mm (Section 6.6.3). The capacity curve was saved at 5.0 mm increments, so the sum comprises 47 full trapezoids and one partial trapezoid, and it returns A = 1,126,240 kN·mm. Figure 6.1 shows the area and the resulting idealization.

A is not a result in its own right. It is the quantity that fixes the yield point: the bilinear curve is drawn so that it encloses exactly the same area as the actual curve up to the same anchor displacement, and the yield base shear V_y that achieves this is the effective yield base shear for that displacement. Each of the three methods has its own maximum displacement (Section 6.3.3), and therefore its own A, V_y and Δ_y. Every factor of this chapter depends on A through V_y and Δ_y: the overstrength $\Omega = V_y / V_d$ directly, and the ductility ratio $\mu = \Delta_{max} / \Delta_y$ through $\Delta_y = V_y / K_e$.

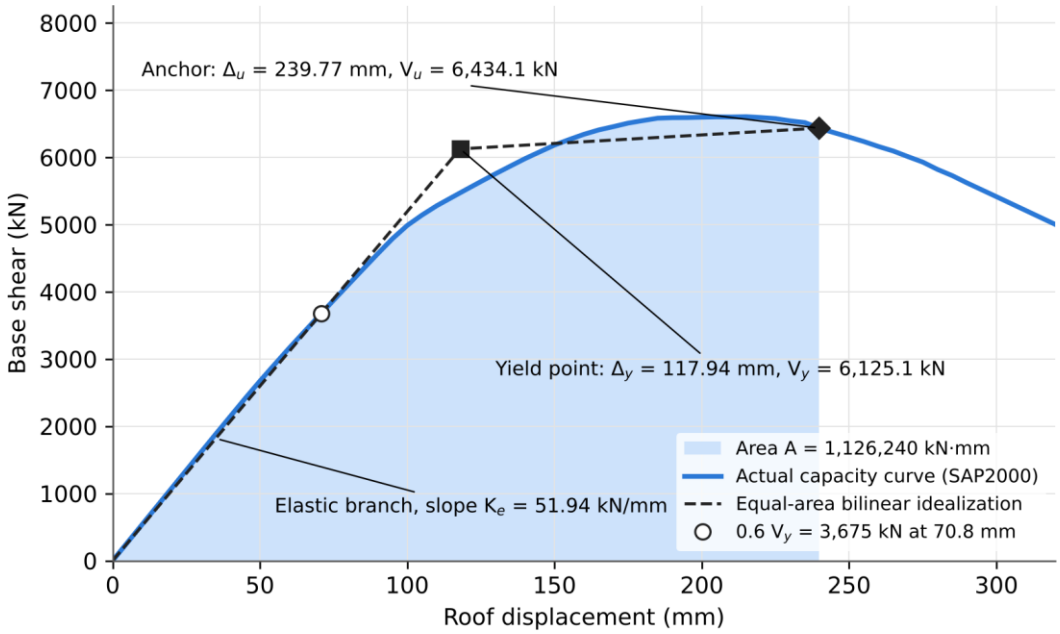

Figure 6.1 Area A and the equal-area idealization, four-story frame.

6.3.2 Derivation of the equal-area equation

The equal-area rule is the condition illustrated in Figure 5.8: the area by which the bilinear curve lies above the actual curve equals the area by which it lies below it. For the four-story frame the two areas are 20,466 kN·mm each. Stating the same condition with the total areas gives an equation that can be solved for V_y directly, without trial and error.

The bilinear idealization consists of an elastic branch of slope K_e from the origin to the yield point (Δ_y, V_y), followed by a post-yield branch from that point to the anchor (Δ_u, V_u). Its area is the sum of the elastic triangle and the post-yield trapezoid, and the equal-area condition sets that sum equal to A:

$$A = 0.5\,\Delta_y\,V_y + 0.5\,(V_y + V_u)(\Delta_u - \Delta_y) \tag{6.8}$$

Substituting $\Delta_y = V_y / K_e$ from Equation (6.3), the two terms in V_y^2 cancel, and solving for V_y gives a closed form:

$$V_y = (A - 0.5\,\Delta_u\,V_u) / (0.5\,\Delta_u - 0.5\,V_u / K_e) \tag{6.9}$$

The units are consistent: the numerator is kN·mm and the denominator is mm, so the quotient is kN. Applying Equation (6.9) to the four-story frame, with A from Section 6.3.1, V_u and Δ_u from Section 6.6.3, and K_e from Section 6.3.5:

$A = 1{,}126{,}239.5$ kN·mm

$0.5\,\Delta_u\,V_u = 0.5 \times 239.77 \times 6{,}434.1 = 771{,}343.0$ kN·mm

numerator = 354,896.5 kN·mm

$0.5\,\Delta_u - 0.5\,V_u / K_e = 119.884 - 0.5 \times 6{,}434.1 / 51.935 = 57.941$ mm

$V_y = 354{,}896.5 / 57.941 = 6{,}125.1$ kN

$\Delta_y = V_y / K_e = 6{,}125.1 / 51.935 = 117.94$ mm

$\Omega = V_y / V_d = 6{,}125.1 / 1{,}219.82 = 5.021$

The denominator is a difference of two quantities of similar size, so the intermediate values are carried to three decimal places.

6.3.3 The anchor displacement

Equation (6.9) requires an end point Δ_u. The end point determines A, and through A it determines the yield point, so the choice is stated rather than assumed. In this study the end point of each method is its own maximum displacement: $\Delta_u = \Delta_{max,A}$ for Method A, $\Delta_u = \delta_t$ for Method B, and $\Delta_u = \Delta_{max,C}$ for Method C. The idealization of each method therefore represents the capacity curve over the range of displacement that the method considers.

Each frame therefore has three effective yield points, one for each method, and each method has its own values of V_y, Δ_y, Ω and μ. They are derived method by method in Sections 6.4 to 6.6, model by model in Section 6.7, and brought together in Table 6.18.

6.3.4 Admissibility of the construction

Equation (6.9) always returns a number, but the number is a yield point only if the frame has yielded before the anchor is reached; otherwise the bilinear curve would have to bend after the end of the curve it represents. The check is therefore:

$$\Delta_y < \Delta_u \tag{6.10}$$

In words: the yield displacement must be smaller than the anchor displacement. The check is passed in all seven models under all three methods (Table 6.18): Δ_y is between 64 and 73 percent of Δ_u under Method A, between 64 and 92 percent under Method B, and between 34 and 50 percent under Method C. In the four-story frame under Method C, for example, $\Delta_y = 117.94$ mm against $\Delta_u = 239.77$ mm.

6.3.5 The effective stiffness

The effective lateral stiffness is the secant stiffness of the capacity curve at sixty percent of the effective yield base shear, following FEMA 356 Section 3.3.3.2.4 and Figure 3-1. Since the yield strength of Equation (6.9) itself depends on that stiffness, the definition is a fixed-point condition. The iteration is started at the secant stiffness of the second analysis step; each cycle evaluates Equation (6.9) and recomputes the secant stiffness at 0.6 V_y by linear interpolation on the capacity curve, and the cycle is repeated until the stiffness changes by less than 10^{-10} kN/mm. The same procedure is applied to all seven models. For the four-story frame under Method C it converges to K_e = 51.935 kN/mm, with the point 0.6 V_y reached at 70.76 mm. Under Methods A and B the point 0.6 V_y lies on the initial linear branch of the capacity curve in every model, so the iteration returns the initial stiffness, $K_e = K_i$ (53.815 kN/mm for the four-story frame).

6.4 Method A: the Code-Amplified Displacement

6.4.1 Definition

The first of the three definitions of the maximum displacement is the code estimate of the inelastic roof displacement. ASCE 7-16 Equation 12.8-15 amplifies the elastic displacement obtained from the design analysis by the deflection amplification factor and divides by the importance factor:

$$\Delta_{max,A} = C_d \, \Delta_d / I_e \tag{6.11}$$

with C_d = 5.5 from Table 12.2-1 and I_e = 1.25 from Table 1.5-2 for Risk Category III. Equation (6.11) is therefore $\Delta_{max,A} = (5.5 / 1.25) \, \Delta_d = 4.40 \, \Delta_d$: the number 4.40 that appears in Tables 6.3 and 6.4 is not a new coefficient but the ratio C_d / I_e of these two code values. The division by the importance factor is a requirement of the equation and not an option. The commentary states the reason: the design forces used to compute the elastic deflection already include the importance factor, so Equation 12.8-15 includes it in the denominator, and the purpose is that the resulting drift be compared with the more stringent drift limits that Table 12.12-1 imposes on the higher risk categories (ASCE, 2016, C12.8.6). The division is applied consistently to all seven models.

6.4.2 Numerical chain

Table 6.3 gives the derivation for the seven models. Every quantity in it is defined in Table 6.1, and the yield quantities are those of the equal-area idealization of Section 6.3 with $\Delta_u = \Delta_{max,A}$.

Table 6.3 Method A, seven models.

Quantity	Four-story	Six-story	Fifteen-story reference	Model 4	Model 5	Model 6	Model 7
Δ_d (mm), ETABS	16.990	25.555	92.554	92.554	92.554	93.044	93.502
$\Delta_{max,A} = (C_d / I_e)\,\Delta_d = 4.40\,\Delta_d$ (mm)	74.76	112.44	407.24	407.24	407.24	409.39	411.41
V_u at $\Delta_{max,A}$ (kN)	3,862.2	5,387.1	7,566.6	7,543.7	7,566.6	7,554.0	7,574.0
A up to $\Delta_{max,A}$ (kN·m)	148.2	308.4	1,640.5	1,638.3	1,640.5	1,646.7	1,657.8
K_e (kN/mm)	53.81	49.11	20.36	20.36	20.36	20.22	20.15
V_y (kN), Equation (6.9)	2,590.8	4,037.5	5,613.7	5,571.7	5,613.7	5,615.0	5,620.2
$\Delta_y = V_y / K_e$ (mm)	48.14	82.22	275.74	273.68	275.74	277.73	278.94
$\mu_A = \Delta_{max,A} / \Delta_y$	1.553	1.368	1.477	1.488	1.477	1.474	1.475
$R_\mu = \mu_A$, Equation (6.4c)	1.553	1.368	1.477	1.488	1.477	1.474	1.475
$\Omega = V_y / V_d$	2.124	3.064	2.547	2.528	2.547	2.553	2.555
$R_A = R_\mu\,\Omega$	3.30	4.19	3.76	3.76	3.76	3.76	3.77
Check: $\Delta_{max,A}\,K_e / V_d$, Eq. (6.5)	3.30	4.19	3.76	3.76	3.76	3.76	3.77

Under Method A the code-amplified displacement exceeds the effective yield displacement in every model, with μ_A between 1.37 and 1.55. Equation (6.4c) governs and R_A lies between 3.30 and 4.19, below 6.40 in every model. The reason is given by Equation (6.6) and Table 6.4. The effective stiffness of the nonlinear model is lower than the design stiffness of the ETABS model, $K_e / K_d < 1$, because the effective-stiffness factors of ASCE 41-17 Table 10-5 are lower than the cracked-section factors of ACI 318-19 Section 6.6.3.1 (Section 5.7.1). The product 4.40 (K_e / K_d) is the Method A factor itself, and it cannot reach 4.40.

Table 6.4 Method A in terms of the two stiffnesses.

Quantity	Four-story	Six-story	Fifteen-story reference	Model 4	Model 5	Model 6	Model 7
$K_d = V_d / \Delta_d$ (kN/mm)	71.80	51.56	23.81	23.81	23.81	23.64	23.53
K_e (kN/mm), Method A	53.81	49.11	20.36	20.36	20.36	20.22	20.15
K_e / K_d	0.750	0.952	0.855	0.855	0.855	0.855	0.856
$R_A = (C_d / I_e)(K_e / K_d)$	3.30	4.19	3.76	3.76	3.76	3.76	3.77

Table 6.4 is read column by column. The last row reproduces R_A of Table 6.3 by a different route, in which the yield point does not appear. In the four-story frame, for example, 4.40 × 53.81 / 71.80 = 3.30. The table shows why R_A is below 6.40 in every model: the code-amplified displacement is $C_d / I_e = 4.40$ times the elastic displacement of the design model, and the effective stiffness of the nonlinear model is 75 to 95 percent of the design stiffness, so the product stays below 4.40.

The result is a property of the adopted definition and of the stiffness assumptions of the two models, not a failure of the analysis. Method A evaluates the frames at a displacement 1.37 to 1.55 times their effective yield displacement, and it therefore mobilizes only a small part of their deformation capacity.

6.4.3 The role of the importance factor in the reported factor

The design base shear in the denominator of Ω carries the importance factor, through both $C_s = S_{D1} I_e / (T R)$ and $C_{s,min} = 0.044 S_{DS} I_e$, whereas the yield strength of the frame does not depend on the occupancy category. The factor estimated from Equation (6.1) with the design base shear of a Risk Category III structure is therefore R divided by the importance factor, not R itself. Put simply, the code asked for 25 percent more design strength because of the occupancy of the building, while the actual strength of the frame is what it is; dividing the actual strength by the increased design strength returns R / 1.25. Table 6.5 demonstrates this for the reference frame by repeating its design base shear in Risk Category II, $I_e = 1.00$, with the site, geometry, sections, reinforcement and mass unchanged, so that the capacity curve is the same.

Table 6.5 Reference frame under two risk categories.

Quantity	Risk Category III, I_e = 1.25	Risk Category II, I_e = 1.00	Changed
$C_{s,min} = 0.044 S_{DS} I_e$	0.0220	0.0176	yes
V_d (kN)	2,203.78	1,763.02	yes
Δ_d (mm), proportional to V_d	92.55	74.04	yes
$\Delta_{max,A} = C_d \Delta_d / I_e$ (mm)	407.24	407.24	no
V_y (kN), Method C	9,304.9	9,304.9	no
Ω, Method C	4.22	5.28	yes
R_A	3.76	4.70	yes
R_B	2.25	2.81	yes
R_C	12.32	15.40	yes

The amplified displacement is identical in the two columns, which confirms that the division by the importance factor performs the function the code intends: the estimated inelastic displacement of a building does not depend on what the building is used for. The estimated factors, however, change by twenty-five percent, and their ratio, 15.40 / 12.32, is exactly the importance factor. The same structure under the same ground motion cannot have two response modification factors because its occupancy changed, so the quantity that changed is not R.

Two published results bear on this point. Banerjee et al. (2023) designed reinforced concrete special moment-resisting frames for importance factors of 1.0, 1.2 and 1.5 and computed the available response reduction factor of each from incremental dynamic analysis over twenty-two ground-motion record pairs; they report that the available response reduction factor remains nearly constant even with an increase in the importance factor. Sukumar et al. (2017) designed a four-story reinforced concrete frame for importance factors from 1.0 to 2.5 and report that the overstrength factor remains between 3.76 and 4.31 across the six designs, without a considerable change. Both studies are consistent with Table 6.5: a correctly estimated factor should not move with the occupancy category.

The point also has a normative dimension. Kircher and Heintz (2008), describing the ATC-63 methodology from which the tabulated values of R in ASCE 7 were quantified, state that design for performance other than life safety was not considered by that project, and that the methodology does not address the special performance or functionality objectives of ASCE 7 for Occupancy Category III and IV structures. The prototype of this study is in Risk Category III, so its occupancy category lies outside the range for which the tabulated factor was quantified. This is a statement about the scope of that work, not a criticism of the tabulated value.

Two equivalent ways of reporting follow. The factors in this chapter are reported as computed, that is as R / I_e, and compared with the code value on the same basis, $8 / 1.25 = 6.40$. Multiplying any reported factor by 1.25 gives the value on the basis of R and the comparison value 8. Comparisons within the study are unaffected, because all seven models share the same importance factor.

6.5 Method B: the FEMA 356 Target Displacement

6.5.1 Definition

The second definition is the target displacement of the displacement coefficient method of FEMA 356 Section 3.3.3.3.2, in which the spectral displacement of an equivalent single-degree-of-freedom system at the effective fundamental period is modified by four coefficients:

$$\delta_t = C_0 \, C_1 \, C_2 \, C_3 \, S_a \, (T_e^2 / 4\pi^2) \, g \tag{6.12}$$

Three of the four coefficients are fixed by explicit conditions of the standard for the structures examined here. Only C_0 is computed. Table 6.6 states the clause that fixes each coefficient and the condition under which it applies.

Table 6.6 Basis of the coefficients of Equation (6.12).

Coefficient	Value	Clause and the condition that fixes it
C_1	1.00	FEMA 356 Section 3.3.3.3.2: $C_1 = 1.0$ for $T_e \geq T_s$. With $S_{DS} = 0.40$ g and $S_{D1} = 0.20$ g, $T_s = 0.50$ s, and the effective period of every model exceeds it.
C_2	1.00	FEMA 356 Table 3-3, Framing Type 2: the special moment frames of this study contain none of the degrading components that define Framing Type 1. The standard additionally permits $C_2 = 1.0$ for nonlinear procedures.
C_3	1.00	FEMA 356 Section 3.3.3.3.2: $C_3 = 1.0$ for structures with positive post-yield stiffness. In every model the capacity curve has a positive slope at the target displacement.
C_0	computed	FEMA 356 Table 3-2 permits a tabulated value, but the standard states that calculation from the deflected shape is preferred. $C_0 = \Gamma \, \varphi_{roof}$ was computed from the first mode of the nonlinear model in the direction of loading, Γ being the modal participation factor and φ_{roof} the mode-shape ordinate at the control node.

6.5.2 Numerical chain

The spectral acceleration is evaluated on the constant-velocity branch of the design spectrum, $S_a = S_{D1} / T_e$, which applies because the effective period of every model lies between $T_s = 0.50$ s and the long-period transition period $T_L = 4$ s. The effective period is taken from the modal analysis of the SAP2000 nonlinear model. Table 6.7 gives the chain for the seven models.

Table 6.7 Method B, seven models.

Quantity	Four-story	Six-story	Fifteen-story reference	Model 4	Model 5	Model 6	Model 7
T_e (s)	1.205	1.561	3.667	3.667	3.667	3.676	3.669
$S_a = S_{D1} / T_e$ (g)	0.1660	0.1281	0.0545	0.0545	0.0545	0.0544	0.0545
$S_d = S_a\, g\, T_e^2 / 4\pi^2$ (mm)	59.88	77.58	182.26	182.26	182.26	182.69	182.36
$C_0 = \Gamma\, \varphi_{roof}$	1.271	1.293	1.336	1.336	1.336	1.334	1.350
$\delta_t = C_0\, S_d$ (mm)	76.09	100.35	243.48	243.48	243.48	243.78	246.24
V_u at δ_t (kN)	3,924.2	4,858.0	4,940.1	4,937.0	4,940.1	4,914.7	4,944.2
A up to δ_t (kN·m)	153.4	246.4	603.3	603.2	603.3	600.6	610.7
K_e (kN/mm)	53.81	49.11	20.36	20.36	20.36	20.22	20.15
V_y (kN), Equation (6.9)	2,606.0	3,752.0	4,553.6	4,522.3	4,553.6	4,544.5	4,558.0
$\Delta_y = V_y / K_e$ (mm)	48.43	76.41	223.67	222.13	223.67	224.78	226.22
$\mu_B = \delta_t / \Delta_y$	1.571	1.313	1.089	1.096	1.089	1.085	1.089
$R_\mu = \mu_B$, Equation (6.4c)	1.571	1.313	1.089	1.096	1.089	1.085	1.089
$\Omega = V_y / V_d$	2.136	2.847	2.066	2.052	2.066	2.066	2.072
$R_B = R_\mu\, \Omega$	3.36	3.74	2.25	2.25	2.25	2.24	2.26
Check: $\delta_t K_e / V_d$, Eq. (6.5)	3.36	3.74	2.25	2.25	2.25	2.24	2.26

The rows are read in order. Method B does not compute the displacement of the building directly. It replaces the building by a single-degree-of-freedom oscillator, finds the displacement of that oscillator under the design spectrum, and converts that displacement back to a roof displacement through C_0. For the six-story frame, with g = 9,810 mm/s^2 and $4\pi^2 = 39.478$:

$S_a = 0.20 / 1.561 = 0.1281$ g

$S_d = 0.1281 \times 9{,}810 \times 1.561^2 / 39.478 = 77.58$ mm

$\delta_t = C_0\, S_d = 1.293 \times 77.58 = 100.35$ mm

A value of C_0 above unity is expected: the roof of a moment frame moves further than the equivalent oscillator that replaces it, and the values tabulated in FEMA 356 Table 3-2 are likewise greater than unity and increase with the number of stories.

6.5.3 The ductility mobilized under this method

Under Method B, μ_B lies between 1.08 and 1.57: 1.57 and 1.31 for the four- and six-story frames, and 1.08 to 1.10 for the fifteen-story models. Equation (6.4c) governs, and R_B lies between 2.24 and 3.74, below 6.40 in every model. In the fifteen-story models the capacity curve up to δ_t departs little from a straight line: Δ_y is 91 to 92 percent of δ_t,

so the idealization is close to its limit $\Delta_y = \Delta_u$ and the yield point it returns has little physical meaning. The factor is then better read from Equation (6.5), $R_B = \delta_t K_e / V_d$, which does not contain the yield point. The comparison with 6.40 does not depend on the value adopted for C_2: with $C_2 = 1.2$, the largest value of FEMA 356 Table 3-3 at Collapse Prevention, δ_t and therefore R_B would be at most 1.2 times larger, that is 4.49 for the six-story frame, which has the largest R_B.

Method B gives a smaller maximum displacement than Method A in every model except the four-story frame, where the two are within 2 percent. The two demands are not expected to coincide. Method A scales the elastic displacement of the cracked-section design model under the design forces, which are computed at the capped period $C_u T_a$ and, for the fifteen-story frame, are governed by the minimum coefficient. Method B evaluates the spectrum directly at the effective period of the nonlinear model, where the spectral acceleration S_{D1} / T_e is small for the long-period frames.

6.6 Method C: the Collapse-Prevention Displacement Capacity

The third definition measures capacity rather than demand. It asks at what roof displacement the frame ceases to satisfy the Collapse-Prevention acceptance criteria of ASCE 41-17, and it answers by comparing the plastic rotation of every hinge with its own acceptance criterion at every saved step of the analysis.

6.6.1 The hinge inventory

Plastic hinges are assigned at both ends of every frame member, so each member carries two. Table 6.8 is read from the SAP2000 frame connectivity and section tables of each model.

Table 6.8 Plastic hinge inventory.

Model	Column hinges	Beam hinges	Total, N
Four-story	160	248	408
Six-story	240	372	612
Fifteen-story (all five models)	600	930	1,530

6.6.2 Definition

For each hinge the demand-capacity ratio at a given analysis step is the ratio of its plastic rotation to its Collapse-Prevention plastic rotation from ASCE 41-17 Table 10-7 or 10-8 (Section 5.3.1):

$$D/C = \theta_p / \theta_{CP},\ \theta_p = \sqrt{(\theta_{p2}^2 + \theta_{p3}^2)} \text{ for columns},\ \theta_p = \theta_{p3} \text{ for beams} \quad (6.13)$$

The maximum displacement of Method C is the roof displacement at which the largest D/C ratio among all hinges of the model first reaches unity. Up to that displacement every deformation-controlled action satisfies its Collapse-Prevention criterion, as ASCE 41-17 Section 7.5.3.2.2 requires; beyond it, at least one does not. The definition contains no parameter chosen by this study.

The ratio D/C reads as follows. D is the plastic rotation that the hinge has actually undergone at a given step of the pushover, read from the SAP2000 Frame Hinge States table; C is the largest plastic rotation that ASCE 41-17 allows for that hinge at the Collapse-Prevention level. D/C = 0.5 means that the hinge has used half of its allowable rotation, D/C = 1 that it has reached the limit, and D/C > 1 that it has exceeded it. Figure 6.3 shows one governing hinge, the base hinge of the 1000 × 1000 mm interior column 2801 of the reference frame, as defined in SAP2000: the backbone A to E of ASCE 41-17 Figure 10-1 with a = 0.0183 rad and b = 0.0503 rad, and the Collapse-Prevention limit 0.7 b = 0.0352 rad. When the plastic rotation of this hinge reaches 0.0352 rad its D/C ratio is 1. The evaluation of this study uses the limit computed directly from Table 10-8 with the gravity axial load of the hinge, 0.0349 rad for this hinge (Table C.2), which is 0.9 percent below the value displayed by SAP2000.

Equation (6.13) is the acceptance check of ASCE 41-17 Section 7.5.3.2.2, reproduced in Figure 6.2, written as a ratio: the clause requires the deformation demand of each deformation-controlled component to be within its acceptance criterion, which is the statement $D/C \leq 1$. The limits θ_{CP} are those of Tables 10-7 and 10-8 (Figures 5.6c and 5.6d). The vector sum of the two plastic rotations of a column hinge is an assumption of this study; ASCE 41-17 requires the deformation capacities to be determined considering all coexisting deformations but does not prescribe how biaxial rotations are combined.

7.5.3.2.2 Acceptance Criteria for Deformation-Controlled Actions for NSP or NDP. Primary and secondary components shall have expected deformation capacities not less than maximum deformation demands calculated at target displacements. Primary and secondary component demands shall be within the acceptance criteria for nonlinear components at the selected Structural Performance Level. Expected deformation capacities shall be determined considering all coexisting forces and deformations in accordance with Chapters 8 through 15.

Figure 6.2 Acceptance criteria of ASCE 41-17 Section 7.5.3.2.2.

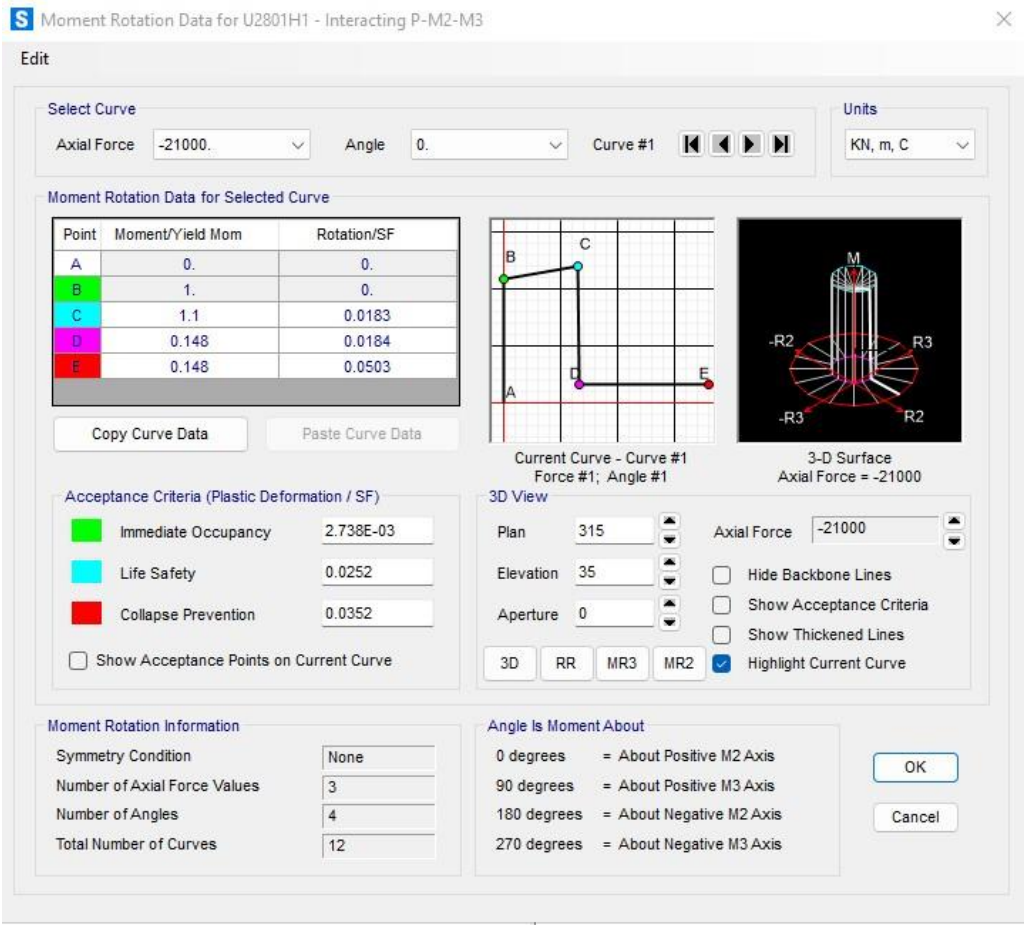

Figure 6.3 Base hinge of column 2801 in SAP2000.

Note. Interior column, 1000 × 1000 mm, first story of the fifteen-story reference frame. The Collapse-Prevention limit, 0.0352 rad, is 0.7 times b = 0.0503 rad.

6.6.3 Locating the limit state between two analysis steps

The largest D/C ratio is available at the saved steps of the analysis, so unity is generally crossed between two steps. The limit state is located by linear interpolation of the largest D/C ratio across the bracketing pair. Writing r_1 and r_2 for the largest ratios at the two bracketing steps and Δ_1 and Δ_2 for their roof displacements:

$$\Delta_{max,C} = \Delta_1 + (1 - r_1) / (r_2 - r_1) \times (\Delta_2 - \Delta_1) \quad (6.14)$$

Equation (6.14) is ordinary linear interpolation and is not taken from a standard. It assumes that the largest D/C ratio varies linearly between two saved steps, which is a close approximation when the steps are small; the two applications below show the arithmetic.

Fifteen-story reference frame

step 67: Δ = 1,340.00 mm, largest D/C = 0.9755

step 68: Δ = 1,360.00 mm, largest D/C = 1.0138

$\Delta_{max,C}$ = 1,340.00 + (0.0245 / 0.0383) × 20.00 = 1,352.80 mm

Four-story frame

step 47: Δ = 235.00 mm, largest D/C = 0.9424

step 48: Δ = 240.00 mm, largest D/C = 1.0028

$\Delta_{max,C}$ = 235.00 + (0.0576 / 0.0603) × 5.00 = 239.77 mm

Figure 6.4 shows the largest D/C ratio of all hinges of each model as the roof is pushed. Each curve starts at zero, rises once the first hinges yield, and crosses the horizontal line D/C = 1 at $\Delta_{max,C}$, marked by a diamond. The four-story frame crosses at 239.77 mm and the six-story frame at 323.54 mm. The four fifteen-story models with the base columns governing follow the reference curve closely and cross between 1,182.86 mm (Model 4) and 1,359.22 mm (Model 7); Model 5 crosses later, at 1,502.15 mm, because its columns are stronger and a beam governs. Every crossing in the figure agrees with the values of Table 6.18.

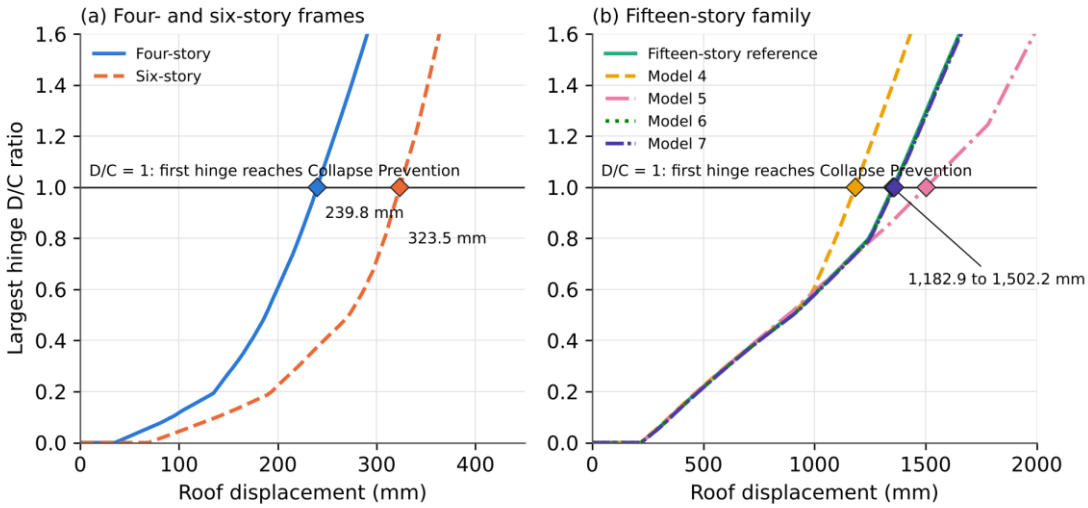

Figure 6.4 Largest hinge D/C ratio against roof displacement.

The interpolation could be avoided by taking, instead of $\Delta_{max,C}$, the last saved step at which every hinge is still within its criterion. That choice gives R_C lower by 0.1 to 1.8 percent across the seven models (0.9 percent for the reference frame). The difference is smaller than any difference between models discussed in Section 6.9, so the interpolation does not affect any conclusion. The analyses were saved at 5.0 mm increments for the four-story frame, 4.3 mm for the six-story frame, and 20 mm for the fifteen-story models.

6.6.4 The components that govern

Under the uniform pattern the first components to reach Collapse Prevention are the base hinges of the first-story interior columns in six of the seven models: the 500 × 500 mm columns of the four-story frame, the 600 × 600 mm interior columns of the six-story frame, and the 1000 × 1000 mm interior columns of the reference frame and of Models 4, 6 and 7. These sections combine the largest axial load ratio with the lowest transverse reinforcement ratio of their schedules (ρ_t = 0.00673 for the 1000 × 1000 mm section, Table 5.4), and the Collapse-Prevention plastic rotation of Table 10-8 decreases as the axial load ratio rises and as ρ_t falls. In Model 5, whose heavier columns carry closer hoops, the first component to reach the criterion is a beam of type B2 at the third-floor level.

At $\Delta_{max,C}$ of the reference frame the beams are still within their criterion, the largest beam D/C ratio being 0.90, at the second and third floor levels; of the 930 beam hinges, 526 have not yielded. Under the first-mode pattern the critical location moves upward: beams of type B2 at the third to fifth floor levels reach the criterion first in the reference

frame and in Models 5 and 6, while the base columns are at D/C ≈ 1.00. Figure 6.5 shows the D/C ratio of every hinge of one frame line at $\Delta_{max,C}$ under the two patterns.

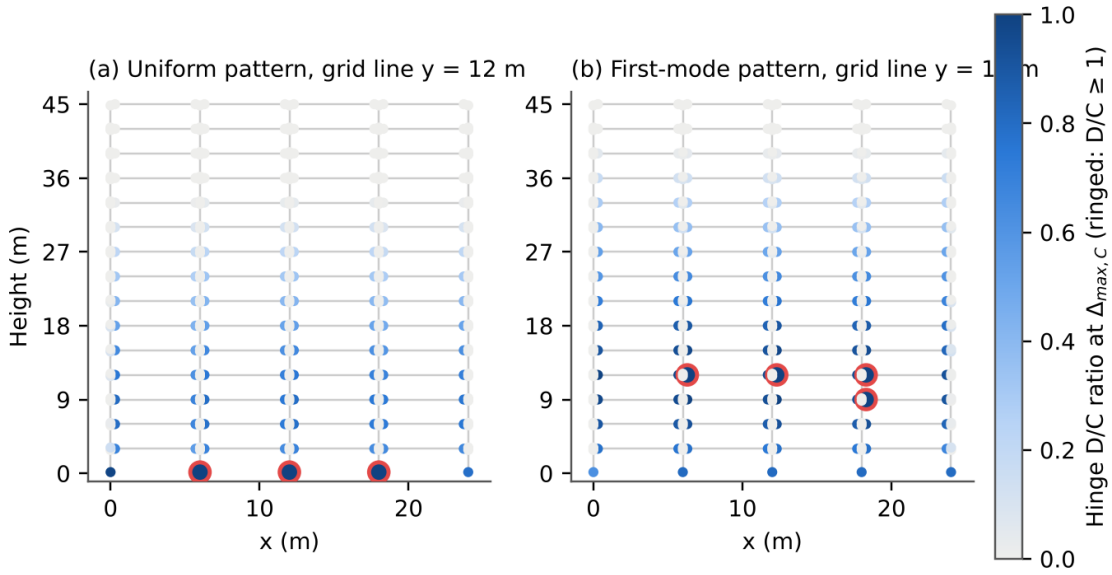

Figure 6.5 Hinge D/C ratios of the reference frame at $\Delta_{max,C}$.

Note. (a) Uniform pattern, interior frame line; (b) first-mode pattern, edge frame line. Ringed hinges have reached the Collapse-Prevention criterion.

6.6.5 Sensitivity to a criterion based on a fraction of the hinges

Method C stops at the first hinge that reaches its limit. Many published studies stop later, so this section asks how much the result would change if a later stopping point were used. The question matters because a reader comparing this study with the literature needs to know whether the difference comes from the frames or from the stopping rule.

Parts of the pushover literature define the ultimate displacement by a global rule, such as a fraction of the hinge population beyond Collapse Prevention, or by a drop of the base shear to eighty percent of its peak, which is the ductility definition of FEMA P-695 for collapse assessment. Neither rule is a provision of ASCE 41-17 for the nonlinear static procedure, and neither is used to define Method C here. Their effect is nevertheless reported, so that the results of this study can be compared with studies that use them. Table 6.9 gives R_C when $\Delta_{max,C}$ is taken at the displacement at which 0.5, 1, 1.5 or 2 percent of the hinges have exceeded their criterion, located by linear interpolation of the hinge count, and Figure 6.6 plots the same values. The last two columns give the overstrength factor at the first-component limit and at the 1-percent limit, since Ω of Method C depends on the definition of $\Delta_{max,C}$.

Table 6.9 Sensitivity of R_C to the criterion that defines $\Delta_{max,C}$.

Model	First component (adopted)	0.5 %	1 %	1.5 %	2 %	Ω at first component	Ω at 1 %
Four-story	10.21	10.22	10.32	11.02	11.07	5.02	5.06
Six-story	11.91	11.93	11.99	12.05	12.12	5.98	6.03
Fifteen-story reference	12.32	12.52	13.20	13.36	13.52	4.22	4.43
Model 4	10.84	11.30	12.14	13.06	13.24	3.96	4.20
Model 5	13.50	13.70	13.91	14.05	14.16	4.62	4.83
Model 6	12.30	12.46	13.24	13.34	13.48	4.25	4.48
Model 7	12.28	12.44	13.24	13.37	13.51	4.23	4.45

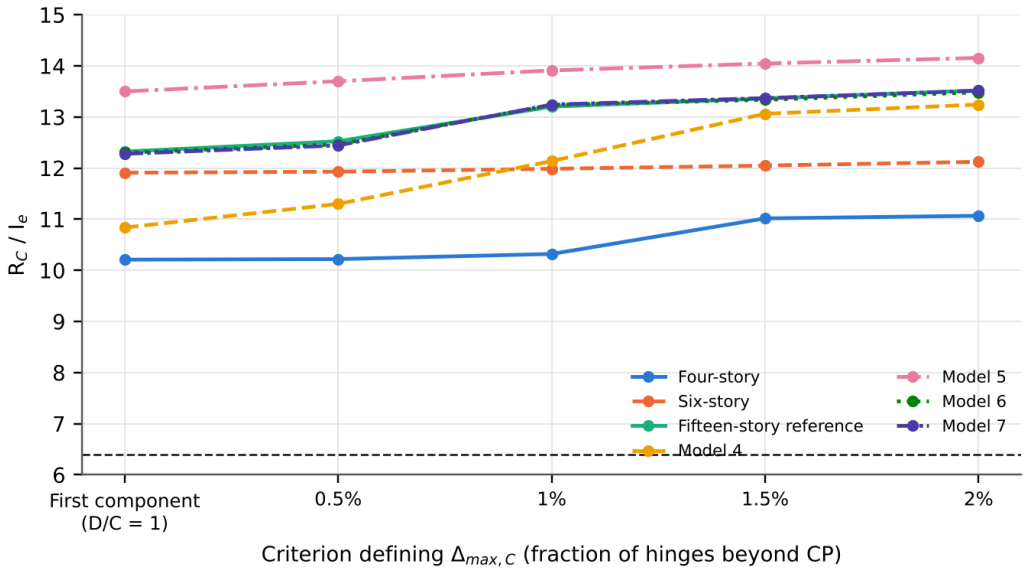

Figure 6.6 R_C against the criterion that defines $\Delta_{max,C}$.

Every value in Table 6.9 lies above 6.40, so the comparison with the code value does not depend on which of these criteria is used. A criterion of 1 percent of the hinges defers the limit state and raises R_C by between 0.6 and 7.9 percent in six of the models, and by 12.0 percent in Model 4, in which several column hinges approach their criterion together. The overstrength factor moves with the anchor, as Section 6.3.3 anticipated, by between 0.8 and 6.1 percent between the adopted definition and the 1-percent criterion. The ordering of the models is the same under every criterion of Table 6.9.

6.7 Model-by-Model Calculation

This section applies the procedure of Sections 6.3 to 6.6 to each model in turn. For every model a table traces the calculation line by line, from the design quantities to the three factors, and states for every value the clause, equation or program output table from

which it comes. The capacity curve of the model follows its table, with the bilinear idealization, the design base shear and the three maximum displacements of Methods A, B and C drawn on it, so that each number of the table can be located on the curve. The values are carried at full precision and rounded only for presentation; a value recomputed from the rounded entries can therefore differ in the last digit. The inputs common to the seven models are listed once, in Table 6.10.

Table 6.10 Inputs common to the seven models.

Quantity	**Value**	**Source of the value**
S_S, S_1	0.75 g, 0.375 g	2.5 Z and 1.25 Z with Z = 0.30 (Section 3.5, Table 3.2)
F_a, F_v	0.8, 0.8	ASCE 7-16 Tables 11.4-1 and 11.4-2, Site Class A (Table 3.2)
S_{DS}, S_{D1}	0.40 g, 0.20 g	ASCE 7-16 Eqs. 11.4-1 to 11.4-4: (2/3)(0.8)(0.75) and (2/3)(0.8)(0.375)
$T_s = S_{D1} / S_{DS}$	0.50 s	ASCE 7-16 Section 11.4.6
T_L	4 s	Adopted value (Table 3.2); ETABS input
R, Ω_0, C_d	8, 3, 5.5	ASCE 7-16 Table 12.2-1, special reinforced concrete moment frame (Table 3.3)
I_e	1.25	ASCE 7-16 Table 1.5-2, Risk Category III (Table 3.2)
C_d / I_e	4.40	Factor of ASCE 7-16 Eq. 12.8-15, Equation (6.11)
f'_{cE}, f_{yE} of the hinges	35 MPa, 455.05 MPa	Expected properties of the nonlinear model (Section 5.3, Table C.1)
θ_{CP} of beams	$\leq$ 0.050 rad	ASCE 41-17 Table 10-7, row i, for each section and sign of moment (Table 5.6, Table C.1)
θ_{CP} of columns	0.7 b	ASCE 41-17 Table 10-8 with $n \geq 0.1$ and ρ_t of each section, Equation (5.2) (Table B.1, Table C.1)
C_1, C_2, C_3	1.00, 1.00, 1.00	FEMA 356 Section 3.3.3.3.2 and Table 3-3 (Table 6.6)
g	9,810 mm/s^2	Standard gravity

6.7.1 Four-story frame

For the four-story frame the design base shear is V_d = 1,219.82 kN and the elastic roof displacement Δ_d = 16.990 mm (Table 6.2). The three methods are evaluated in turn, each with the equal-area idealization up to its own maximum displacement (Section 6.3.3). Method A: $\Delta_{max,A}$ = 74.76 mm, V_y = 2,590.8 kN and Δ_y = 48.14 mm, so Ω = 2.124, μ_A = 1.553 and R_A = 3.30. Method B: δ_t = 76.09 mm, V_y = 2,606.0 kN and Δ_y = 48.43 mm, so Ω = 2.136, μ_B = 1.571 and R_B = 3.36. Method C: V_y = 6,125.1 kN and Δ_y = 117.94 mm, so Ω = 5.021. The first column hinge reaches its Collapse-Prevention limit at $\Delta_{max,C}$ = 239.77 mm, which gives μ_C = 2.033 and R_C = 10.21 on the basis of R / I_e, or 12.76 on the basis of R. The capacity curve peaks at about 215 mm and $\Delta_{max,C}$ lies just beyond the peak, on the descending branch. Table 6.11 gives the calculation and Figure 6.7 the capacity curve.

Table 6.11 Calculation for the four-story frame.

Quantity	Value	Source of the value
Elastic design model (ETABS, load case EQX)		
Period used in design	0.654 s	C_u T_a, ASCE 7-16 Section 12.8.2.1; ETABS Auto Seismic table, Period Used
C_s	0.0478	S_{D1} / (T R / I_e), ASCE 7-16 Eq. 12.8-3
W	25,545.0 kN	ETABS Auto Seismic table (ASCE 7-16), load pattern EQX, Weight Used
V_d	1,219.82 kN	ETABS Base Reactions table, load case EQX, global FX
Δ_d	16.990 mm	ETABS Joint Displacements table, load case EQX, largest U_x at the roof
$K_d = V_d / \Delta_d$	71.80 kN/mm	Derived
Nonlinear model (SAP2000)		
N, plastic hinges	408	SAP2000 model, two hinges per member (Table 6.8)
T_e	1.205 s	SAP2000 Modal Participating Mass Ratios table: X-direction mode with the largest U_X ratio
Γ	46.109	SAP2000 Modal Participation Factors table, U_X, same mode (mass-normalized)
φ_{roof}	0.027561	SAP2000 Joint Displacements table, case MODAL, U_1 of control joint 746
Capacity curve	100 steps to 500.0 mm	SAP2000 Pushover Capacity Curve table, case Pushover-X, uniform pattern, saved at 5.0 mm increments
V_{max} within the run	6,604.6 kN	Largest base shear of the capacity curve
Method C: Collapse-Prevention displacement		
Step 47: Δ, largest D/C	235.00 mm, 0.9424	SAP2000 Frame Hinge States table (θ_{p2}, θ_{p3}); Equation (6.13) with the θ_{CP} of each hinge
Step 48: Δ, largest D/C	240.00 mm, 1.0028	As above
$\Delta_{max,C}$	239.77 mm	Linear interpolation to D/C = 1, Equation (6.14); ASCE 41-17 Section 7.5.3.2.2
Roof drift at $\Delta_{max,C}$	2.00 %	$\Delta_{max,C}$ / 12 m
Hinges with D/C > 1 at step 48	2: frames 2831, 2861	SAP2000 Frame Hinge States table; section Col 50X50
V_u at $\Delta_{max,C}$	6,434.1 kN	Capacity curve, linear interpolation at $\Delta_{max,C}$
Method C: bilinear idealization (Section 6.3)		
A up to $\Delta_u = \Delta_{max,C}$	1,126,240 kN·mm	Trapezoidal sum on the capacity curve, Equation (6.7)

Quantity	Value	Source of the value
K_i	53.815 kN/mm	V / Δ at the first saved step after the origin; starting value of the iteration (Section 6.3.5)
K_e	51.935 kN/mm	Secant at 0.6 V_y, reached at 70.76 mm; FEMA 356 Section 3.3.3.2.4 and Figure 3-1 (Section 6.3.5)
V_y	6,125.1 kN	Equal-area condition, Equation (6.9)
$\Delta_y = V_y / K_e$	117.94 mm	Equation (6.3)
$V_u / K_e < \Delta_u$	123.9 < 239.8 mm	Admissibility, Equation (6.10): satisfied
$\Omega = V_y / V_d$	5.021	Equation (6.2)
Method A: code-amplified displacement		
$\Delta_{max,A} = C_d \Delta_d / I_e$	74.76 mm	ASCE 7-16 Eq. 12.8-15, Equation (6.11)
V_u at $\Delta_{max,A}$	3,862.2 kN	Capacity curve, linear interpolation at $\Delta_{max,A}$
A up to $\Delta_u = \Delta_{max,A}$	148,231 kN·mm	Trapezoidal sum on the capacity curve, Equation (6.7)
K_e	53.815 kN/mm	Secant at 0.6 V_y, reached at 28.89 mm on the initial linear branch, so $K_e = K_i$ (Section 6.3.5)
V_y	2,590.8 kN	Equal-area condition, Equation (6.9)
$\Delta_y = V_y / K_e$	48.14 mm	Equation (6.3)
$V_u / K_e < \Delta_u$	71.8 < 74.8 mm	Admissibility, Equation (6.10): satisfied
$\mu_A = \Delta_{max,A} / \Delta_y$	1.553	Equation (6.3)
$R_\mu = \mu_A$	1.553	Equation (6.4c), $\mu_A > 1$ and $T_e > 0.5$ s
$\Omega = V_y / V_d$	2.124	Equation (6.2)
$R_A = R_\mu \Omega$	3.30	Equation (6.1), reported as R / I_e
Check $(C_d / I_e)(K_e / K_d)$, Eq. (6.6)	3.30	equals R_A
Method B: FEMA 356 target displacement		
$S_a = S_{D1} / T_e$	0.1660 g	ASCE 7-16 Eq. 11.4-6, $T_s < T_e \leq T_L$
$S_d = S_a g T_e^2 / 4\pi^2$	59.88 mm	Spectral displacement of the equivalent oscillator
$C_0 = \Gamma \varphi_{roof}$	1.271	FEMA 356 Section 3.3.3.3.2, calculated from the mode shape
$\delta_t = C_0 C_1 C_2 C_3 S_d$	76.09 mm	FEMA 356 Eq. 3-15, Equation (6.12)
V_u at δ_t	3,924.2 kN	Capacity curve, linear interpolation at δ_t
A up to $\Delta_u = \delta_t$	153,438 kN·mm	Trapezoidal sum on the capacity curve, Equation (6.7)
K_e	53.815 kN/mm	Secant at 0.6 V_y, reached at 29.06 mm on the initial linear branch, so $K_e = K_i$ (Section 6.3.5)
V_y	2,606.0 kN	Equal-area condition, Equation (6.9)
$\Delta_y = V_y / K_e$	48.43 mm	Equation (6.3)
$V_u / K_e < \Delta_u$	72.9 < 76.1 mm	Admissibility, Equation (6.10): satisfied
$\mu_B = \delta_t / \Delta_y$	1.571	Equation (6.3)
$R_\mu = \mu_B$	1.571	Equation (6.4c), $\mu_B > 1$ and $T_e > 0.5$ s
$\Omega = V_y / V_d$	2.136	Equation (6.2)
$R_B = R_\mu \Omega$	3.36	Equation (6.1), reported as R / I_e
Check $\delta_t K_e / V_d$, Eq. (6.5)	3.36	equals R_B
Method C: factor		
$\mu_C = \Delta_{max,C} / \Delta_y$	2.033	Equation (6.3)
$R_\mu = \mu_C$	2.033	Equation (6.4c), $\mu_C > 1$ and $T_e > 0.5$ s
$R_C = R_\mu \Omega$	10.21	Equation (6.1), reported as R / I_e
Check $\Delta_{max,C} K_e / V_d$	10.21	Equation (6.5); equals R_C
Comparison with the code value		
R_A, R_B, R_C (as R / I_e)	3.30, 3.36, 10.21	Compared with 8 / 1.25 = 6.40 (Section 6.4.3)
R_A, R_B, R_C (as R)	4.12, 4.20, 12.76	1.25 × the values above; compared with 8
R_C, first-mode pattern	10.73	Same chain under the first-mode pattern (Table 6.19)

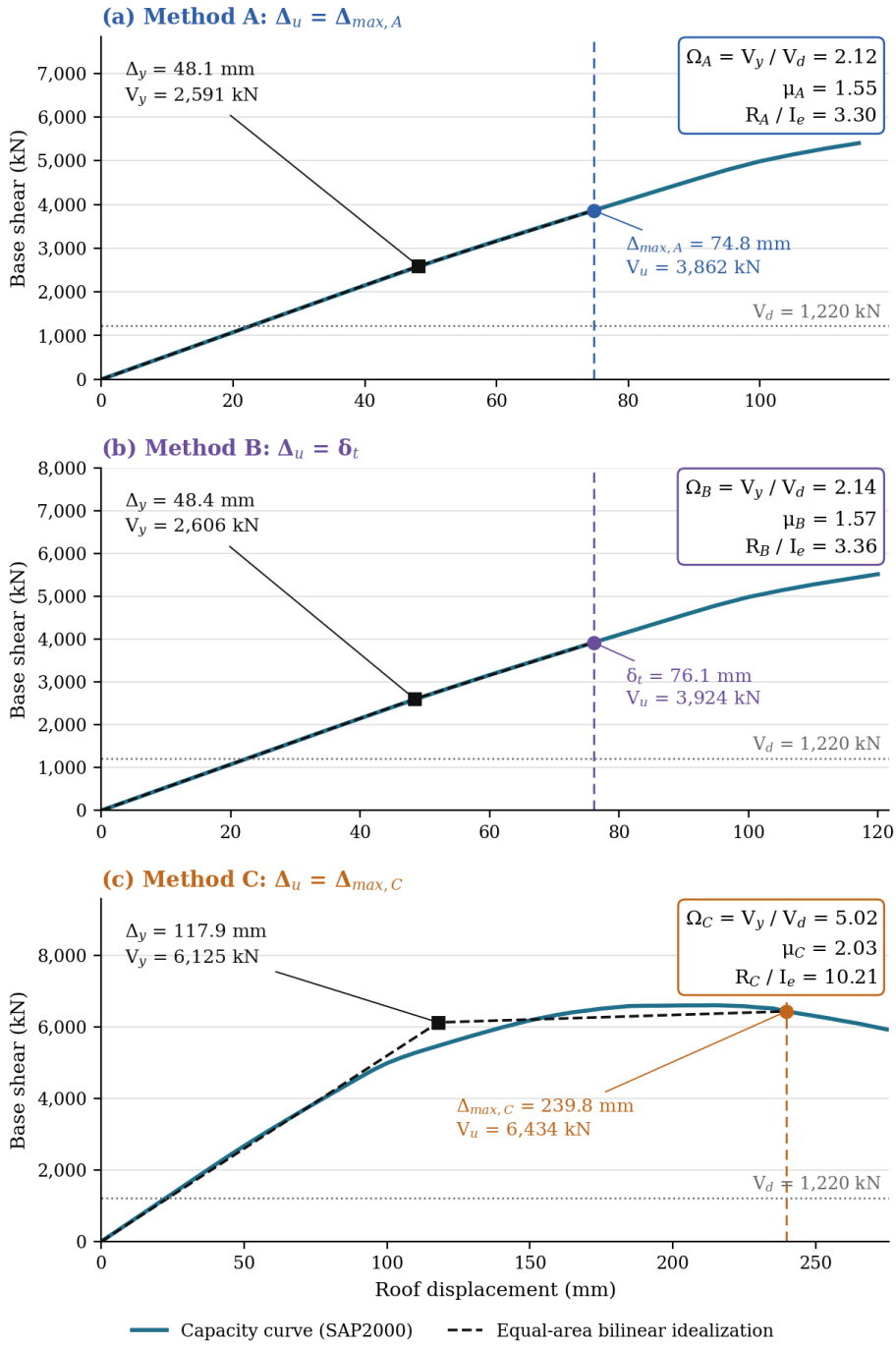

Figure 6.7 Four-story frame: capacity curve and bilinear idealizations.

6.7.2 Six-story frame

For the six-story frame the design base shear is V_d = 1,317.71 kN and the elastic roof displacement Δ_d = 25.555 mm (Table 6.2). The three methods are evaluated in turn, each with the equal-area idealization up to its own maximum displacement (Section 6.3.3). Method A: $\Delta_{max,A}$ = 112.44 mm, V_y = 4,037.5 kN and Δ_y = 82.22 mm, so Ω = 3.064, μ_A = 1.368 and R_A = 4.19. Method B: δ_t = 100.35 mm, V_y = 3,752.0 kN and Δ_y = 76.41 mm, so Ω = 2.847, μ_B = 1.313 and R_B = 3.74. Method C: V_y = 7,882.1 kN and Δ_y = 162.51 mm, so Ω = 5.982. The first column hinge reaches its Collapse-Prevention limit at $\Delta_{max,C}$ = 323.54 mm, which gives μ_C = 1.991 and R_C = 11.91 on the basis of R / I_e, or 14.89 on the basis of R. The capacity curve peaks at about 297 mm and $\Delta_{max,C}$ lies just beyond the peak, on the descending branch. Table 6.12 gives the calculation and Figure 6.8 the capacity curve.

Table 6.12 Calculation for the six-story frame.

Quantity	Value	Source of the value
Elastic design model (ETABS, load case EQX)		
Period used in design	0.943 s	$C_u T_a = 1.5 \times 0.0466 \times 18^{0.9}$, ASCE 7-16 Section 12.8.2.1 and Tables 12.8-1 and 12.8-2; equal to S_{D1} / (C_s R / I_e) with $C_s = V_d$ / W
C_s	0.0332	S_{D1} / (T R / I_e), ASCE 7-16 Eq. 12.8-3
W	39,747.8 kN	ETABS Auto Seismic table (ASCE 7-16), load pattern EQX, Weight Used
V_d	1,317.71 kN	ETABS Base Reactions table, load case EQX, global FX
Δ_d	25.555 mm	ETABS Joint Displacements table, load case EQX, largest U_x at the roof
$K_d = V_d / \Delta_d$	51.56 kN/mm	Derived
Nonlinear model (SAP2000)		
N, plastic hinges	612	SAP2000 model, two hinges per member (Table 6.8)
T_e	1.561 s	SAP2000 Modal Participating Mass Ratios table: X-direction mode with the largest U_X ratio
Γ	56.670	SAP2000 Modal Participation Factors table, U_X, same mode (mass-normalized)
φ_{roof}	0.022824	SAP2000 Joint Displacements table, case MODAL, U_1 of control joint 808
Capacity curve	100 steps to 430.0 mm	SAP2000 Pushover Capacity Curve table, case Pushover-X, uniform pattern, saved at 4.3 mm increments
V_{max} within the run	8,987.6 kN	Largest base shear of the capacity curve
Method C: Collapse-Prevention displacement		
Step 75: Δ, largest D/C	322.50 mm, 0.9866	SAP2000 Frame Hinge States table (θ_{p2}, θ_{p3}); Equation (6.13) with the θ_{CP} of each hinge
Step 76: Δ, largest D/C	326.80 mm, 1.0422	As above
$\Delta_{max,C}$	323.54 mm	Linear interpolation to D/C = 1, Equation (6.14); ASCE 41-17 Section 7.5.3.2.2
Roof drift at $\Delta_{max,C}$	1.80 %	$\Delta_{max,C}$ / 18 m
Hinges with D/C > 1 at step 76	8: frames 2786, 2801, 2816, 2831, 2846, 2861, 2966, 2981	SAP2000 Frame Hinge States table; section Col 50X50, Col 60X60 int
V_u at $\Delta_{max,C}$	8,571.4 kN	Capacity curve, linear interpolation at $\Delta_{max,C}$

Quantity	Value	Source of the value
Method C: bilinear idealization (Section 6.3)		
A up to $\Delta_u = \Delta_{max,C}$	1,965,194 kN·mm	Trapezoidal sum on the capacity curve, Equation (6.7)
K_i	49.107 kN/mm	V / Δ at the first saved step after the origin; starting value of the iteration (Section 6.3.5)
K_e	48.502 kN/mm	Secant at 0.6 V_y, reached at 97.51 mm; FEMA 356 Section 3.3.3.2.4 and Figure 3-1 (Section 6.3.5)
V_y	7,882.1 kN	Equal-area condition, Equation (6.9)
$\Delta_y = V_y / K_e$	162.51 mm	Equation (6.3)
$V_u / K_e < \Delta_u$	176.7 < 323.5 mm	Admissibility, Equation (6.10): satisfied
$\Omega = V_y / V_d$	5.982	Equation (6.2)
Method A: code-amplified displacement		
$\Delta_{max,A} = C_d \Delta_d / I_e$	112.44 mm	ASCE 7-16 Eq. 12.8-15, Equation (6.11)
V_u at $\Delta_{max,A}$	5,387.1 kN	Capacity curve, linear interpolation at $\Delta_{max,A}$
A up to $\Delta_u = \Delta_{max,A}$	308,395 kN·mm	Trapezoidal sum on the capacity curve, Equation (6.7)
K_e	49.106 kN/mm	Secant at 0.6 V_y, reached at 49.33 mm on the initial linear branch, so $K_e = K_i$ (Section 6.3.5)
V_y	4,037.5 kN	Equal-area condition, Equation (6.9)
$\Delta_y = V_y / K_e$	82.22 mm	Equation (6.3)
$V_u / K_e < \Delta_u$	109.7 < 112.4 mm	Admissibility, Equation (6.10): satisfied
$\mu_A = \Delta_{max,A} / \Delta_y$	1.368	Equation (6.3)
$R_\mu = \mu_A$	1.368	Equation (6.4c), $\mu_A > 1$ and $T_e > 0.5$ s
$\Omega = V_y / V_d$	3.064	Equation (6.2)
$R_A = R_\mu \Omega$	4.19	Equation (6.1), reported as R / I_e
Check $(C_d / I_e)(K_e / K_d)$, Eq. (6.6)	4.19	equals R_A
Method B: FEMA 356 target displacement		
$S_a = S_{D1} / T_e$	0.1281 g	ASCE 7-16 Eq. 11.4-6, $T_s < T_e \le T_L$
$S_d = S_a g T_e^2 / 4\pi^2$	77.58 mm	Spectral displacement of the equivalent oscillator
$C_0 = \Gamma \varphi_{roof}$	1.293	FEMA 356 Section 3.3.3.3.2, calculated from the mode shape
$\delta_t = C_0 C_1 C_2 C_3 S_d$	100.35 mm	FEMA 356 Eq. 3-15, Equation (6.12)
V_u at δ_t	4,858.0 kN	Capacity curve, linear interpolation at δ_t
A up to $\Delta_u = \delta_t$	246,399 kN·mm	Trapezoidal sum on the capacity curve, Equation (6.7)
K_e	49.106 kN/mm	Secant at 0.6 V_y, reached at 45.84 mm on the initial linear branch, so $K_e = K_i$ (Section 6.3.5)
V_y	3,752.0 kN	Equal-area condition, Equation (6.9)
$\Delta_y = V_y / K_e$	76.41 mm	Equation (6.3)
$V_u / K_e < \Delta_u$	98.9 < 100.3 mm	Admissibility, Equation (6.10): satisfied
$\mu_B = \delta_t / \Delta_y$	1.313	Equation (6.3)
$R_\mu = \mu_B$	1.313	Equation (6.4c), $\mu_B > 1$ and $T_e > 0.5$ s
$\Omega = V_y / V_d$	2.847	Equation (6.2)
$R_B = R_\mu \Omega$	3.74	Equation (6.1), reported as R / I_e
Check $\delta_t K_e / V_d$, Eq. (6.5)	3.74	equals R_B
Method C: factor		
$\mu_C = \Delta_{max,C} / \Delta_y$	1.991	Equation (6.3)
$R_\mu = \mu_C$	1.991	Equation (6.4c), $\mu_C > 1$ and $T_e > 0.5$ s
$R_C = R_\mu \Omega$	11.91	Equation (6.1), reported as R / I_e
Check $\Delta_{max,C} K_e / V_d$	11.91	Equation (6.5); equals R_C
Comparison with the code value		
R_A, R_B, R_C (as R / I_e)	4.19, 3.74, 11.91	Compared with 8 / 1.25 = 6.40 (Section 6.4.3)
R_A, R_B, R_C (as R)	5.24, 4.67, 14.89	1.25 × the values above; compared with 8
R_C, first-mode pattern	not reached	Largest D/C = 0.738 at 425.7 mm, the end of the run (Table 6.19)

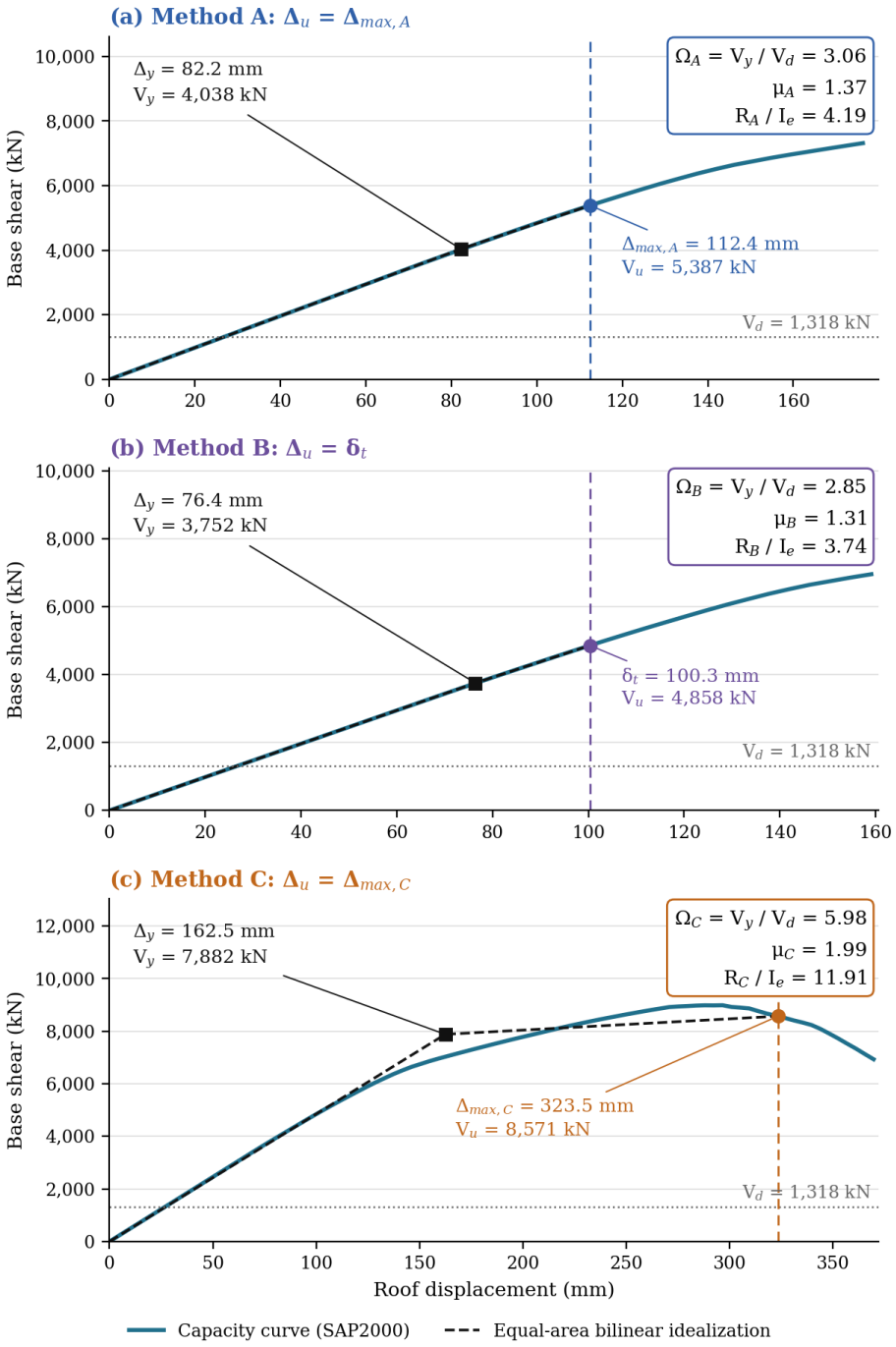

Figure 6.8 Six-story frame: capacity curve and bilinear idealizations.

6.7.3 Fifteen-story reference frame

For the fifteen-story reference frame the design base shear is V_d = 2,203.78 kN and the elastic roof displacement Δ_d = 92.554 mm (Table 6.2). The three methods are evaluated in turn, each with the equal-area idealization up to its own maximum displacement (Section 6.3.3). Method A: $\Delta_{max,A}$ = 407.24 mm, V_y = 5,613.7 kN and Δ_y = 275.74 mm, so Ω = 2.547, μ_A = 1.477 and R_A = 3.76. Method B: δ_t = 243.48 mm, V_y = 4,553.6 kN and Δ_y = 223.67 mm, so Ω = 2.066, μ_B = 1.089 and R_B = 2.25. Method C: V_y = 9,304.9 kN and Δ_y = 463.53 mm, so Ω = 4.222. The first column hinge reaches its Collapse-Prevention limit at $\Delta_{max,C}$ = 1,352.80 mm, which gives μ_C = 2.918 and R_C = 12.32 on the basis of R / I_e, or 15.40 on the basis of R. The capacity curve still rises at the end of the analysis, at 2.0 m, so $\Delta_{max,C}$ lies on the rising branch. Table 6.13 gives the calculation and Figure 6.9 the capacity curve.

Table 6.13 Calculation for the fifteen-story reference frame.

Quantity	Value	Source of the value
Elastic design model (ETABS, load case EQX)		
Period used in design	2.150 s	$C_u T_a$ = 1.5 × 1.433, ASCE 7-16 Section 12.8.2.1 (Appendix A.2)
C_s	0.0220	0.044 $S_{DS} I_e$, ASCE 7-16 Eq. 12.8-5 (governs; Table A.2)
W	100,171.9 kN	V_d / C_s (derived)
V_d	2,203.78 kN	ETABS Base Reactions table, load case EQX, global FX
Δ_d	92.554 mm	ETABS Joint Displacements table, load case EQX, largest U_x at the roof
$K_d = V_d / \Delta_d$	23.81 kN/mm	Derived
Nonlinear model (SAP2000)		
N, plastic hinges	1,530	SAP2000 model, two hinges per member (Table 6.8)
T_e	3.667 s	SAP2000 Modal Participating Mass Ratios table: X-direction mode with the largest U_X ratio
Γ	86.608	SAP2000 Modal Participation Factors table, U_X, same mode (mass-normalized)
φ_{roof}	0.015424	SAP2000 Joint Displacements table, case MODAL, U_1 of control joint 1087
Capacity curve	100 steps to 2,000.0 mm	SAP2000 Pushover Capacity Curve table, case Pushover-X, uniform pattern, saved at 20.0 mm increments
V_{max} within the run	18,994.2 kN	Largest base shear of the capacity curve
Method C: Collapse-Prevention displacement		
Step 67: Δ, largest D/C	1,340.00 mm, 0.9755	SAP2000 Frame Hinge States table (θ_{p2}, θ_{p3}); Equation (6.13) with the θ_{CP} of each hinge
Step 68: Δ, largest D/C	1,360.00 mm, 1.0138	As above
$\Delta_{max,C}$	1,352.80 mm	Linear interpolation to D/C = 1, Equation (6.14); ASCE 41-17 Section 7.5.3.2.2
Roof drift at $\Delta_{max,C}$	3.01 %	$\Delta_{max,C}$ / 45 m
Hinges with D/C > 1 at step 68	6: frames 2786, 2801, 2816, 2831, 2846, 2861	SAP2000 Frame Hinge States table; section Col 1000X1000
V_u at $\Delta_{max,C}$	16,209.9 kN	Capacity curve, linear interpolation at $\Delta_{max,C}$
Method C: bilinear idealization (Section 6.3)		
A up to $\Delta_u = \Delta_{max,C}$	13,501,301 kN·mm	Trapezoidal sum on the capacity curve, Equation (6.7)

Quantity	Value	Source of the value
K_i	20.358 kN/mm	V / Δ at the first saved step after the origin; starting value of the iteration (Section 6.3.5)
K_e	20.074 kN/mm	Secant at 0.6 V_y, reached at 278.12 mm; FEMA 356 Section 3.3.3.2.4 and Figure 3-1 (Section 6.3.5)
V_y	9,304.9 kN	Equal-area condition, Equation (6.9)
$\Delta_y = V_y / K_e$	463.53 mm	Equation (6.3)
$V_u / K_e < \Delta_u$	807.5 < 1,352.8 mm	Admissibility, Equation (6.10): satisfied
$\Omega = V_y / V_d$	4.222	Equation (6.2)
Method A: code-amplified displacement		
$\Delta_{max,A} = C_d \Delta_d / I_e$	407.24 mm	ASCE 7-16 Eq. 12.8-15, Equation (6.11)
V_u at $\Delta_{max,A}$	7,566.6 kN	Capacity curve, linear interpolation at $\Delta_{max,A}$
A up to $\Delta_u = \Delta_{max,A}$	1,640,542 kN·mm	Trapezoidal sum on the capacity curve, Equation (6.7)
K_e	20.358 kN/mm	Secant at 0.6 V_y, reached at 165.45 mm on the initial linear branch, so $K_e = K_i$ (Section 6.3.5)
V_y	5,613.7 kN	Equal-area condition, Equation (6.9)
$\Delta_y = V_y / K_e$	275.74 mm	Equation (6.3)
$V_u / K_e < \Delta_u$	371.7 < 407.2 mm	Admissibility, Equation (6.10): satisfied
$\mu_A = \Delta_{max,A} / \Delta_y$	1.477	Equation (6.3)
$R_\mu = \mu_A$	1.477	Equation (6.4c), $\mu_A > 1$ and $T_e > 0.5$ s
$\Omega = V_y / V_d$	2.547	Equation (6.2)
$R_A = R_\mu \Omega$	3.76	Equation (6.1), reported as R / I_e
Check $(C_d / I_e)(K_e / K_d)$, Eq. (6.6)	3.76	equals R_A
Method B: FEMA 356 target displacement		
$S_a = S_{D1} / T_e$	0.0545 g	ASCE 7-16 Eq. 11.4-6, $T_s < T_e \leq T_L$
$S_d = S_a g T_e^2 / 4\pi^2$	182.26 mm	Spectral displacement of the equivalent oscillator
$C_0 = \Gamma \varphi_{roof}$	1.336	FEMA 356 Section 3.3.3.3.2, calculated from the mode shape
$\delta_t = C_0 C_1 C_2 C_3 S_d$	243.48 mm	FEMA 356 Eq. 3-15, Equation (6.12)
V_u at δ_t	4,940.1 kN	Capacity curve, linear interpolation at δ_t
A up to $\Delta_u = \delta_t$	603,269 kN·mm	Trapezoidal sum on the capacity curve, Equation (6.7)
K_e	20.358 kN/mm	Secant at 0.6 V_y, reached at 134.20 mm on the initial linear branch, so $K_e = K_i$ (Section 6.3.5)
V_y	4,553.6 kN	Equal-area condition, Equation (6.9)
$\Delta_y = V_y / K_e$	223.67 mm	Equation (6.3)
$V_u / K_e < \Delta_u$	242.7 < 243.5 mm	Admissibility, Equation (6.10): satisfied
$\mu_B = \delta_t / \Delta_y$	1.089	Equation (6.3)
$R_\mu = \mu_B$	1.089	Equation (6.4c), $\mu_B > 1$ and $T_e > 0.5$ s
$\Omega = V_y / V_d$	2.066	Equation (6.2)
$R_B = R_\mu \Omega$	2.25	Equation (6.1), reported as R / I_e
Check $\delta_t K_e / V_d$, Eq. (6.5)	2.25	equals R_B
Method C: factor		
$\mu_C = \Delta_{max,C} / \Delta_y$	2.918	Equation (6.3)
$R_\mu = \mu_C$	2.918	Equation (6.4c), $\mu_C > 1$ and $T_e > 0.5$ s
$R_C = R_\mu \Omega$	12.32	Equation (6.1), reported as R / I_e
Check $\Delta_{max,C} K_e / V_d$	12.32	Equation (6.5); equals R_C
Comparison with the code value		
R_A, R_B, R_C (as R / I_e)	3.76, 2.25, 12.32	Compared with 8 / 1.25 = 6.40 (Section 6.4.3)
R_A, R_B, R_C (as R)	4.70, 2.81, 15.40	1.25 × the values above; compared with 8
R_C, first-mode pattern	11.08	Same chain under the first-mode pattern (Table 6.19)

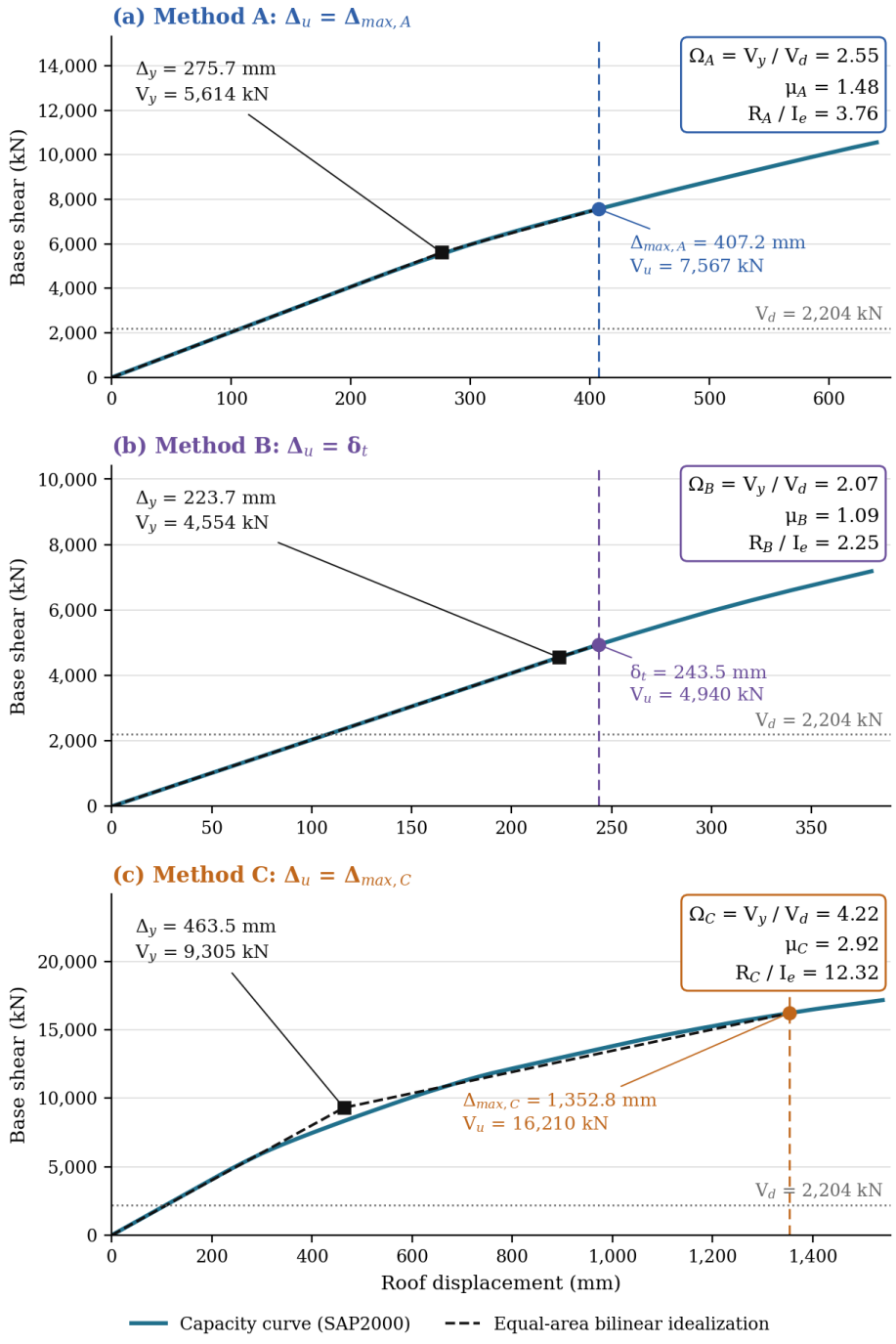

Figure 6.9 Reference frame: capacity curve and bilinear idealizations.

6.7.4 Model 4: wider hoop spacing and lower concrete strength

For Model 4 the design base shear is V_d = 2,203.78 kN and the elastic roof displacement Δ_d = 92.554 mm (Table 6.2). The three methods are evaluated in turn, each with the equal-area idealization up to its own maximum displacement (Section 6.3.3). Method A: $\Delta_{max,A}$ = 407.24 mm, V_y = 5,571.7 kN and Δ_y = 273.68 mm, so Ω = 2.528, μ_A = 1.488 and R_A = 3.76. Method B: δ_t = 243.48 mm, V_y = 4,522.3 kN and Δ_y = 222.13 mm, so Ω = 2.052, μ_B = 1.096 and R_B = 2.25. Method C: V_y = 8,719.3 kN and Δ_y = 431.90 mm, so Ω = 3.957. The first column hinge reaches its Collapse-Prevention limit at $\Delta_{max,C}$ = 1,182.86 mm, which gives μ_C = 2.739 and R_C = 10.84 on the basis of R / I_e, or 13.54 on the basis of R. Model 4 shares the design model of the reference frame (Section 6.2), so its design quantities are those of Table 6.13. Its base columns, with 100 mm hoops and 29 MPa concrete, reach their limit earlier than in the reference frame. Table 6.14 gives the calculation and Figure 6.10 the capacity curve.

Table 6.14 Calculation for Model 4.

Quantity	Value	Source of the value
Elastic design model (ETABS, load case EQX)		
Period used in design	2.150 s	$C_u T_a$ = 1.5 × 1.433, ASCE 7-16 Section 12.8.2.1 (Appendix A.2)
C_s	0.0220	0.044 $S_{DS} I_e$, ASCE 7-16 Eq. 12.8-5 (governs; Table A.2)
W	100,171.9 kN	V_d / C_s (derived)
V_d	2,203.78 kN	ETABS design model of the reference frame, shared by Models 4 and 5 (Section 6.2)
Δ_d	92.554 mm	ETABS design model of the reference frame, shared by Models 4 and 5 (Section 6.2)
$K_d = V_d / \Delta_d$	23.81 kN/mm	Derived
Nonlinear model (SAP2000)		
N, plastic hinges	1,530	SAP2000 model, two hinges per member (Table 6.8)
T_e	3.667 s	SAP2000 Modal Participating Mass Ratios table: X-direction mode with the largest U_X ratio
Γ	86.608	SAP2000 Modal Participation Factors table, U_X, same mode (mass-normalized)
φ_{roof}	0.015424	SAP2000 Joint Displacements table, case MODAL, U_1 of control joint 1087
Capacity curve	101 steps to 2,000.0 mm	SAP2000 Pushover Capacity Curve table, case Pushover-X, uniform pattern, saved at 20.0 mm increments
V_{max} within the run	18,290.6 kN	Largest base shear of the capacity curve
Method C: Collapse-Prevention displacement		
Step 59: Δ, largest D/C	1,180.00 mm, 0.9932	SAP2000 Frame Hinge States table (θ_{p2}, θ_{p3}); Equation (6.13) with the θ_{CP} of each hinge
Step 60: Δ, largest D/C	1,200.00 mm, 1.0409	As above
$\Delta_{max,C}$	1,182.86 mm	Linear interpolation to D/C = 1, Equation (6.14); ASCE 41-17 Section 7.5.3.2.2
Roof drift at $\Delta_{max,C}$	2.63 %	$\Delta_{max,C}$ / 45 m
Hinges with D/C > 1 at step 60	6: frames 2786, 2801, 2816, 2831, 2846, 2861	SAP2000 Frame Hinge States table; section Col 1000X1000
V_u at $\Delta_{max,C}$	14,769.1 kN	Capacity curve, linear interpolation at $\Delta_{max,C}$

Quantity	Value	Source of the value
Method C: bilinear idealization (Section 6.3)		
A up to $\Delta_u = \Delta_{max,C}$	10,702,338 kN·mm	Trapezoidal sum on the capacity curve, Equation (6.7)
K_i	20.358 kN/mm	V / Δ at the first saved step after the origin; starting value of the iteration (Section 6.3.5)
K_e	20.188 kN/mm	Secant at 0.6 V_y, reached at 259.14 mm; FEMA 356 Section 3.3.3.2.4 and Figure 3-1 (Section 6.3.5)
V_y	8,719.3 kN	Equal-area condition, Equation (6.9)
$\Delta_y = V_y / K_e$	431.90 mm	Equation (6.3)
$V_u / K_e < \Delta_u$	731.6 < 1,182.9 mm	Admissibility, Equation (6.10): satisfied
$\Omega = V_y / V_d$	3.957	Equation (6.2)
Method A: code-amplified displacement		
$\Delta_{max,A} = C_d \Delta_d / I_e$	407.24 mm	ASCE 7-16 Eq. 12.8-15, Equation (6.11)
V_u at $\Delta_{max,A}$	7,543.7 kN	Capacity curve, linear interpolation at $\Delta_{max,A}$
A up to $\Delta_u = \Delta_{max,A}$	1,638,263 kN·mm	Trapezoidal sum on the capacity curve, Equation (6.7)
K_e	20.358 kN/mm	Secant at 0.6 V_y, reached at 164.21 mm on the initial linear branch, so $K_e = K_i$ (Section 6.3.5)
V_y	5,571.7 kN	Equal-area condition, Equation (6.9)
$\Delta_y = V_y / K_e$	273.68 mm	Equation (6.3)
$V_u / K_e < \Delta_u$	370.5 < 407.2 mm	Admissibility, Equation (6.10): satisfied
$\mu_A = \Delta_{max,A} / \Delta_y$	1.488	Equation (6.3)
$R_\mu = \mu_A$	1.488	Equation (6.4c), $\mu_A > 1$ and $T_e > 0.5$ s
$\Omega = V_y / V_d$	2.528	Equation (6.2)
$R_A = R_\mu \Omega$	3.76	Equation (6.1), reported as R / I_e
Check $(C_d / I_e)(K_e / K_d)$, Eq. (6.6)	3.76	equals R_A
Method B: FEMA 356 target displacement		
$S_a = S_{D1} / T_e$	0.0545 g	ASCE 7-16 Eq. 11.4-6, $T_s < T_e \leq T_L$
$S_d = S_a g T_e^2 / 4\pi^2$	182.26 mm	Spectral displacement of the equivalent oscillator
$C_0 = \Gamma \varphi_{roof}$	1.336	FEMA 356 Section 3.3.3.3.2, calculated from the mode shape
$\delta_t = C_0 C_1 C_2 C_3 S_d$	243.48 mm	FEMA 356 Eq. 3-15, Equation (6.12)
V_u at δ_t	4,937.0 kN	Capacity curve, linear interpolation at δ_t
A up to $\Delta_u = \delta_t$	603,224 kN·mm	Trapezoidal sum on the capacity curve, Equation (6.7)
K_e	20.358 kN/mm	Secant at 0.6 V_y, reached at 133.28 mm on the initial linear branch, so $K_e = K_i$ (Section 6.3.5)
V_y	4,522.3 kN	Equal-area condition, Equation (6.9)
$\Delta_y = V_y / K_e$	222.13 mm	Equation (6.3)
$V_u / K_e < \Delta_u$	242.5 < 243.5 mm	Admissibility, Equation (6.10): satisfied
$\mu_B = \delta_t / \Delta_y$	1.096	Equation (6.3)
$R_\mu = \mu_B$	1.096	Equation (6.4c), $\mu_B > 1$ and $T_e > 0.5$ s
$\Omega = V_y / V_d$	2.052	Equation (6.2)
$R_B = R_\mu \Omega$	2.25	Equation (6.1), reported as R / I_e
Check $\delta_t K_e / V_d$, Eq. (6.5)	2.25	equals R_B
Method C: factor		
$\mu_C = \Delta_{max,C} / \Delta_y$	2.739	Equation (6.3)
$R_\mu = \mu_C$	2.739	Equation (6.4c), $\mu_C > 1$ and $T_e > 0.5$ s
$R_C = R_\mu \Omega$	10.84	Equation (6.1), reported as R / I_e
Check $\Delta_{max,C} K_e / V_d$	10.84	Equation (6.5); equals R_C
Comparison with the code value		
R_A, R_B, R_C (as R / I_e)	3.76, 2.25, 10.84	Compared with 8 / 1.25 = 6.40 (Section 6.4.3)
R_A, R_B, R_C (as R)	4.70, 2.81, 13.54	1.25 × the values above; compared with 8
R_C, first-mode pattern	9.98	Same chain under the first-mode pattern (Table 6.19)

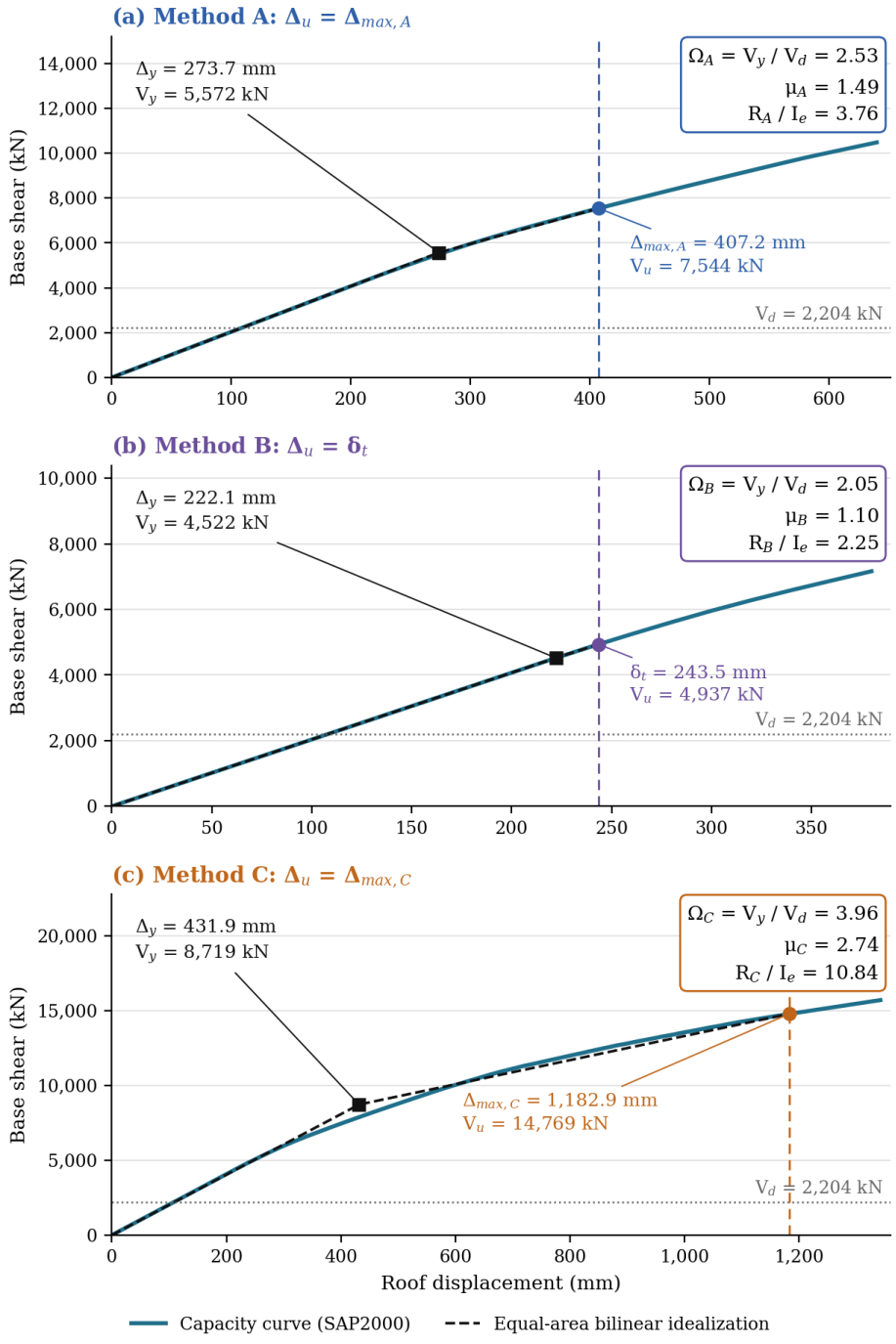

Figure 6.10 Model 4: capacity curve and bilinear idealizations.

6.7.5 Model 5: about 2 percent longitudinal reinforcement

For Model 5 the design base shear is V_d = 2,203.78 kN and the elastic roof displacement Δ_d = 92.554 mm (Table 6.2). The three methods are evaluated in turn, each with the equal-area idealization up to its own maximum displacement (Section 6.3.3). Method A: $\Delta_{max,A}$ = 407.24 mm, V_y = 5,613.7 kN and Δ_y = 275.74 mm, so Ω = 2.547, μ_A = 1.477 and R_A = 3.76. Method B: δ_t = 243.48 mm, V_y = 4,553.6 kN and Δ_y = 223.67 mm, so Ω = 2.066, μ_B = 1.089 and R_B = 2.25. Method C: V_y = 10,177.9 kN and Δ_y = 513.93 mm, so Ω = 4.618. The first beam hinge reaches its Collapse-Prevention limit at $\Delta_{max,C}$ = 1,502.15 mm, which gives μ_C = 2.923 and R_C = 13.50 on the basis of R / I_e, or 16.87 on the basis of R. Model 5 shares the design model of the reference frame (Section 6.2). Its heavier columns carry closer hoops, and the first hinge to reach the limit is a beam of type B2, not a column. Table 6.15 gives the calculation and Figure 6.11 the capacity curve.

Table 6.15 Calculation for Model 5.

Quantity	Value	Source of the value
Elastic design model (ETABS, load case EQX)		
Period used in design	2.150 s	$C_u T_a$ = 1.5 × 1.433, ASCE 7-16 Section 12.8.2.1 (Appendix A.2)
C_s	0.0220	0.044 $S_{DS} I_e$, ASCE 7-16 Eq. 12.8-5 (governs; Table A.2)
W	100,171.9 kN	V_d / C_s (derived)
V_d	2,203.78 kN	ETABS design model of the reference frame, shared by Models 4 and 5 (Section 6.2)
Δ_d	92.554 mm	ETABS design model of the reference frame, shared by Models 4 and 5 (Section 6.2)
$K_d = V_d / \Delta_d$	23.81 kN/mm	Derived
Nonlinear model (SAP2000)		
N, plastic hinges	1,530	SAP2000 model, two hinges per member (Table 6.8)
T_e	3.667 s	SAP2000 Modal Participating Mass Ratios table: X-direction mode with the largest U_X ratio
Γ	86.608	SAP2000 Modal Participation Factors table, U_X, same mode (mass-normalized)
φ_{roof}	0.015424	SAP2000 Joint Displacements table, case MODAL, U_1 of control joint 1087
Capacity curve	100 steps to 2,000.0 mm	SAP2000 Pushover Capacity Curve table, case Pushover-X, uniform pattern, saved at 20.0 mm increments
V_{max} within the run	20,862.4 kN	Largest base shear of the capacity curve
Method C: Collapse-Prevention displacement		
Step 75: Δ, largest D/C	1,500.00 mm, 0.9981	SAP2000 Frame Hinge States table (θ_{p2}, θ_{p3}); Equation (6.13) with the θ_{CP} of each hinge
Step 76: Δ, largest D/C	1,520.00 mm, 1.0157	As above
$\Delta_{max,C}$	1,502.15 mm	Linear interpolation to D/C = 1, Equation (6.14); ASCE 41-17 Section 7.5.3.2.2
Roof drift at $\Delta_{max,C}$	3.34 %	$\Delta_{max,C}$ / 45 m
Hinges with D/C > 1 at step 76	2: frames 2395, 2399	SAP2000 Frame Hinge States table; section B2 45x50
V_u at $\Delta_{max,C}$	18,409.5 kN	Capacity curve, linear interpolation at $\Delta_{max,C}$

Quantity	Value	Source of the value
Method C: bilinear idealization (Section 6.3)		
A up to $\Delta_u = \Delta_{max,C}$	16,740,674 kN·mm	Trapezoidal sum on the capacity curve, Equation (6.7)
K_i	20.358 kN/mm	V / Δ at the first saved step after the origin; starting value of the iteration (Section 6.3.5)
K_e	19.804 kN/mm	Secant at 0.6 V_y, reached at 308.36 mm; FEMA 356 Section 3.3.3.2.4 and Figure 3-1 (Section 6.3.5)
V_y	10,177.9 kN	Equal-area condition, Equation (6.9)
$\Delta_y = V_y / K_e$	513.93 mm	Equation (6.3)
$V_u / K_e < \Delta_u$	929.6 < 1,502.2 mm	Admissibility, Equation (6.10): satisfied
$\Omega = V_y / V_d$	4.618	Equation (6.2)
Method A: code-amplified displacement		
$\Delta_{max,A} = C_d \Delta_d / I_e$	407.24 mm	ASCE 7-16 Eq. 12.8-15, Equation (6.11)
V_u at $\Delta_{max,A}$	7,566.6 kN	Capacity curve, linear interpolation at $\Delta_{max,A}$
A up to $\Delta_u = \Delta_{max,A}$	1,640,542 kN·mm	Trapezoidal sum on the capacity curve, Equation (6.7)
K_e	20.358 kN/mm	Secant at 0.6 V_y, reached at 165.45 mm on the initial linear branch, so $K_e = K_i$ (Section 6.3.5)
V_y	5,613.7 kN	Equal-area condition, Equation (6.9)
$\Delta_y = V_y / K_e$	275.74 mm	Equation (6.3)
$V_u / K_e < \Delta_u$	371.7 < 407.2 mm	Admissibility, Equation (6.10): satisfied
$\mu_A = \Delta_{max,A} / \Delta_y$	1.477	Equation (6.3)
$R_\mu = \mu_A$	1.477	Equation (6.4c), $\mu_A > 1$ and $T_e > 0.5$ s
$\Omega = V_y / V_d$	2.547	Equation (6.2)
$R_A = R_\mu \Omega$	3.76	Equation (6.1), reported as R / I_e
Check $(C_d / I_e)(K_e / K_d)$, Eq. (6.6)	3.76	equals R_A
Method B: FEMA 356 target displacement		
$S_a = S_{D1} / T_e$	0.0545 g	ASCE 7-16 Eq. 11.4-6, $T_s < T_e \leq T_L$
$S_d = S_a g T_e^2 / 4\pi^2$	182.26 mm	Spectral displacement of the equivalent oscillator
$C_0 = \Gamma \varphi_{roof}$	1.336	FEMA 356 Section 3.3.3.3.2, calculated from the mode shape
$\delta_t = C_0 C_1 C_2 C_3 S_d$	243.48 mm	FEMA 356 Eq. 3-15, Equation (6.12)
V_u at δ_t	4,940.1 kN	Capacity curve, linear interpolation at δ_t
A up to $\Delta_u = \delta_t$	603,269 kN·mm	Trapezoidal sum on the capacity curve, Equation (6.7)
K_e	20.358 kN/mm	Secant at 0.6 V_y, reached at 134.20 mm on the initial linear branch, so $K_e = K_i$ (Section 6.3.5)
V_y	4,553.6 kN	Equal-area condition, Equation (6.9)
$\Delta_y = V_y / K_e$	223.67 mm	Equation (6.3)
$V_u / K_e < \Delta_u$	242.7 < 243.5 mm	Admissibility, Equation (6.10): satisfied
$\mu_B = \delta_t / \Delta_y$	1.089	Equation (6.3)
$R_\mu = \mu_B$	1.089	Equation (6.4c), $\mu_B > 1$ and $T_e > 0.5$ s
$\Omega = V_y / V_d$	2.066	Equation (6.2)
$R_B = R_\mu \Omega$	2.25	Equation (6.1), reported as R / I_e
Check $\delta_t K_e / V_d$, Eq. (6.5)	2.25	equals R_B
Method C: factor		
$\mu_C = \Delta_{max,C} / \Delta_y$	2.923	Equation (6.3)
$R_\mu = \mu_C$	2.923	Equation (6.4c), $\mu_C > 1$ and $T_e > 0.5$ s
$R_C = R_\mu \Omega$	13.50	Equation (6.1), reported as R / I_e
Check $\Delta_{max,C} K_e / V_d$	13.50	Equation (6.5); equals R_C
Comparison with the code value		
R_A, R_B, R_C (as R / I_e)	3.76, 2.25, 13.50	Compared with 8 / 1.25 = 6.40 (Section 6.4.3)
R_A, R_B, R_C (as R)	4.70, 2.81, 16.87	1.25 × the values above; compared with 8
R_C, first-mode pattern	10.84	Same chain under the first-mode pattern (Table 6.19)

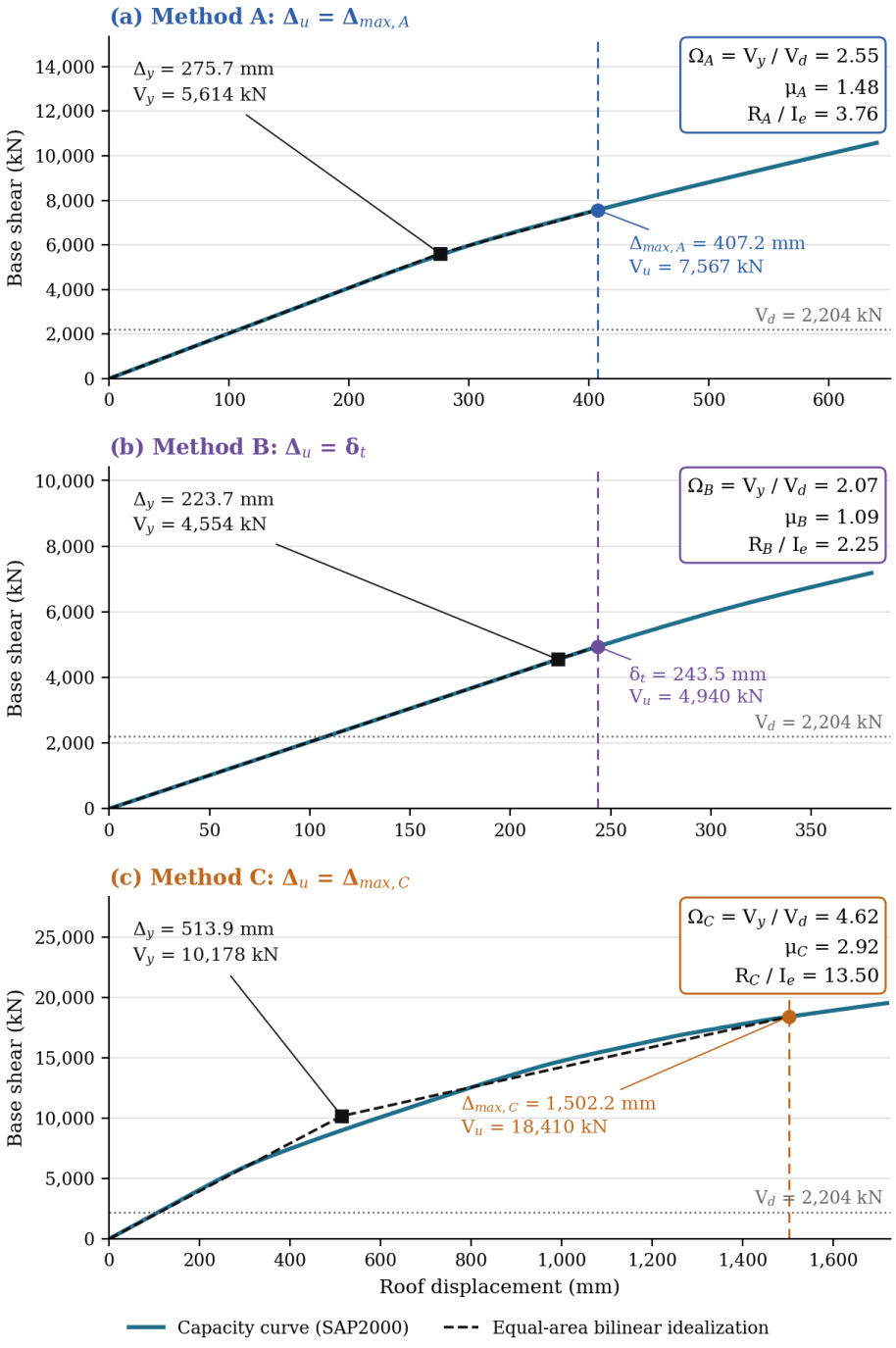

Figure 6.11 Model 5: capacity curve and bilinear idealizations.

6.7.6 Model 6: reduced columns in stories 3 to 5

For Model 6 the design base shear is V_d = 2,199.11 kN and the elastic roof displacement Δ_d = 93.044 mm (Table 6.2). The three methods are evaluated in turn, each with the equal-area idealization up to its own maximum displacement (Section 6.3.3). Method A: $\Delta_{max,A}$ = 409.39 mm, V_y = 5,615.0 kN and Δ_y = 277.73 mm, so Ω = 2.553, μ_A = 1.474 and R_A = 3.76. Method B: δ_t = 243.78 mm, V_y = 4,544.5 kN and Δ_y = 224.78 mm, so Ω = 2.066, μ_B = 1.085 and R_B = 2.24. Method C: V_y = 9,340.7 kN and Δ_y = 468.50 mm, so Ω = 4.247. The first column hinge reaches its Collapse-Prevention limit at $\Delta_{max,C}$ = 1,356.80 mm, which gives μ_C = 2.896 and R_C = 12.30 on the basis of R / I_e, or 15.38 on the basis of R. Model 6 has its own design model, with the perimeter columns of stories 3 to 5 reduced (Table 5.5). Table 6.16 gives the calculation and Figure 6.12 the capacity curve.

Table 6.16 Calculation for Model 6.

Quantity	Value	Source of the value
Elastic design model (ETABS, load case EQX)		
Period used in design	2.150 s	C_u T_a, ASCE 7-16 Section 12.8.2.1; ETABS Auto Seismic table, Period Used
C_s	0.0220	0.044 S_{DS} I_e, ASCE 7-16 Eq. 12.8-5 (governs); ETABS Auto Seismic table, Coeff Used
W	99,959.5 kN	ETABS Auto Seismic table (ASCE 7-16), load pattern EQX, Weight Used
V_d	2,199.11 kN	ETABS Base Reactions table, load case EQX, global FX
Δ_d	93.044 mm	ETABS Joint Displacements table, load case EQX, largest U_x at the roof
$K_d = V_d / \Delta_d$	23.64 kN/mm	Derived
Nonlinear model (SAP2000)		
N, plastic hinges	1,530	SAP2000 model, two hinges per member (Table 6.8)
T_e	3.676 s	SAP2000 Modal Participating Mass Ratios table: X-direction mode with the largest U_X ratio
Γ	86.560	SAP2000 Modal Participation Factors table, U_X, same mode (mass-normalized)
φ_{roof}	0.015416	SAP2000 Joint Displacements table, case MODAL, U_1 of control joint 1087
Capacity curve	100 steps to 2,000.0 mm	SAP2000 Pushover Capacity Curve table, case Pushover-X, uniform pattern, saved at 20.0 mm increments
V_{max} within the run	18,756.4 kN	Largest base shear of the capacity curve
Method C: Collapse-Prevention displacement		
Step 67: Δ, largest D/C	1,340.00 mm, 0.9682	SAP2000 Frame Hinge States table (θ_{p2}, θ_{p3}); Equation (6.13) with the θ_{CP} of each hinge
Step 68: Δ, largest D/C	1,360.00 mm, 1.0061	As above
$\Delta_{max,C}$	1,356.80 mm	Linear interpolation to D/C = 1, Equation (6.14); ASCE 41-17 Section 7.5.3.2.2
Roof drift at $\Delta_{max,C}$	3.02 %	$\Delta_{max,C}$ / 45 m
Hinges with D/C > 1 at step 68	6: frames 2786, 2801, 2816, 2831, 2846, 2861	SAP2000 Frame Hinge States table; section Col 1000X1000
V_u at $\Delta_{max,C}$	16,143.6 kN	Capacity curve, linear interpolation at $\Delta_{max,C}$

Quantity	Value	Source of the value
Method C: bilinear idealization (Section 6.3)		
A up to $\Delta_u = \Delta_{max,C}$	13,506,946 kN·mm	Trapezoidal sum on the capacity curve, Equation (6.7)
K_i	20.217 kN/mm	V / Δ at the first saved step after the origin; starting value of the iteration (Section 6.3.5)
K_e	19.937 kN/mm	Secant at 0.6 V_y, reached at 281.10 mm; FEMA 356 Section 3.3.3.2.4 and Figure 3-1 (Section 6.3.5)
V_y	9,340.7 kN	Equal-area condition, Equation (6.9)
$\Delta_y = V_y / K_e$	468.50 mm	Equation (6.3)
$V_u / K_e < \Delta_u$	809.7 < 1,356.8 mm	Admissibility, Equation (6.10): satisfied
$\Omega = V_y / V_d$	4.247	Equation (6.2)
Method A: code-amplified displacement		
$\Delta_{max,A} = C_d \Delta_d / I_e$	409.39 mm	ASCE 7-16 Eq. 12.8-15, Equation (6.11)
V_u at $\Delta_{max,A}$	7,554.0 kN	Capacity curve, linear interpolation at $\Delta_{max,A}$
A up to $\Delta_u = \Delta_{max,A}$	1,646,665 kN·mm	Trapezoidal sum on the capacity curve, Equation (6.7)
K_e	20.217 kN/mm	Secant at 0.6 V_y, reached at 166.64 mm on the initial linear branch, so $K_e = K_i$ (Section 6.3.5)
V_y	5,615.0 kN	Equal-area condition, Equation (6.9)
$\Delta_y = V_y / K_e$	277.73 mm	Equation (6.3)
$V_u / K_e < \Delta_u$	373.6 < 409.4 mm	Admissibility, Equation (6.10): satisfied
$\mu_A = \Delta_{max,A} / \Delta_y$	1.474	Equation (6.3)
$R_\mu = \mu_A$	1.474	Equation (6.4c), $\mu_A > 1$ and $T_e > 0.5$ s
$\Omega = V_y / V_d$	2.553	Equation (6.2)
$R_A = R_\mu \Omega$	3.76	Equation (6.1), reported as R / I_e
Check $(C_d / I_e)(K_e / K_d)$, Eq. (6.6)	3.76	equals R_A
Method B: FEMA 356 target displacement		
$S_a = S_{D1} / T_e$	0.0544 g	ASCE 7-16 Eq. 11.4-6, $T_s < T_e \leq T_L$
$S_d = S_a g T_e^2 / 4\pi^2$	182.69 mm	Spectral displacement of the equivalent oscillator
$C_0 = \Gamma \varphi_{roof}$	1.334	FEMA 356 Section 3.3.3.3.2, calculated from the mode shape
$\delta_t = C_0 C_1 C_2 C_3 S_d$	243.78 mm	FEMA 356 Eq. 3-15, Equation (6.12)
V_u at δ_t	4,914.7 kN	Capacity curve, linear interpolation at δ_t
A up to $\Delta_u = \delta_t$	600,621 kN·mm	Trapezoidal sum on the capacity curve, Equation (6.7)
K_e	20.217 kN/mm	Secant at 0.6 V_y, reached at 134.87 mm on the initial linear branch, so $K_e = K_i$ (Section 6.3.5)
V_y	4,544.5 kN	Equal-area condition, Equation (6.9)
$\Delta_y = V_y / K_e$	224.78 mm	Equation (6.3)
$V_u / K_e < \Delta_u$	243.1 < 243.8 mm	Admissibility, Equation (6.10): satisfied
$\mu_B = \delta_t / \Delta_y$	1.085	Equation (6.3)
$R_\mu = \mu_B$	1.085	Equation (6.4c), $\mu_B > 1$ and $T_e > 0.5$ s
$\Omega = V_y / V_d$	2.066	Equation (6.2)
$R_B = R_\mu \Omega$	2.24	Equation (6.1), reported as R / I_e
Check $\delta_t K_e / V_d$, Eq. (6.5)	2.24	equals R_B
Method C: factor		
$\mu_C = \Delta_{max,C} / \Delta_y$	2.896	Equation (6.3)
$R_\mu = \mu_C$	2.896	Equation (6.4c), $\mu_C > 1$ and $T_e > 0.5$ s
$R_C = R_\mu \Omega$	12.30	Equation (6.1), reported as R / I_e
Check $\Delta_{max,C} K_e / V_d$	12.30	Equation (6.5); equals R_C
Comparison with the code value		
R_A, R_B, R_C (as R / I_e)	3.76, 2.24, 12.30	Compared with 8 / 1.25 = 6.40 (Section 6.4.3)
R_A, R_B, R_C (as R)	4.70, 2.80, 15.38	1.25 × the values above; compared with 8
R_C, first-mode pattern	10.98	Same chain under the first-mode pattern (Table 6.19)

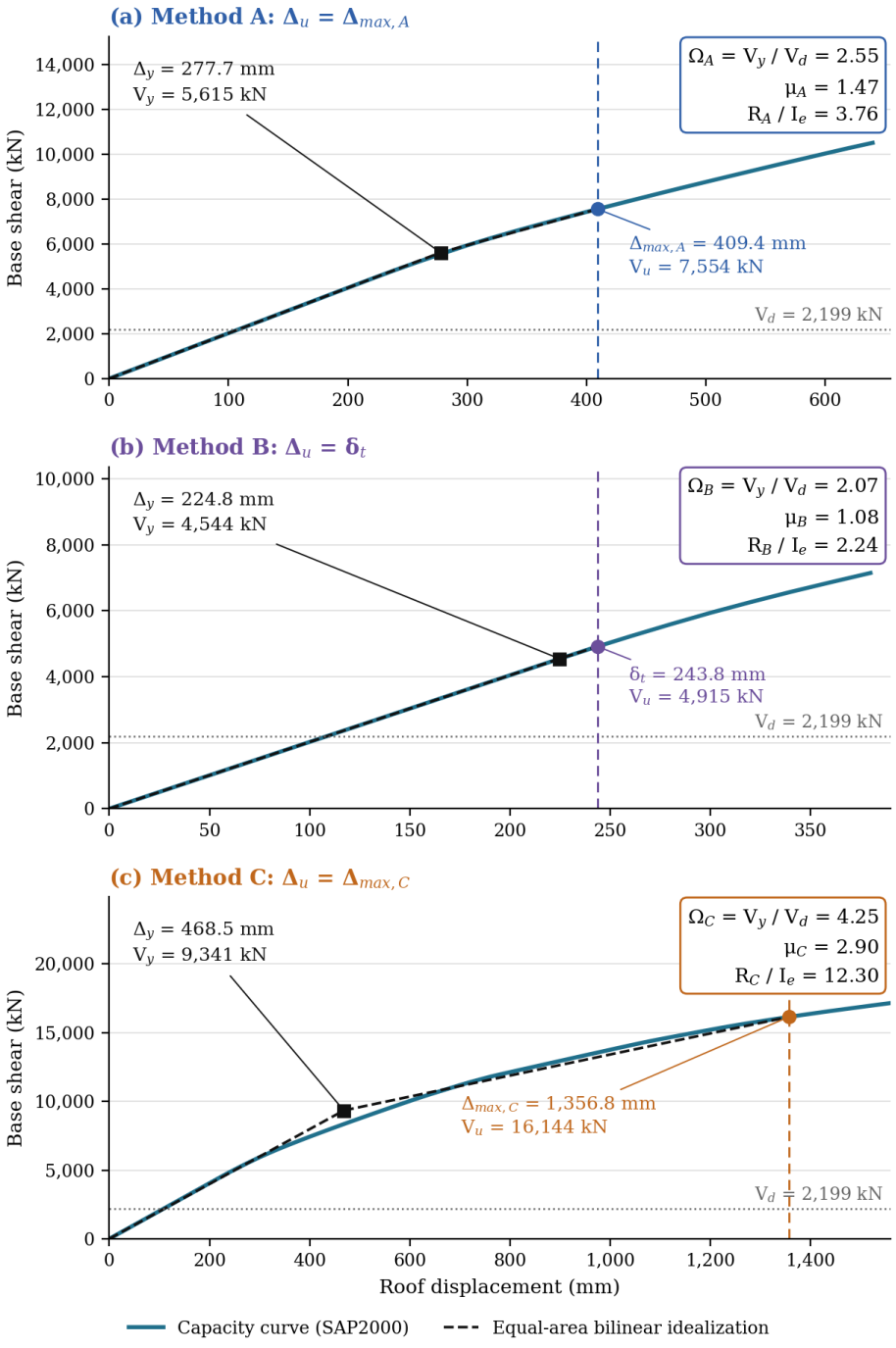

Figure 6.12 Model 6: capacity curve and bilinear idealizations.

6.7.7 Model 7: reduced columns in stories 13 to 15

For Model 7 the design base shear is V_d = 2,199.65 kN and the elastic roof displacement Δ_d = 93.502 mm (Table 6.2). The three methods are evaluated in turn, each with the equal-area idealization up to its own maximum displacement (Section 6.3.3). Method A: $\Delta_{max,A}$ = 411.41 mm, V_y = 5,620.2 kN and Δ_y = 278.94 mm, so Ω = 2.555, μ_A = 1.475 and R_A = 3.77. Method B: δ_t = 246.24 mm, V_y = 4,558.0 kN and Δ_y = 226.22 mm, so Ω = 2.072, μ_B = 1.089 and R_B = 2.26. Method C: V_y = 9,314.8 kN and Δ_y = 468.80 mm, so Ω = 4.235. The first column hinge reaches its Collapse-Prevention limit at $\Delta_{max,C}$ = 1,359.22 mm, which gives μ_C = 2.899 and R_C = 12.28 on the basis of R / I_e, or 15.35 on the basis of R. Model 7 has its own design model, with all columns of stories 13 to 15 reduced to 450 mm (Table 5.5). Table 6.17 gives the calculation and Figure 6.13 the capacity curve.

Table 6.17 Calculation for Model 7.

Quantity	Value	Source of the value
Elastic design model (ETABS, load case EQX)		
Period used in design	2.150 s	C_u T_a, ASCE 7-16 Section 12.8.2.1; ETABS Auto Seismic table, Period Used
C_s	0.0220	0.044 S_{DS} I_e, ASCE 7-16 Eq. 12.8-5 (governs); ETABS Auto Seismic table, Coeff Used
W	99,984.3 kN	ETABS Auto Seismic table (ASCE 7-16), load pattern EQX, Weight Used
V_d	2,199.65 kN	ETABS Base Reactions table, load case EQX, global FX
Δ_d	93.502 mm	ETABS Joint Displacements table, load case EQX, largest U_x at the roof
$K_d = V_d / \Delta_d$	23.53 kN/mm	Derived
Nonlinear model (SAP2000)		
N, plastic hinges	1,530	SAP2000 model, two hinges per member (Table 6.8)
T_e	3.669 s	SAP2000 Modal Participating Mass Ratios table: X-direction mode with the largest U_X ratio
Γ	86.372	SAP2000 Modal Participation Factors table, U_X, same mode (mass-normalized)
φ_{roof}	0.015634	SAP2000 Joint Displacements table, case MODAL, U_1 of control joint 1087
Capacity curve	100 steps to 2,000.0 mm	SAP2000 Pushover Capacity Curve table, case Pushover-X, uniform pattern, saved at 20.0 mm increments
V_{max} within the run	18,981.2 kN	Largest base shear of the capacity curve
Method C: Collapse-Prevention displacement		
Step 67: Δ, largest D/C	1,340.00 mm, 0.9634	SAP2000 Frame Hinge States table (θ_{p2}, θ_{p3}); Equation (6.13) with the θ_{CP} of each hinge
Step 68: Δ, largest D/C	1,360.00 mm, 1.0015	As above
$\Delta_{max,C}$	1,359.22 mm	Linear interpolation to D/C = 1, Equation (6.14); ASCE 41-17 Section 7.5.3.2.2
Roof drift at $\Delta_{max,C}$	3.02 %	$\Delta_{max,C}$ / 45 m
Hinges with D/C > 1 at step 68	2: frames 2831, 2861	SAP2000 Frame Hinge States table; section Col 1000X1000
V_u at $\Delta_{max,C}$	16,208.0 kN	Capacity curve, linear interpolation at $\Delta_{max,C}$
Method C: bilinear idealization (Section 6.3)		
A up to $\Delta_u = \Delta_{max,C}$	13,546,377 kN·mm	Trapezoidal sum on the capacity curve, Equation (6.7)

Quantity	Value	Source of the value
K_i	20.149 kN/mm	V / Δ at the first saved step after the origin; starting value of the iteration (Section 6.3.5)
K_e	19.869 kN/mm	Secant at 0.6 V_y, reached at 281.28 mm; FEMA 356 Section 3.3.3.2.4 and Figure 3-1 (Section 6.3.5)
V_y	9,314.8 kN	Equal-area condition, Equation (6.9)
$\Delta_y = V_y / K_e$	468.80 mm	Equation (6.3)
$V_u / K_e < \Delta_u$	815.7 < 1,359.2 mm	Admissibility, Equation (6.10): satisfied
$\Omega = V_y / V_d$	4.235	Equation (6.2)
Method A: code-amplified displacement		
$\Delta_{max,A} = C_d \Delta_d / I_e$	411.41 mm	ASCE 7-16 Eq. 12.8-15, Equation (6.11)
V_u at $\Delta_{max,A}$	7,574.0 kN	Capacity curve, linear interpolation at $\Delta_{max,A}$
A up to $\Delta_u = \Delta_{max,A}$	1,657,765 kN·mm	Trapezoidal sum on the capacity curve, Equation (6.7)
K_e	20.149 kN/mm	Secant at 0.6 V_y, reached at 167.36 mm on the initial linear branch, so $K_e = K_i$ (Section 6.3.5)
V_y	5,620.2 kN	Equal-area condition, Equation (6.9)
$\Delta_y = V_y / K_e$	278.94 mm	Equation (6.3)
$V_u / K_e < \Delta_u$	375.9 < 411.4 mm	Admissibility, Equation (6.10): satisfied
$\mu_A = \Delta_{max,A} / \Delta_y$	1.475	Equation (6.3)
$R_\mu = \mu_A$	1.475	Equation (6.4c), $\mu_A > 1$ and $T_e > 0.5$ s
$\Omega = V_y / V_d$	2.555	Equation (6.2)
$R_A = R_\mu \Omega$	3.77	Equation (6.1), reported as R / I_e
Check $(C_d / I_e)(K_e / K_d)$, Eq. (6.6)	3.77	equals R_A
Method B: FEMA 356 target displacement		
$S_a = S_{D1} / T_e$	0.0545 g	ASCE 7-16 Eq. 11.4-6, $T_s < T_e \leq T_L$
$S_d = S_a g T_e^2 / 4\pi^2$	182.36 mm	Spectral displacement of the equivalent oscillator
$C_0 = \Gamma \varphi_{roof}$	1.350	FEMA 356 Section 3.3.3.3.2, calculated from the mode shape
$\delta_t = C_0 C_1 C_2 C_3 S_d$	246.24 mm	FEMA 356 Eq. 3-15, Equation (6.12)
V_u at δ_t	4,944.2 kN	Capacity curve, linear interpolation at δ_t
A up to $\Delta_u = \delta_t$	610,689 kN·mm	Trapezoidal sum on the capacity curve, Equation (6.7)
K_e	20.149 kN/mm	Secant at 0.6 V_y, reached at 135.73 mm on the initial linear branch, so $K_e = K_i$ (Section 6.3.5)
V_y	4,558.0 kN	Equal-area condition, Equation (6.9)
$\Delta_y = V_y / K_e$	226.22 mm	Equation (6.3)
$V_u / K_e < \Delta_u$	245.4 < 246.2 mm	Admissibility, Equation (6.10): satisfied
$\mu_B = \delta_t / \Delta_y$	1.089	Equation (6.3)
$R_\mu = \mu_B$	1.089	Equation (6.4c), $\mu_B > 1$ and $T_e > 0.5$ s
$\Omega = V_y / V_d$	2.072	Equation (6.2)
$R_B = R_\mu \Omega$	2.26	Equation (6.1), reported as R / I_e
Check $\delta_t K_e / V_d$, Eq. (6.5)	2.26	equals R_B
Method C: factor		
$\mu_C = \Delta_{max,C} / \Delta_y$	2.899	Equation (6.3)
$R_\mu = \mu_C$	2.899	Equation (6.4c), $\mu_C > 1$ and $T_e > 0.5$ s
$R_C = R_\mu \Omega$	12.28	Equation (6.1), reported as R / I_e
Check $\Delta_{max,C} K_e / V_d$	12.28	Equation (6.5); equals R_C
Comparison with the code value		
R_A, R_B, R_C (as R / I_e)	3.77, 2.26, 12.28	Compared with 8 / 1.25 = 6.40 (Section 6.4.3)
R_A, R_B, R_C (as R)	4.71, 2.82, 15.35	1.25 × the values above; compared with 8
R_C, first-mode pattern	not reached	Largest D/C = 0.981 at 1,641.7 mm, the end of the run (Table 6.19)

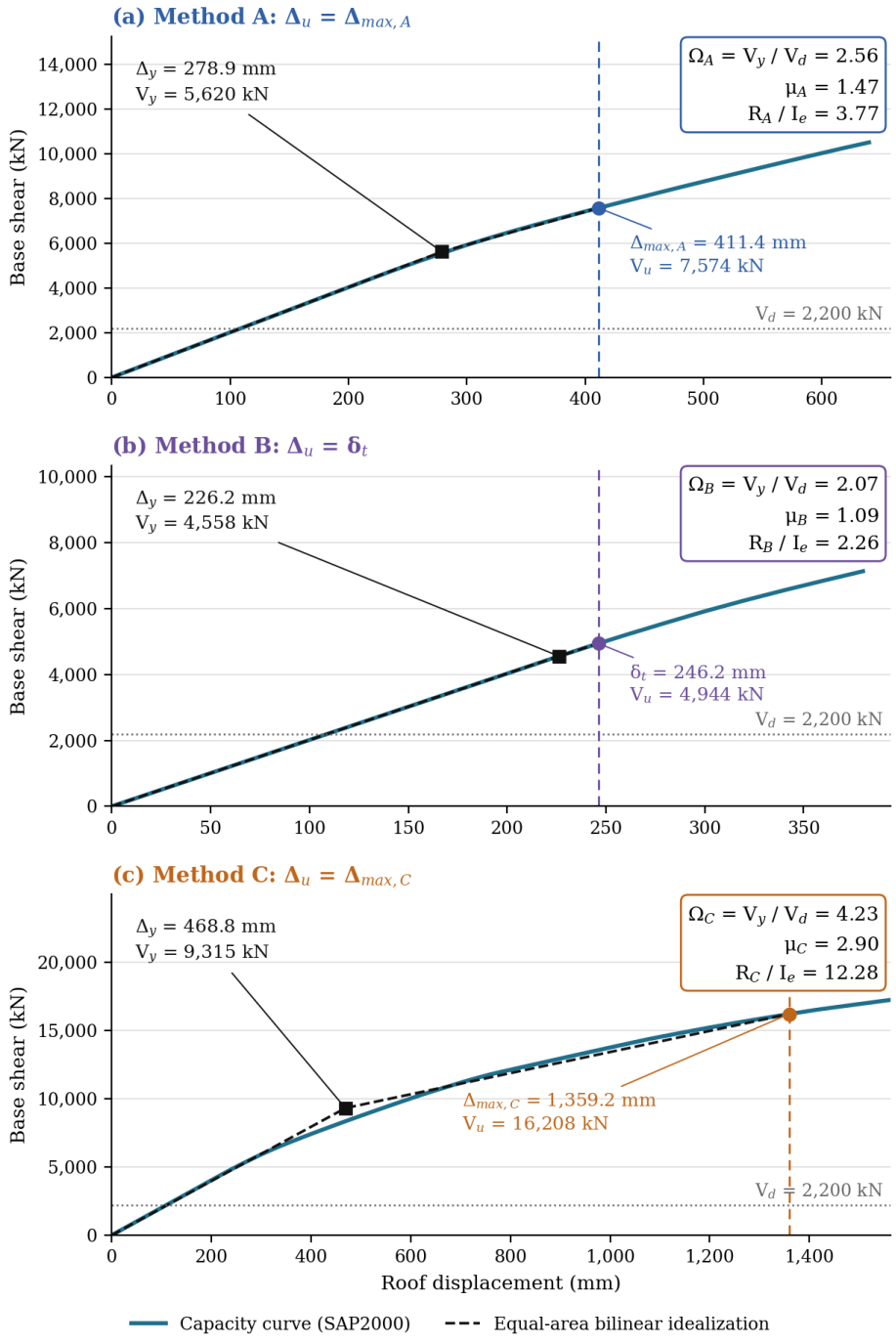

Figure 6.13 Model 7: capacity curve and bilinear idealizations.

6.8 Consolidated Results

6.8.1 Uniform pattern

Table 6.18 brings together the results of Section 6.7 for the seven models under the uniform pattern, and Figure 6.14 compares the capacity curves of Models 4 to 7 with that of the reference frame.

Table 6.18 Consolidated results, uniform pattern.

Quantity	Four-story	Six-story	Fifteen-story reference	Model 4	Model 5	Model 6	Model 7
V_d (kN)	1,219.82	1,317.71	2,203.78	2,203.78	2,203.78	2,199.11	2,199.65
$\Delta_{max,A}$ (mm)	74.76	112.44	407.24	407.24	407.24	409.39	411.41
δ_t (mm)	76.09	100.35	243.48	243.48	243.48	243.78	246.24
$\Delta_{max,C}$ (mm)	239.77	323.54	1,352.80	1,182.86	1,502.15	1,356.80	1,359.22
V_u (kN)	6,434.1	8,571.4	16,209.9	14,769.1	18,409.5	16,143.6	16,208.0
A (kN·m), Method C	1,126.2	1,965.2	13,501.3	10,702.3	16,740.7	13,506.9	13,546.4
K_e (kN/mm), Method C	51.94	48.50	20.07	20.19	19.80	19.94	19.87
V_y (kN), Method C	6,125.1	7,882.1	9,304.9	8,719.3	10,177.9	9,340.7	9,314.8
Δ_y (mm), Method C	117.94	162.51	463.53	431.90	513.93	468.50	468.80
Δ_y / $\Delta_{max,C}$	0.492	0.502	0.343	0.365	0.342	0.345	0.345
Ω, Method C	5.021	5.982	4.222	3.957	4.618	4.247	4.235
V_y (kN), Method A	2,590.8	4,037.5	5,613.7	5,571.7	5,613.7	5,615.0	5,620.2
Δ_y / $\Delta_{max,A}$	0.644	0.731	0.677	0.672	0.677	0.678	0.678
μ_A	1.553	1.368	1.477	1.488	1.477	1.474	1.475
$R_A = \Delta_{max,A} K_e / V_d$	3.30	4.19	3.76	3.76	3.76	3.76	3.77
V_y (kN), Method B	2,606.0	3,752.0	4,553.6	4,522.3	4,553.6	4,544.5	4,558.0
Δ_y / δ_t	0.636	0.761	0.919	0.912	0.919	0.922	0.919
μ_B	1.571	1.313	1.089	1.096	1.089	1.085	1.089
$R_B = \delta_t K_e / V_d$	3.36	3.74	2.25	2.25	2.25	2.24	2.26
μ_C	2.033	1.991	2.918	2.739	2.923	2.896	2.899
$R_C = \mu_C \Omega$	10.21	11.91	12.32	10.84	13.50	12.30	12.28
Check: $\Delta_{max,C} K_e / V_d$, Eq. (6.5)	10.21	11.91	12.32	10.84	13.50	12.30	12.28
$R_A \times 1.25$	4.12	5.24	4.70	4.70	4.70	4.70	4.71
$R_B \times 1.25$	4.20	4.67	2.81	2.81	2.81	2.80	2.82
$R_C \times 1.25$	12.76	14.89	15.40	13.54	16.87	15.38	15.35

Note. Factors are R / I_e, compared with 6.40; the last three rows are R, compared with 8.

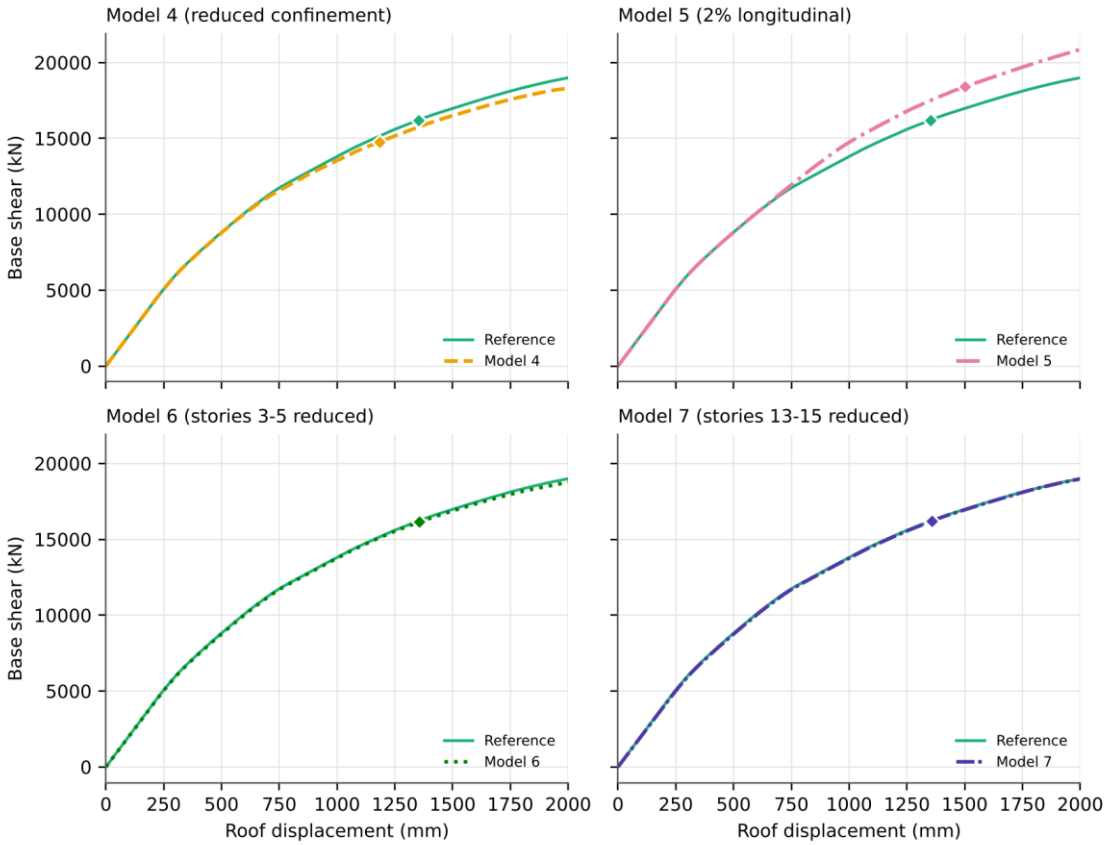

Figure 6.14 Capacity curves of Models 4 to 7 and the reference frame.

The four-story frame reaches the Collapse-Prevention criterion at 239.77 mm, a roof drift of 2.00 percent, and the six-story frame at 323.54 mm (1.80 percent); in both, $\Delta_{max,C}$ falls just beyond the peak of the capacity curve. The fifteen-story models reach it between 1,182.86 and 1,502.15 mm, roof drifts of 2.63 to 3.34 percent, on a capacity curve that is still rising; at $\Delta_{max,C}$ the base shear of the reference frame is 7.36 times the design base shear, while the effective yield base shear is 4.22 times it.

The factors of Table 6.18 satisfy Equation (6.5) in every model and under every method, since $\mu > 1$ throughout. The yield displacement lies between 64 and 73 percent of the anchor displacement under Method A, between 64 and 92 percent under Method B, and between 34 and 50 percent under Method C, so condition (6.10) is satisfied in every case, with the smallest margin under Method B for the fifteen-story models.

6.8.2 First-mode load pattern and the envelope of the two patterns

Two lateral load patterns were analyzed (Section 5.7.3). The uniform pattern applies to each floor a force proportional to its mass, the same acceleration at every level; it loads the lower stories relatively more and is the second of the two patterns that FEMA

356 Section 3.3.3.2.3 requires. The first-mode pattern applies forces proportional to the mass times the fundamental mode shape, so the forces grow with height; it is the single pattern prescribed by ASCE 41-17 Section 7.4.3.2.3, whose commentary notes that multiple patterns add little accuracy. The uniform pattern is reported as the primary basis of Sections 6.3 to 6.8.1, and the first-mode results are given here. Because the two standards differ, the conclusions of this chapter are stated for the lower of the two patterns in each model as well.

The same chain was evaluated for the first-mode pattern. Table 6.19 gives the results, and Figure 6.15 compares the capacity curves of the two patterns.

Table 6.19 Results under the first-mode pattern.

Quantity	Four-story	Six-story	Fifteen-story reference	Model 4	Model 5	Model 6	Model 7
$\Delta_{max,C}$ (mm)	317.31	—	1,720.73	1,530.65	1,660.46	1,710.96	—
V_y (kN)	5,753.9	—	8,070.4	7,385.2	7,373.1	8,054.8	—
K_e (kN/mm)	41.25	—	14.19	14.37	14.39	14.11	—
Ω, Method C	4.717	—	3.662	3.351	3.346	3.663	—
R_A, first-mode pattern	2.66	3.26	2.70	2.70	2.70	2.70	2.68
R_B, first-mode pattern	2.71	2.91	1.61	1.61	1.61	1.61	1.61
μ_C	2.275	—	3.025	2.978	3.240	2.996	—
R_C	10.73	—	11.08	9.98	10.84	10.98	—
R_C, uniform pattern	10.21	11.91	12.32	10.84	13.50	12.30	12.28
R_C, lower of the two patterns	10.21	11.91	11.08	9.98	10.84	10.98	12.28
Largest D/C at end of run	—	0.738 at 425.7 mm	—	—	—	—	0.981 at 1,641.7 mm

Note. Factors are R / I_e. A dash marks a run in which no component reached the Collapse-Prevention criterion.

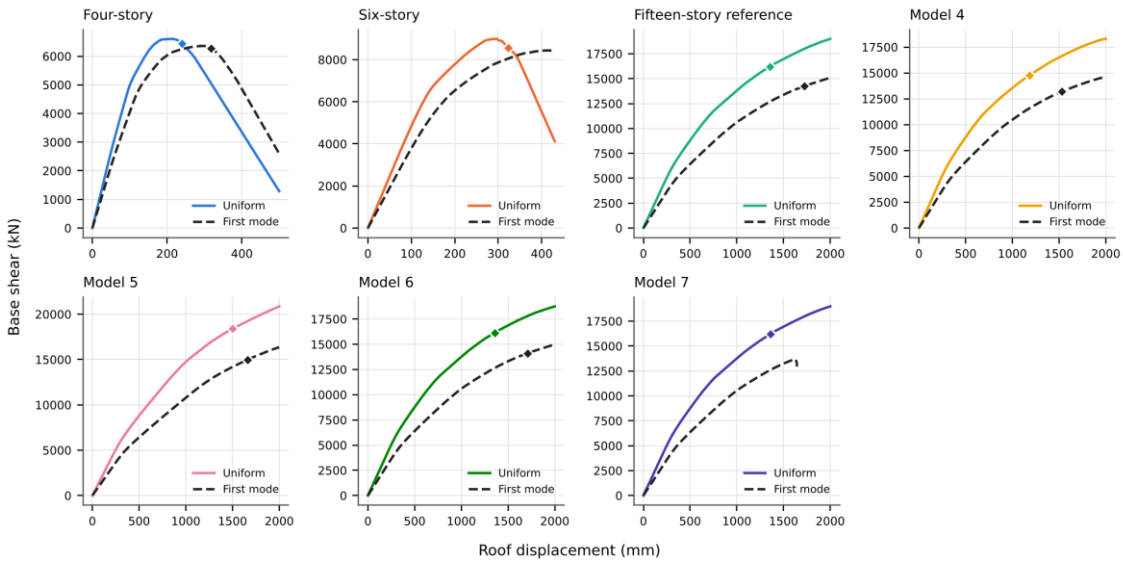

Figure 6.15 Capacity curves under the two load patterns.

In the six-story frame and in Model 7 no component reached its Collapse-Prevention criterion within the analyzed range under the first-mode pattern: the largest D/C ratio at the end of the run was 0.738 at 425.7 mm and 0.981 at 1,641.7 mm, where the Model 7 analysis stopped converging. For these two runs $\Delta_{max,C}$ is larger than the last analyzed displacement, no first-mode factor is reported, and the lower-bound row of Table 6.19 carries the uniform value.

For the five models that reached the criterion, the first-mode pattern gives a lower overstrength factor in every case, since it applies a larger share of the lateral load to the upper stories and the base shear at a given roof displacement is lower (Figure 6.15). R_C is lower under the first-mode pattern for the four fifteen-story models, by between 7.9 and 19.7 percent, and higher by 5.1 percent for the four-story frame, where the larger $\Delta_{max,C}$ outweighs the lower Ω. Under the first-mode pattern the initial stiffness of the capacity curve is lower, so R_A and R_B are lower than under the uniform pattern: R_A lies between 2.66 and 3.26 and R_B between 1.61 and 2.91.

Taking the lower of the two patterns in each model, R_C lies between 9.98 and 12.28 on the basis of R / I_e (12.47 to 15.35 on the basis of R), above 6.40 in every model, while R_A and R_B lie below 6.40 under both patterns. The comparison with the code value is therefore the same under either pattern.

6.9 Comparative Discussion

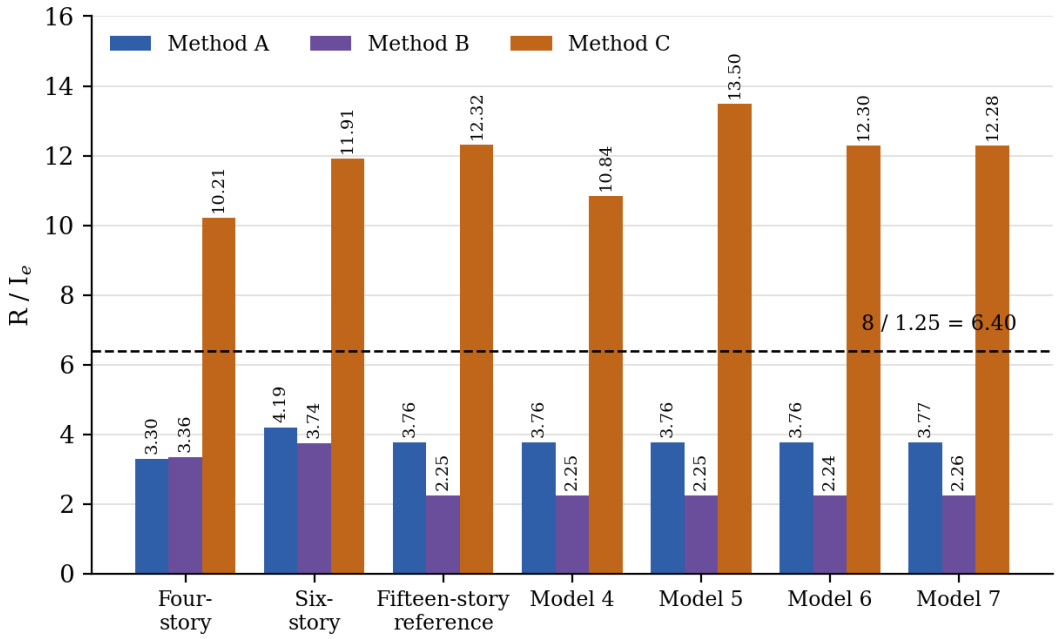

Figure 6.16 Estimated factors of the seven models.

6.9.1 The three definitions compared

All three methods give a ductility ratio above unity, but of very different size: μ_A between 1.37 and 1.55, μ_B between 1.08 and 1.57, and μ_C between 1.99 and 2.92. Methods A and B evaluate the frames at displacements at which they have only begun to yield, and their factors, 3.30 to 4.19 and 2.24 to 3.74, are the smallest in every model. Method C, which measures the displacement capacity at the Collapse-Prevention level, gives the largest factor in every model. The ordering $R_C > R_A$ and $R_C > R_B$ is a consequence of the definitions and of the modeling framework adopted in this study, in particular of the stiffness of the nonlinear model relative to the design model (Equation 6.6); it is not evidence that one definition is generally superior to the others.

6.9.2 Comparison with the tabulated value of ASCE 7-16

On the basis of R / I_e, the factors of Method A lie between 3.30 and 4.19 and those of Method B between 2.24 and 3.74, below the comparison value of 6.40 in every model, and the factors of Method C lie between 10.21 and 13.50, above it in every model. On the basis of R the same statements read 4.12 to 5.24, 2.80 to 4.67, and 12.76 to 16.87 against 8.

The two results answer different questions and must not be read as a contradiction. Methods A and B measure the factor that a prescribed displacement demand mobilizes. The code-amplified displacement and the target displacement lie at 1.1 to 1.6 times the corresponding effective yield displacement, so only a small part of the ductility capacity of the frames enters them. A value below 6.40 under these methods does not indicate that the tabulated factor is unsafe. Method C measures the strength and the deformation capacity available up to the Collapse-Prevention level of ASCE 41-17, and it is the comparison that bears on the adequacy of the tabulated factor. On that comparison the code value is conservative for all the archetypes examined.

In engineering terms, the results mean the following. A response modification factor says by how much the elastic earthquake force may be reduced for design because the frame will be stronger than designed and will deform inelastically without collapse. A value of R_C above the code value means that the frames, designed with R = 8, can tolerate the design earthquake with margin to the Collapse-Prevention limit: the code value is on the safe side for these frames, and it is not too large. A value of R_A or R_B below the code value does not mean the opposite. Methods A and B stop at a prescribed displacement shortly beyond first yield, so they leave out most of the deformation capacity of the frames; they underestimate the available R by construction rather than reveal that the code overestimates it. Neither result supports lowering the code value. Under the lower of the two load patterns of Section 6.8.2, R_C lies between 9.98 and 12.28 on the basis of R / I_e, and the statement does not change.

The overstrength factors of Method C are also well above the tabulated system overstrength factor $\Omega_0 = 3.0$ of ASCE 7-16 Table 12.2-1: 4.95 to 7.48 on the basis of R. The two quantities are not the same: Ω_0 is a design amplification factor for force-controlled elements, whereas Ω is computed from the capacity curve. The sources of the margin, which include member sizing for drift and for the strong-column weak-beam requirement, minimum reinforcement and detailing, strength reduction factors, and expected material strengths, are not separated in this study.

Table 6.20 places these ranges beside published estimates for moment-resisting frames. The comparison is made on the basis of R, since the published values are for structures in occupancy categories in which the importance factor is unity. The studies listed differ from this one, and from each other, in structural system, design code, hazard

level and definition of the maximum displacement, which the table states for each; the table is therefore a comparison of ranges and not of like-for-like values.

Table 6.20 Present ranges and published estimates of R.

Source	System	Method of estimation	Range of R
ASCE 7-16 Table 12.2-1	Special moment frame	Tabulated	8
AlHamaydeh et al. (2011)	Special moment frame	Nonlinear dynamic analysis (IDARC-2D)	4 to 7
Mondal et al. (2013)	Ductile RC frame (IS 1893)	Pushover, two performance levels	4.23 to 4.96 (stability level); 5.46 to 8.48 (ultimate level)
Al-Ahmar and Al-Samara (2015)	Special moment frame	Pushover, 25 frames, 3 to 15 stories	5 to 12
Suquillo et al. (2026)	Reinforced concrete moment frame	Pushover, 0.8 V_{max}, with redundancy index	3.80 to 14.56
Abuznaid (2023); Shrouf (2025)	Intermediate moment frame	Pushover, 0.8 V_{max} criterion	4.5 to 6.9
Present study, Methods A and B	Special moment frame	Demand displacement of ASCE 7-16 and FEMA 356	2.80 to 5.24
Present study, Method C	Special moment frame	ASCE 41-17 Collapse-Prevention capacity	12.76 to 16.87

The range of Methods A and B, 2.80 to 5.24, overlaps the lower part of the range of Suquillo et al. (2026) and lies almost entirely below the range of Al-Ahmar and Al-Samara (2015). The range of Method C lies above the range of Al-Ahmar and Al-Samara (2015); it overlaps the upper part of the range of Suquillo et al. (2026) and extends above it. The difference is consistent with the definition of the ultimate displacement: several of the studies listed use the strength drop to 0.8 V_{max}, which the fifteen-story capacity curves of this study do not reach within 2.0 m, whereas Method C uses the component acceptance criteria of ASCE 41-17. The comparison with the intermediate-frame theses at this institution is in addition a comparison across two structural systems and is presented as a range comparison for that reason.

6.9.3 The effect of building height

Across the height family R_C is 10.21, 11.91 and 12.32 for the four-, six- and fifteen-story frames, while Ω is 5.02, 5.98 and 4.22 and μ_C is 2.03, 1.99 and 2.92. The capacity-based factor increases with height in this family, but its two components do not: the overstrength factor is highest for the six-story frame and lowest for the fifteen-story

frame, and the ductility ratio is highest for the fifteen-story frame. The three frames are code-designed archetypes whose member dimensions, reinforcement, axial forces, stiffness, strength distribution and periods all change with height, so the observed differences cannot be attributed to height alone, and three heights do not establish a general trend.

6.9.4 The parametric variants

Model 4, the variant with 100 mm hoop spacing and f'_{cE} = 29 MPa, gives R_C = 10.84 against 12.32 for the reference frame (-12.1 percent). Both components fall: Ω from 4.22 to 3.96, through the lower concrete strength, and μ_C from 2.92 to 2.74, through the lower ρ_t of the base columns, which reach their criterion earlier (1,182.86 mm against 1,352.80 mm). Because the two parameters change together, the result measures their combined effect and cannot be attributed to the hoop spacing alone.

Model 5, with about 2 percent longitudinal reinforcement in most column sections, gives the largest factor of the family, R_C = 13.50 (+9.5 percent). The increase comes from the overstrength factor, 4.62 against 4.22, while μ_C is practically unchanged (2.92 against 2.92). The stronger columns also move the first component to reach its criterion from the base columns to a beam (Section 6.6.4).

Models 6 and 7, with reduced columns in stories 3 to 5 and in stories 13 to 15, give R_C = 12.30 and 12.28, within 0.4 percent of the reference frame. In both variants the base columns of the first story still govern, and neither reduction changed the capacity curve materially up to $\Delta_{max,C}$ (Figure 6.14). Within the range examined, a section reduction away from the first story had no measurable effect on the estimated factor, whatever its location over the height, which is consistent with the expectation stated in Section 3.8.

The ordering of the variants is the same under the 1-percent criterion of Table 6.9, so these conclusions do not depend on the definition of $\Delta_{max,C}$. They apply to the archetypes examined and are not generalized beyond them.

6.9.5 The effect of the load pattern

The first-mode pattern lowers the overstrength factor of every model that reached the criterion under it and lowers R_C of the four fifteen-story models evaluated, and in the reference frame and Models 5 and 6 it moves the first component to reach Collapse Prevention to beams of type B2 at the third to fifth floor levels (Figure 6.5). The two

patterns therefore bound the capacity-based factor of the tall frames from above and below, and the factor remains above the code value under both. For the low-rise frames the effect of the pattern is small. Higher-mode effects beyond those represented by the two patterns are not captured by the nonlinear static procedure (Section 6.10).

6.10 Limitations of the Estimation

Model 4 combines two changes. It changes the hoop spacing and the concrete strength together, so its result cannot be attributed to the spacing alone. A variant with 100 mm spacing and 35 MPa concrete would isolate the effect of spacing; it was not analyzed.

Material and load assumptions. The expected yield strength of the reinforcement, 455.05 MPa, is lower than 1.25 f_y of ASCE 41-17 Table 10-1, and the gravity load case is 1.0 D + 0.25 L rather than 1.1 (D + 0.25 L). Both are declared departures (Sections 5.3 and 5.7.3); a higher steel strength would raise V_y and Ω (inference, not quantified).

Design and analysis stiffness. The design models use the cracked-section factors of ACI 318-19 and the nonlinear models the effective-stiffness factors of ASCE 41-17. The ratio K_e / K_d enters Method A directly through Equation (6.6), so R_A holds for these stiffness assumptions; with equal stiffness in the two models, it would equal C_d / I_e = 4.40, still below 6.40.

Nonlinear static analysis only. The fifteen-story frames have an effective period of about 3.67 s, where higher modes contribute to the response. Two lateral load patterns were analyzed, but no modal pushover or nonlinear dynamic analysis was performed, so no result of this chapter is verified against a time-history response, and the ductility reduction factors rest on the Newmark-Hall relations rather than on computed inelastic spectra.

Hinge modeling. The column hinges are generated automatically by SAP2000 to ASCE 41-17 Table 10-8, so that both their backbone and their acceptance criterion depend on the same section properties and axial load; the beam backbones are symmetric, with the sign-dependent criteria applied in the evaluation (Section 5.7.2). Shear and joint failures are not modeled; the design checks of Section 5.6 indicate that they do not govern.

Axial load in the column criteria. ASCE 41-17 Table 10-8 defines N_{UD} as the maximum compressive axial load including the effects of the lateral forces (Equation 7-

34). The Collapse-Prevention limits of the columns in this study were evaluated with the axial load of the gravity case. For the exterior columns, whose axial load rises with overturning, this overestimates the limit and is unconservative; for the interior first-story columns that govern Method C, whose axial load changes little under lateral load, the effect is expected to be small (inference, not quantified). This is a declared departure.

Load pattern. ASCE 41-17 Section 7.4.3.2.3 prescribes a single pattern proportional to the fundamental mode, and the results of that pattern are reported in Section 6.8.2. The uniform pattern used as the primary basis is that of FEMA 356 Section 3.3.3.2.3. FEMA 356 also requires, for fundamental periods above 1.0 s, a modal pattern based on a response spectrum analysis; that pattern was not analyzed.

Runs that did not reach the criterion. Under the first-mode pattern the six-story frame and Model 7 did not reach the Collapse-Prevention criterion within the analyzed range, and no factor is reported for them.

One site, one hazard level, one plan. The seven models share one site (Site Class A), one hazard level, one plan and one set of nominal materials, and the redundancy of the system was not varied. The design of the fifteen-story models is governed by the minimum base shear coefficient. The results are specific to these conditions.

6.11 Summary of Findings

F1. Under the uniform pattern, Method A gives R_A between 3.30 and 4.19 and Method B gives R_B between 2.24 and 3.74 on the basis of R / I_e (4.12 to 5.24 and 2.80 to 4.67 on the basis of R), with ductility ratios between 1.08 and 1.57. These values are below 6.40 (and 8); they measure the factor mobilized at a prescribed demand, not the capacity of the frames.

F2. Method C, defined by the first component that reaches its ASCE 41-17 Collapse-Prevention criterion, gives R_C between 10.21 and 13.50 on the basis of R / I_e (12.76 to 16.87 on the basis of R), above the code value in every model.

F3. $R_A = (C_d / I_e)(K_e / K_d)$ (Equation 6.6). Because the effective stiffness of the nonlinear model is 75 to 95 percent of the design stiffness, R_A cannot exceed $C_d / I_e = 4.40$.

F4. Under the uniform pattern the first components to reach Collapse Prevention are the base hinges of the first-story interior columns, except in Model 5, where a beam governs.

Under the first-mode pattern beams of the third to fifth floor levels govern in the reference frame and in Models 5 and 6.

F5. R_C increases from the four-story (10.21) to the six-story (11.91) and fifteen-story (12.32) frames, but Ω does not follow height, and the frames differ in more than height.

F6. Model 4 lowers R_C by 12.1 percent, as the combined effect of 100 mm hoops and 29 MPa concrete; the variant with about 2 percent longitudinal reinforcement raises it by 9.5 percent through Ω; the two column-reduction variants leave it practically unchanged.

F7. The first-mode pattern, which is the pattern of ASCE 41-17, lowers Ω in every model that reached the criterion under it and R_C in the fifteen-story models that reached it. Taking the lower of the two patterns in each model, R_C lies between 9.98 and 12.28 on the basis of R / I_e, and all values remain above 6.40.

F8. Criteria based on a fraction of the hinges beyond Collapse Prevention (0.5 to 2 percent) raise R_C by up to 22 percent but do not change the comparison with the code value or the ordering of the variants.

F9. The factor estimated with the design base shear of a Risk Category III structure is R / I_e; it must be compared with $8 / 1.25 = 6.40$, or multiplied by 1.25 and compared with 8.

CHAPTER 7 CONCLUSIONS AND RECOMMENDATIONS

7.1 Summary of the Study

This study estimated the response modification factor of reinforced concrete special moment-resisting frames designed to ASCE 7-16 (ASCE, 2016) and detailed to ACI 318-19 Chapter 18 (ACI, 2019), for a Site Class A rock site with the hazard of seismic Zone 3 of Palestine (S_{DS} = 0.40 g, S_{D1} = 0.20 g) and Risk Category III. Seven three-dimensional models were designed in ETABS and analyzed by nonlinear static pushover analysis in SAP2000 under a uniform and a first-mode load pattern: frames of four, six and fifteen stories, and four variants of the fifteen-story frame. The factor was estimated under three code-based definitions of the maximum displacement (Methods A, B and C). All factors are reported as R / I_e and compared with 8 / 1.25 = 6.40.

7.2 Conclusions

1. Method A, the code-amplified displacement, gives R_A between 3.30 and 4.19, and Method B, the FEMA 356 target displacement, gives R_B between 2.24 and 3.74, with ductility ratios between 1.08 and 1.57. Both are below 6.40 in every model. Method A reduces to $R_A = (C_d / I_e)(K_e / K_d)$; since the effective stiffness of the nonlinear models is 75 to 95 percent of the design stiffness, R_A cannot exceed C_d / I_e = 4.40. These two methods measure the factor mobilized at a prescribed demand and do not indicate that the tabulated factor is unsafe.

2. Method C, the displacement at which the first component reaches the Collapse-Prevention limit of ASCE 41-17, gives R_C between 10.21 and 13.50 (12.76 to 16.87 against 8), with ductility ratios between 1.99 and 2.92. Under the uniform pattern all seven models exceed 6.40. Under the first-mode pattern five models reached the limit and give 9.98 to 11.08; the six-story frame and Model 7 did not reach it within the analyzed range, and no factor is reported for them under that pattern. For the seven frames examined, and under the assumptions of this study, the tabulated factor R = 8 is therefore conservative with respect to the strength and deformation capacity available up to Collapse Prevention. This conclusion is not extended to other configurations, site classes or hazard levels.

3. The overstrength factor of Method C is 3.96 to 5.98 (4.95 to 7.48 on the basis of R), above the tabulated Ω_0 = 3.0. Its sources, which include member sizing for drift and

for the strong-column weak-beam requirement, minimum reinforcement, strength reduction factors and expected material strengths, were not separated.

4. Under the uniform pattern the base hinges of the first-story interior columns are the first components to reach Collapse Prevention in six of the seven models; in Model 5 a beam governs. R_C is 10.21, 11.91 and 12.32 for the four-, six- and fifteen-story frames, but the three frames differ in more than height, and no general trend with height is inferred.

5. Among the variants of the fifteen-story frame, Model 4 (100 mm hoops with 29 MPa concrete) lowered R_C by 12.1 percent, a combined effect that cannot be attributed to hoop spacing alone; Model 5 (about 2 percent column reinforcement) raised it by 9.5 percent, through overstrength; and Models 6 and 7 (reduced column sections in stories 3 to 5 and 13 to 15) changed it by less than 0.5 percent.

6. The estimated factor depends strongly on the definition of the maximum displacement: for the same frame, the capacity-based definition gives about 3 to 6 times the value of the demand-based definitions. For a structure with $I_e \neq 1$, the factor estimated from the design base shear is R / I_e and must be compared on that basis.

7.3 Limitations

1. Method. The study is deterministic and based on nonlinear static analysis under two load patterns. Record-to-record variability, cyclic degradation and higher-mode effects beyond those two patterns are not represented, and no collapse probability is established.

2. Modeling. R_A depends on the stiffness assumptions of the two models (ACI 318-19 cracked-section factors in design, ASCE 41-17 Table 10-5 in the nonlinear model). The column hinges follow ASCE 41-17 Table 10-8; shear failure, joint failure and bond slip are not modeled.

3. Declared departures. The expected steel strength, 455.05 MPa, is below 1.25 f_y; the gravity load case is 1.0 D + 0.25 L; and the column Collapse-Prevention limits use the gravity axial load, which is expected to be unconservative for exterior columns (inference, not quantified).

4. Scope. The models share one site class, one hazard level, one plan and one set of nominal materials. The design of the fifteen-story frames is governed by the minimum

base shear coefficient. The analysis is unidirectional, and accidental torsion, masonry infill and soil-structure interaction are not considered.

5. Incomplete cases. Model 4 changes the hoop spacing and the concrete strength together. Under the first-mode pattern the six-story frame and Model 7 did not reach the Collapse-Prevention limit within the analyzed range.

7.4 Recommendations

For practice:

- For frames of the type and in the seismic setting examined, the capacity-based results give no evidence for lowering the tabulated value R = 8.

- An analytical estimate of R should state the definition of the maximum displacement, take it from a code or standard, report more than one definition, and state the basis of comparison where I_e differs from unity.

- The stiffness assumptions of the design model and of the nonlinear model should be reported together, since their ratio controls the demand-based estimates.

For future research:

- Nonlinear response-history and incremental dynamic analysis following FEMA P-695 (FEMA, 2009), with ground motions representative of the Dead Sea Transform, to verify the pushover-based values and to establish the collapse margin associated with R = 8.

- Extension to Site Classes C and D and to other hazard levels, where spectral demand rather than the minimum base shear coefficient would govern the design of the taller frames.

- A variant with 100 mm hoop spacing and the reference concrete strength, to isolate the effect of hoop spacing, together with sensitivity studies of the expected steel strength and of the effective stiffness of the nonlinear model.

- A broader family of archetypes and load patterns, including masonry infill and bidirectional loading, so that trends with height can be separated from the design changes that accompany it.

REFERENCES

Abdi, H., Hejazi, F. and Jaafar, M.S., 2019. Response modification factor: Review paper. IOP Conference Series: Earth and Environmental Science. 357, 012003.

Abou-Elfath, H. and Elhout, E., 2018. Evaluating the response modification factors of RC frames designed with different geometric configurations. International Journal of Civil Engineering. 16, 1699-1711.

Abuznaid, H.A., 2023. Response modification factor in intermediate moment resisting frame building (Master's thesis). Palestine Polytechnic University, Hebron.

Ahmad, N., Rizwan, M., Ashraf, M., Khan, A.N. and Ali, Q., 2021. Seismic collapse safety of reinforced concrete moment resisting frames with/without beam-column joint detailing. Bulletin of the New Zealand Society for Earthquake Engineering. 54, 1-20.

Ahmed, M.M.M., Abdo, M.A.-B. and Mohamed, W.A.E.-W., 2021. Evaluation of seismic response modification factor (R) for moderate-rise RC buildings with vertical irregular configurations (Preprint). Research Square. https://doi.org/10.21203/rs.3.rs-1141410/v1

Al-Ahmar, R. and Al-Samara, M., 2015. An evaluation of the seismic response modification factor R for RC special moment-resisting frame system. International Journal of Structural Engineering. 6, 368-387.

Al-Dabbeek, J.N., 2007. Vulnerability and expected seismic performance of buildings in West Bank, Palestine. The Islamic University Journal (Series of Natural Studies and Engineering). 15, 193-217.

Al-Dabbeek, J.N. and Al-Jawhari, A.H.W., 2002. Reinforced concrete frame with infill walls designed for gravity loading (Housing Report 48, Palestinian Territories). World Housing Encyclopedia, Earthquake Engineering Research Institute and International Association for Earthquake Engineering. https://www.world-housing.net/WHEReports/wh100032.pdf (accessed 11 November 2026).

AlHamaydeh, M., Abdullah, S., Hamid, A. and Mustapha, A., 2011. Seismic design factors for RC special moment resisting frames in Dubai, UAE. Earthquake Engineering and Engineering Vibration. 10, 495-506.

Ambraseys, N., 2009. Earthquakes in the Mediterranean and Middle East: A multidisciplinary study of seismicity up to 1900. Cambridge University Press, Cambridge.

American Concrete Institute, 2019. Building code requirements for structural concrete (ACI 318-19). American Concrete Institute, Farmington Hills, MI.

American Society of Civil Engineers, 2016. Minimum design loads and associated criteria for buildings and other structures (ASCE/SEI 7-16). ASCE, Reston, VA.

American Society of Civil Engineers, 2017. Seismic evaluation and retrofit of existing buildings (ASCE/SEI 41-17). ASCE, Reston, VA.

An-Najah National University, n.d. Seismic hazard map for building codes in the Levant. Earth Sciences and Seismic Engineering Unit, Urban Planning and Disaster Risk Reduction Center, Nablus. https://www.najah.edu/en/research/scientific-centers/urban-planning-and-disaster-risk-reduction-center/earth-sciences-and-seismic-engineering-unit/seismic-hazard-map/ (accessed 11 November 2026).

Applied Technology Council, 1978. Tentative provisions for the development of seismic regulations for buildings (ATC 3-06). ATC, Palo Alto, CA.

Applied Technology Council, 1995. Structural response modification factors (ATC-19). ATC, Redwood City, CA.

Applied Technology Council, 1996. Seismic evaluation and retrofit of concrete buildings (ATC-40). ATC, Redwood City, CA.

Ariyanto, M., Purba, R.H. and Riyanto, H., 2026. Seismic response of reinforced concrete structures using pushover analysis with varying number of stories. Reka Buana: Jurnal Ilmiah Teknik Sipil dan Teknik Kimia. 11, 169-181.

Attia, R.A., El-Tahawy, R.M.G. and Fayed, M.N., 2020. Seismic response modification factor for special concrete structures based on pushover and nonlinear time history analyses. Advances in Science, Technology and Engineering Systems Journal. 5, 436-445.

Avni, R., Bowman, D., Shapira, A. and Nur, A., 2002. Erroneous interpretation of historical documents related to the epicenter of the 1927 Jericho earthquake in the Holy Land. Journal of Seismology. 6, 469-476.

Balendra, T., Tan, K.-H. and Kong, S.-K., 1999. Vulnerability of reinforced concrete frames in low seismic region, when designed according to BS 8110. Earthquake Engineering and Structural Dynamics. 28, 1361-1381.

Banerjee, S., Singh, D. and Shiradhonkar, S., 2023. Estimation of seismic design factors for RC-SMRF buildings in seismic risk framework, in: COMPDYN 2023 Proceedings. pp. 5202-5217.

Bathe, K.-J., 1996. Finite element procedures. Prentice Hall, Upper Saddle River, NJ.

Boore, D.M., Joyner, W.B. and Fumal, T.E., 1997. Equations for estimating horizontal response spectra and peak acceleration from western North American earthquakes: A summary of recent work. Seismological Research Letters. 68, 128-153.

Borzi, B. and Elnashai, A.S., 2000. Refined force reduction factors for seismic design. Engineering Structures. 22, 1244-1260.

Bresler, B. and Scordelis, A.C., 1963. Shear strength of reinforced concrete beams. ACI Journal Proceedings. 60, 51-74.

Bureau of Indian Standards, 2016. Criteria for earthquake resistant design of structures: Part 1. General provisions and buildings (IS 1893-1). Bureau of Indian Standards, New Delhi.

Charney, F.A., 2015. Seismic loads: Guide to the seismic load provisions of ASCE 7-10. ASCE Press, Reston, VA.

Chaulagain, H., Rodrigues, H., Spacone, E., Guragain, R., Mallik, R. and Varum, H., 2014. Response reduction factor of irregular RC buildings in Kathmandu valley. Earthquake Engineering and Engineering Vibration. 13, 455-470.

Computers and Structures, Inc., 2022. ETABS: Integrated building analysis and design software, Version 20.3.0 (Computer software). Computers and Structures, Inc., Walnut Creek, CA.

Computers and Structures, Inc., 2023. SAP2000: Integrated software for structural analysis and design, Version 24.2.0 (Computer software). Computers and Structures, Inc., Walnut Creek, CA.

Cui, S., Chen, Y. and Lu, D., 2021. Probability assessment of structural response modification factor of RC frames by the demand-capacity-factor method. Structures. 30, 628-637.

Damayanti, F. and Muin, R.B., 2023. Comparison of real response modification factors and performance of SMRSF structure with OMRSF structure using pushover method. Rekayasa Sipil. 12, 32-42.

Elnashai, A.S. and Mwafy, A.M., 2002. Overstrength and force reduction factors of multistory reinforced-concrete buildings. The Structural Design of Tall Buildings. 11, 329-351.

European Committee for Standardization, 2004. Eurocode 8: Design of structures for earthquake resistance. Part 1: General rules, seismic actions and rules for buildings (EN 1998-1). CEN, Brussels.

Fayed, M.N., Aboul Nour, L.A. and El-Masry, S.S., 2018. Evaluation of seismic response modification factor of multistory buildings designed according to Egyptian code. IOSR Journal of Mechanical and Civil Engineering. 15, 66-86.

Federal Emergency Management Agency, 2000. Prestandard and commentary for the seismic rehabilitation of buildings (FEMA 356). FEMA, Washington, DC.

Federal Emergency Management Agency, 2005. Improvement of nonlinear static seismic analysis procedures (FEMA 440). FEMA, Washington, DC.

Federal Emergency Management Agency, 2009. Quantification of building seismic performance factors (FEMA P-695). FEMA, Washington, DC.

Ferraioli, M., 2021. Behaviour factor of ductile code-designed reinforced concrete frames. Advances in Civil Engineering. 2021, 6666687.

Foutch, D.A. and Wilcoski, J., 2005. A rational approach for determining response modification factors for seismic design of buildings using current code provisions. Earthquake Spectra. 21, 339-352.

Garfunkel, Z., 2014. Lateral motion and deformation along the Dead Sea Transform, in: Garfunkel, Z., Ben-Avraham, Z. and Kagan, E. (Eds.), Dead Sea Transform Fault System: Reviews. Springer, Dordrecht, pp. 109-150.

Goud, S.S. and Pradeep Kumar, R., 2014. Rationalizing response reduction factor (R) for better performance of reinforced concrete framed buildings, in: Proceedings of the National Conference on Recent Research Advances in Civil Engineering (RRACE-2014). IIIT-Hyderabad, India.

Haselton, C.B., Liel, A.B., Deierlein, G.G., Dean, B.S. and Chou, J.H., 2011. Seismic collapse safety of reinforced concrete buildings. I: Assessment of ductile moment frames. Journal of Structural Engineering. 137, 481-491.

Haselton, C.B., Liel, A.B., Taylor Lange, S. and Deierlein, G.G., 2007. Beam-column element model calibrated for predicting flexural response leading to global collapse of RC frame buildings (PEER Report 2007/03). Pacific Earthquake Engineering Research Center, University of California, Berkeley.

Humar, J.L. and Rahgozar, M.A., 2000. Concept of overstrength in seismic design, in: Proceedings of the 12th World Conference on Earthquake Engineering. Auckland, New Zealand, Paper 0794.

Karanja Kuria, K. and Kegyes-Brassai, O.K., 2023. Pushover analysis in seismic engineering: A detailed chronology and review of techniques for structural assessment. Applied Sciences. 14, 151.

Keerthi, S. and Vivek Philip, 2017. Evaluation of response reduction factor based on redundancy for high rise buildings. International Research Journal of Engineering and Technology. 4, 3161-3164.

Kim, T., Chu, Y., Park, H.-G. and Shin, Y.S., 2016. Over-strength, ductility and response modification factor of small-size reinforced concrete moment frame buildings. Journal of the Earthquake Engineering Society of Korea. 20, 145-153.

Kircher, C.A. and Heintz, J.A., 2008. Overview and key concepts of the ATC-63 methodology, in: Structures Congress 2008: Crossing Borders. American Society of Civil Engineers, Reston, VA.

Kumar, M.S., Rama Rao, R., Bhanuji Rao, K. and Himala Kumari, G., 2017. Analysis of moment resisting RC frames of response reduction factors. International Journal for Technological Research in Engineering. 5, 3020-3024.

Layas, F.M., Karakale, V., Aras, F. and Demircan, K., 2026. Quantifying the response modification factor of RC buildings: A comparative study using nonlinear pushover analysis. World Journal of Advanced Engineering Technology and Sciences. 19, 190-201.

Magar Patil, H.R., 2017. Evaluation of seismic response modification factor for asymmetric structures. Journal of Civil Engineering and Urbanism. 7, 87-94.

Mander, J.B., Priestley, M.J.N. and Park, R., 1988. Theoretical stress-strain model for confined concrete. Journal of Structural Engineering. 114, 1804-1826.

Miranda, E. and Bertero, V.V., 1994. Evaluation of strength reduction factors for earthquake-resistant design. Earthquake Spectra. 10, 357-379.

Mitchell, D. and Paultre, P., 1994. Ductility and overstrength in seismic design of reinforced concrete structures. Canadian Journal of Civil Engineering. 21, 1049-1060.

Mondal, A., Ghosh, S. and Reddy, G.R., 2013. Performance-based evaluation of the response reduction factor for ductile RC frames. Engineering Structures. 56, 1808-1819.

Mueller, G., 1977. Numerical problems in nonlinear analysis of reinforced concrete (Report No. UC SESM 77-5). Structural Engineering and Structural Mechanics, University of California, Berkeley.

Newmark, N.M. and Hall, W.J., 1982. Earthquake spectra and design. Earthquake Engineering Research Institute, Berkeley, CA.

Nishanth, M., Visuvasam, J., Simon, J. and Packiaraj, J.S., 2017. Assessment of seismic response reduction factor for moment resisting RC frames. IOP Conference Series: Materials Science and Engineering. 263, 032034.

Oggu, P., Gopikrishna, K. and Nagariya, A., 2021. Seismic behavior and response reduction factors for concrete moment-resisting frames. Bulletin of Earthquake Engineering. 19, 5643-5670.

Patel, A.M. and Parikh, K.B., 2022. Computation of R factor for SMRF and OMRF frame using nonlinear time history analysis. International Journal for Research in Applied Science & Engineering Technology. 10, 381-386.

Paulay, T. and Priestley, M.J.N., 1992. Seismic design of reinforced concrete and masonry buildings. John Wiley & Sons, New York.

Prasanth, S. and Ghosh, G., 2022. Role of resilience in selection of R factors for an RC building. Frontiers in Built Environment. 8, 1029209.

Prasanth, S., Ghosh, G., Gupta, P.K., Kumar, V., Paramasivam, P. and Dhanasekaran, S., 2023. Selection of response reduction factor considering resilience aspect. Buildings. 13, 626.

Priestley, M.J.N., Seible, F. and Calvi, G.M., 1996. Seismic design and retrofit of bridges. John Wiley & Sons, New York.

Qubajeh, M., 2026. Response modification factor in intermediate moment resisting frame building (Master's thesis). Palestine Polytechnic University, Hebron.

Sadeghian, V., Erochko, J., Lau, D., Fazileh, F. and Fathi-Fazl, R., 2023. Determination of seismic response modification factors in Canada and the United States: A critical review, in: Canadian-Pacific Conference on Earthquake Engineering 2023. Vancouver.

Safi, M. and Karaki, G., 2024. Seismic performance of deficient reinforced concrete frames in developing countries: a case study in Ramallah city. Discover Civil Engineering. 1, 95.

Sattar, S., 2018. Evaluating the consistency between prescriptive and performance-based seismic design approaches for reinforced concrete moment frame buildings. Engineering Structures. 174, 919-931.

Shaban, A., 2024. Response modification factor in special reinforced concrete moment-resisting frame system and dual systems with shear walls (Master's thesis). Palestine Polytechnic University, Hebron.

Sharon, M., Sagy, A., Kurzon, I., Marco, S. and Rosensaft, M., 2020. Assessment of seismic sources and capable faults through hierarchic tectonic criteria: Implications for seismic hazard in the Levant. Natural Hazards and Earth System Sciences. 20, 125-148.

Shrouf, M., 2025. Response modification factor in intermediate moment resisting frame building (Master's thesis). Palestine Polytechnic University, Hebron.

Sukumar, V., Arunachalam, J. and Haran Pragalath, D.C., 2017. Efficacy of importance factor in seismic design of Indian buildings. Applied Mechanics and Materials. 857, 71-75.

Suquillo, B., Villavicencio, S., Medina, C.D. and Cagua, B., 2026. Configuration-sensitive decomposition of the response modification factor in reinforced concrete moment frames. Buildings. 16, 2752.

Tsopelas, P. and Husain, M., 2004. Measures of structural redundancy in reinforced concrete buildings. II: Redundancy response modification factor RR. Journal of Structural Engineering. 130, 1659-1666.

Uang, C.-M., 1991. Establishing R (or Rw) and Cd factors for building seismic provisions. Journal of Structural Engineering. 117, 19-28.

Vamvatsikos, D. and Cornell, C.A., 2002. Incremental dynamic analysis. Earthquake Engineering and Structural Dynamics. 31, 491-514.

Vidic, T., Fajfar, P. and Fischinger, M., 1994. Consistent inelastic design spectra: Strength and displacement. Earthquake Engineering and Structural Dynamics. 23, 507-521.

Xiao, J., Sun, Y. and Falkner, H., 2006. Seismic performance of frame structures with recycled aggregate concrete. Engineering Structures. 28, 1-8.

Zafar, A., 2009. Response modification factor of reinforced concrete moment resisting frames in developing countries (Master's thesis). University of Illinois at Urbana-Champaign.

Zameeruddin, M. and Sangle, K.K., 2021. Performance-based seismic assessment of reinforced concrete moment resisting frame. Journal of King Saud University - Engineering Sciences. 33, 153-165.

Zohar, M. and Marco, S., 2012. Re-estimating the epicenter of the 1927 Jericho earthquake using spatial distribution of intensity data. Journal of Applied Geophysics. 82, 19-29.

APPENDIX A ELASTIC DESIGN CALCULATIONS AND CODE CHECKS

This appendix documents the seismic design quantities of the fifteen-story reference frame, the derivation of its design base shear, and the story-drift and stability checks of ASCE 7-16 Chapter 12. All quantities are taken from the ETABS design model of the reference frame. The corresponding design base shears of the four- and six-story frames are given in Table 3.4.

A.1 Seismic Design Parameters

Table A.1 Seismic design parameters of the prototype.

Parameter	Symbol	Value	Source
Mapped short-period acceleration	Ss	0.75 g	2.5 Z, Z = 0.30 (Section 3.5)
Mapped 1-second acceleration	S1	0.375 g	1.25 Z, Z = 0.30 (Section 3.5)
Site class	—	A	ASCE 7-16 Table 20.3-1
Site coefficients	Fa, Fv	0.8, 0.8	ASCE 7-16 Tables 11.4-1, 11.4-2
Design short-period acceleration	S_{DS}	0.40 g	ASCE 7-16 Eq. 11.4-3
Design 1-second acceleration	S_{D1}	0.20 g	ASCE 7-16 Eq. 11.4-4
Spectrum corner period	T_s	0.50 s	S_{D1}/S_{DS}
Risk category	—	III	ASCE 7-16 Table 1.5-1
Importance factor	Ie	1.25	ASCE 7-16 Table 1.5-2
Seismic design category	—	D	ASCE 7-16 Tables 11.6-1, 11.6-2
Response modification factor	R	8	ASCE 7-16 Table 12.2-1
Deflection amplification factor	Cd	5.5	ASCE 7-16 Table 12.2-1
Redundancy factor	ρ	1.3	ASCE 7-16 Section 12.3.4 (retained in design; see A.3)

A.2 Design Base Shear

The approximate fundamental period follows ASCE 7-16 Equation 12.8-7 with the coefficients for concrete moment-resisting frames of Table 12.8-2, Ct = 0.0466 and x = 0.9, and a structural height hn = 45.0 m:

$$T_a = C_t\, h_n^{\,x} = 0.0466\,(45.0)^{0.9} = 1.433 \text{ s} \tag{A.1}$$

The upper-limit coefficient is $C_u = 1.5$ from Table 12.8-1 at $S_{D1} = 0.20$ g, so that $C_u T_a = 1.5 \times 1.433 = 2.150$ s, which is the period at which the seismic response coefficient is evaluated for load case EQX. The fundamental period computed by the ETABS modal

analysis in the direction of loading is 2.897 s, which exceeds the cap, so the seismic response coefficient is evaluated at the capped period in accordance with Section 12.8.2.

Table A.2 Seismic response coefficient, reference frame.

Expression	Equation	Value of C_s	Status
$S_{DS} / (R / I_e)$	12.8-2	0.0625	Base value
$S_{D1} / (T (R / I_e))$ at T = 2.150 s	12.8-3	0.0145	Upper limit, $T \leq T_L$
$0.044 S_{DS} I_e \geq 0.01$	12.8-5	0.0220	Governs

The minimum coefficient of Equation 12.8-5 exceeds the period-dependent value of Equation 12.8-3 by the factor $0.044 S_{DS} T R / S_{D1} = 0.044 (0.40) (2.150) (8) / 0.20 = 1.51$, and therefore governs the design. With an effective seismic weight of W = 100,172 kN,

$$V_d = Cs\ W = 0.0220\ (100{,}172) = 2{,}203.78\ \text{kN} \tag{A.2}$$

The ETABS story-force output returns a base shear of 2,203.78 kN for load case EQX, which confirms the hand calculation. The total dead load reported at the base of the first story is 100,750.4 kN; the effective seismic weight is 0.6 percent lower because the mass source is defined from the dead load pattern without the base-level tributary. The magnitude of the total dead load confirms that the self-weight of the structural members is carried in the dead load pattern, since the superimposed dead load alone would amount to 32,400 kN.

A.3 Story Drift Check

The design story drift is obtained from the elastic story drift of the equivalent lateral force analysis through ASCE 7-16 Equation 12.8-15. The redundancy factor is taken as unity for drift calculations in accordance with Section 12.3.4.1, item 2. The allowable drift for Risk Category III under the heading of all other structures is $0.015 h_{sx}$ from Table 12.12-1.

Table A.3 Story drift check, reference frame.

Quantity	Value
Maximum elastic story drift ratio, $\delta xe/h_{sx}$ (story 7, EQX)	0.002703
Amplification, Cd/Ie	4.40
Design story drift ratio, Δ/h_{sx}	0.01189
Design story drift, Δ (h_{sx} = 3,000 mm)	35.68 mm
Allowable story drift, $\Delta a = 0.015\ h_{sx}$	45.00 mm
Utilization, $\Delta/\Delta a$	0.793
Result	Satisfied

ASCE 7-16 Section 12.12.1.1, referenced by footnote b to Table 12.12-1, requires the design story drift not to exceed $\Delta a/\rho$ for seismic force-resisting systems comprising only moment frames in Seismic Design Categories D through F. The conditions of Section 12.3.4.2 under which ρ may be taken as 1.0 are examined here. Condition (b) of that section is met directly: the structure is regular in plan at all levels, and its seismic force-resisting system has four bays of perimeter moment framing on each side in the direction of loading and three bays on each side in the orthogonal direction, more than the two bays required. Condition (a) is also met. Stories 1 to 13 each resist more than 35 percent of the base shear (Table A.4), so Table 12.3-3 applies to them. In the direction of loading each story contains four bays on each of four frame lines, giving sixteen beams; the loss of moment resistance at both ends of any one of them removes of the order of six percent of the story strength, well below the 33 percent threshold of the table. The plan is doubly symmetric with a rigid diaphragm and develops no extreme torsional irregularity of Type 1b. Both conditions are therefore satisfied and $\rho = 1.0$ is permitted, so the limit of Section 12.12.1.1 coincides with Δa = 45.00 mm and the check is satisfied at the utilization reported in Table A.3. Had $\rho = 1.3$ been retained the limit would be 34.62 mm and the governing drift would exceed it by 3.1 percent; the outcome of this provision is therefore governed by the redundancy assessment rather than by the stiffness of the frame, and the assessment is recorded here for that reason. The redundancy factor was nevertheless retained at 1.3 in the strength load combinations of Section 3.7, which is conservative: adopting 1.0 there would reduce the seismic load effect on every member. The design base shear is unaffected either way, because it is governed by the minimum base shear floor of Equation 12.8-5, in which the redundancy factor does not appear.

A.4 Stability Coefficient

The stability coefficient of ASCE 7-16 Equation 12.8-16 is

$$\theta = P_x \, \Delta \, I_e / (V_x \, h_{sx} \, C_d) \qquad \text{(A.3)}$$

in which P_x is the total unfactored vertical design load at and above the level considered and Δ is the design story drift. Since $\Delta = C_d \, \delta_{xe} / I_e$, the coefficient equals $P_x \, \delta_{xe} / (V_x \, h_{sx})$, with δ_{xe} the elastic story drift of the design analysis. Section 12.8.7 does not require P-delta effects to be considered where $\theta \leq 0.10$, and it limits θ to $\theta_{max} = 0.5 / (\beta \, C_d) \leq 0.25$, in which β is the ratio of shear demand to shear capacity of the story and may conservatively be taken as 1.0. Table A.4 gives θ for every story.

The coefficient is largest in story 5, $\theta = 0.107$, and exceeds 0.10 in stories 3 to 6; at the story of maximum drift, story 7, $\theta = 71{,}725 \times 0.002703 / 2{,}006.4 = 0.097$. The elastic design analysis in ETABS did not include P-delta effects, so in stories 3 to 6 the displacements and member forces are to be multiplied by $1 / (1 - \theta)$, at most 1.12 (Section 12.8.7). Applied to every story, this raises the largest design story drift from 35.68 mm to 39.6 mm (story 6), which remains below the allowable 45.00 mm. For the member forces, the amplification of at most 12 percent is covered by the redundancy factor of 1.3 that was retained in the strength load combinations although 1.0 is permitted (Section A.3): the seismic load effect used in design, $1.3 \, Q_E$, exceeds the required $1.12 \, Q_E$. For the same reason the shear capacity of each story is at least 1.3 times its demand, so $\beta \leq 0.77$ and $\theta_{max} = 0.5 / (0.77 \times 5.5) = 0.118$, above the largest θ. The nonlinear analyses of Chapters 5 and 6 include P-delta effects directly and are not affected by this check.

The vertical loads and story shears from which the coefficient is evaluated at any level are listed below. The story-force distribution is that of the ETABS design model, scaled to the total weight and base shear of the final design (increases of 1.6 and 1.4 percent respectively).

Table A.4 Vertical load and story shear, reference frame.

Story	**Dead (kN)**	**Live (kN)**	**Px = D + L (kN)**	**Vx, EQX (kN)**	**δ_{xe} / h_{sx}**	**θ, Equation (A.3)**
15	6,536	1,360	7,896	366.7	0.000800	0.017
14	13,072	2,720	15,792	699.7	0.001289	0.029
13	19,609	4,079	23,688	990.5	0.001762	0.042
12	26,145	5,439	31,584	1,241.8	0.002109	0.054
11	32,681	6,799	39,480	1,456.3	0.002305	0.062
10	39,217	8,158	47,375	1,636.4	0.002491	0.072
9	45,753	9,518	55,271	1,785.1	0.002578	0.080
8	52,620	10,878	63,498	1,907.6	0.002634	0.088
7	59,487	12,238	71,725	2,006.4	0.002703	0.097
6	66,354	13,598	79,952	2,080.9	0.002692	0.103
5	73,221	14,957	88,178	2,134.3	0.002583	0.107
4	80,087	16,317	96,404	2,169.8	0.002399	0.107
3	86,955	17,677	104,632	2,190.9	0.002115	0.101
2	93,821	19,036	112,857	2,201.0	0.001639	0.084
1	100,750	20,396	121,146	2,203.8	0.000752	0.041

APPENDIX B COLUMN CONFINEMENT: DESIGN AND MANDER PARAMETERS

This appendix documents the design of the column hoops to ACI 318-19 Section 18.7.5, which fixes the transverse reinforcement ratio ρ_t that enters the column hinges through ASCE 41-17 Table 10-8, and the inputs and outputs of the confined-concrete model of Mander, Priestley and Park (1988) in the SAP2000 parametric material, from which the concrete strength of Model 4 is taken (Section 5.3).

B.1 Design of the Column Hoops

Where $P_u > 0.3\ A_g\ f'_c$, ACI 318-19 Section 18.7.5.2(f) requires every longitudinal bar around the perimeter to be laterally supported by a corner of a hoop or a crosstie, so the number of hoop legs in each direction equals the number of bars on that face. The required area A_{sh} is the largest of the expressions of Table 18.7.5.4, with $b_c = b - 80$ mm (40 mm clear cover). The axial forces P_u are the largest values from the ETABS load combinations that include earthquake effects; for the fifteen-story variants the values of the reference frame at the same story are used (assumption). The hoop diameter is kept at Ø10 with the smallest reduction of spacing that provides the required area, and Ø12 is used where Ø10 does not suffice.

Table B.1 Design of the column hoops.

Model	Column (mm)	P_u (kN)	$P_u / (A_g f'_c)$	A_{sh} required at s = 75 mm (mm²)	Hoops provided	ρ_t
4	500	3,164	0.53	323	Ø10, 4 × 4 legs @ 70	0.00898
6	600	4,783	0.55	394	Ø12, 4 × 4 legs @ 75	0.01005
6	500	3,049	0.51	324	Ø12, 4 × 3 legs @ 75	0.00905
15	1000	11,793	0.49	504	Ø10, 7 × 6 legs @ 70	0.00673
15	950	10,952	0.51	500	Ø10, 6 × 6 legs @ 70	0.00709
15	900	9,300	0.48	439	Ø10, 7 × 8 legs @ 75	0.00814
15	850	8,485	0.49	429	Ø10, 7 × 7 legs @ 75	0.00862
15	800	7,677	0.50	419	Ø10, 6 × 7 legs @ 75	0.00785
15	750	6,878	0.51	412	Ø10, 6 × 5 legs @ 70	0.00748
15	700	5,309	0.45	340	Ø10, 6 × 6 legs @ 75	0.00898
15	650	4,698	0.46	331	Ø10, 6 × 5 legs @ 75	0.00806
15	600	3,759	0.44	295	Ø10, 5 × 5 legs @ 75	0.00873
15	550	2,998	0.41	260	Ø10, 5 × 5 legs @ 75	0.00952
15	500	2,242	0.37	225	Ø10, 4 × 5 legs @ 75	0.00838

Note. $\rho_t = A_v / (b\ s)$ with A_v taken in the direction with fewer legs, as defined in ASCE 41-17 Table 10-8. Model 4 keeps the legs and diameters of the reference frame with the spacing increased to 100 mm, which deliberately does not satisfy Table 18.7.5.4 (Section 3.8).

B.2 Mander Parameters of a Representative Column

The confined properties of Table 5.1 are those returned by the SAP2000 parametric Mander material for a representative 800 × 800 mm column with Ø10 hoops of four legs in each direction, a confined core $b_c = 710$ mm measured to the centerline of the perimeter hoop, and hoop spacings of 75 and 100 mm. The derivation follows.

B.3 Volumetric Confinement Ratio

The volumetric ratio of transverse reinforcement to the confined core is computed for the reference column as

$$\rho_s = 2\ A_{sh} / (s \cdot b_c) \tag{B.1}$$

in which A_{sh} is the total area of transverse reinforcement crossing one principal direction, s is the tie spacing and b_c is the core dimension. For four legs of Ø10, $A_{sh} = 4 \times 78.54 = 314.2$ mm², and $b_c = 710$ mm.

Table B.2 Volumetric confinement ratio.

Tie spacing, s (mm)	A_{sh} (mm²)	b_c (mm)	ρ_s
75	314.2	710	0.01180
100	314.2	710	0.00885

B.4 Derived Confined Properties

The confined strength f'_{cc} is the value returned by the SAP2000 parametric Mander material for the representative section at each hoop spacing, computed by the program from the core geometry, the transverse reinforcement layout and its yield strength. The confined strains follow the Mander formulation applied to that strength. The peak strain is $\varepsilon_{cc} = \varepsilon_{co}\ [1 + 5\ (f'_{cc} / f'_c - 1)]$ with $\varepsilon_{co} = 0.002$, the secant modulus at peak stress is $E_{sec} = f'_{cc} / \varepsilon_{cc}$, and the curve-shape parameter is $r = E_c / (E_c - E_{sec})$ with $E_c = 23{,}025$ MPa from ACI 318-19 Section 19.2.2. The ultimate compressive strain follows the energy-balance approximation of Priestley, Seible and Calvi (1996),

$$\varepsilon_{cu} = 0.004 + 1.4\ \rho_s\ f_{yh}\ \varepsilon_{su} / f'_{cc} \tag{B.2}$$

in which $f_{yh} = 420$ MPa is the yield strength of the transverse reinforcement and $\varepsilon_{su} = 0.09$ is the steel strain at maximum stress.

Table B.3 Mander confined-concrete parameters.

Quantity	Symbol	75 mm	100 mm
Unconfined strength (MPa)	f'_c	24.0	24.0
Confined strength (MPa)	f'_{cc}	35.0	29.0
Confinement ratio	f'_{cc}/f'_c	1.458	1.208
Unconfined peak strain	ε_{co}	0.00200	0.00200
Confined peak strain	ε_{cc}	0.00658	0.00408
Elastic modulus (MPa)	E_c	23,025	23,025
Secant modulus at peak (MPa)	E_{sec}	5,316	7,102
Curve-shape parameter	r	1.300	1.446
Volumetric confinement ratio	ρ_s	0.01180	0.00885
Transverse yield strength (MPa)	f_{yh}	420	420
Steel strain at maximum stress	ε_{su}	0.090	0.090
Confined ultimate strain	ε_{cu}	0.01738	0.01611

B.5 Internal Consistency Check

Equation (B.2) was evaluated independently at both tie spacings using the quantities of Table B.3:

$$\text{At } s = 75 \text{ mm:}\quad \varepsilon_{cu} = 0.004 + 1.4\,(0.00885)\,(420)\,(0.09)/35.0 = 0.01738$$

$$\text{At } s = 100 \text{ mm:}\quad \varepsilon_{cu} = 0.004 + 1.4\,(0.00664)\,(420)\,(0.09)/29.0 = 0.01611$$

Both values reproduce Table 5.1 of the main text. A stronger form of the same check is obtained by inverting Equation (B.2). Taking ρs from the section geometry alone and f'cc and εcu from the two SAP2000 material definitions, the steel strain at maximum stress is recovered as 0.090004 at 75 mm spacing and 0.089995 at 100 mm. Two independent tie spacings, two independent confined strengths and a single recovered steel model, agreeing to five decimal places with the value of 0.09 adopted by Priestley, Seible and Calvi (1996), confirm that both material definitions were generated from the same section geometry and the same constitutive assumptions. The ratio ρs (100 mm)/ρs (75 mm) returns 0.7499 against the exact 0.750 required by the inverse proportionality to tie spacing.

APPENDIX C PLASTIC HINGE PROPERTIES

This appendix documents the plastic-hinge formulation used in the nonlinear static analyses, the modeling parameters and acceptance criteria of representative beam and column hinges, and the evolution of the hinge demand-capacity ratio through the pushover of the fifteen-story reference frame.

C.1 Hinge Assignment Scheme

Table C.1 Plastic hinge assignment scheme.

Item	Beams	Columns
Hinge type	Moment (M3), user-defined for each beam section	Interacting axial-biaxial moment (P-M2-M3), generated automatically
Modeling parameters	ASCE 41-17 Table 10-7, row i: a = 0.025, b = 0.05, c = 0.2	ASCE 41-17 Table 10-8, from the axial load of the gravity case and ρ_t of the section
Yield moment	M_y^+ and M_y^- from the SAP2000 section analysis (Table 5.6)	From the P-M interaction of the section
Peak point C	1.1 M_y	1.1 M_y
Backbone symmetry	Symmetric in rotation	As generated
Collapse-Prevention criterion used in Method C	Table 10-7, for each section and each sign of moment, with $(\rho - \rho')/\rho_{bal}$	0.7 b of Table 10-8, Equation (5.2), with $N_{UD} / (A_g f'_{cE}) \geq 0.1$
Location	Both ends of every member	Both ends of every member
Material basis	Expected properties, f'_{cE} = 35 MPa, f_{yE} = 455.05 MPa	Expected properties, f'_{cE} = 35 MPa, f_{yE} = 455.05 MPa

C.2 Representative Hinges

Table C.2 gives the parameters of the beam type B3 and of the base hinge of a first-story interior column of the fifteen-story reference frame. For the column, with N_{UD} = 8,219 kN under the gravity case, A_g = 1.0 m² and f'_{cE} = 35 MPa, the axial load ratio is 0.235 and ρ_t = 0.00673, so Equation (5.2) gives b = 0.5 / [5 + (0.235 / 0.8) (1 / 0.00673) (35 / 455.05)] − 0.01 = 0.0498 and θ_{CP} = 0.7 b = 0.0349 rad.

Table C.2 Parameters of representative hinges, reference frame.

Quantity	**Beam B3 (500 × 450 mm)**	**Column, 1000 × 1000 mm, story 1, base**
M_y (kN·m)	171.3 (positive) / 309.7 (negative)	From the P-M interaction
a / b / c	0.025 / 0.050 / 0.20	Table 10-8 with n = 0.235, ρ_t = 0.00673
θ_{CP} (rad)	0.0500 (positive) / 0.0470 (negative)	0.0349
D/C at $\Delta_{max,C}$ of the reference frame	≤ 0.90 (largest of all beams)	1.01 (governing)

C.3 Evolution of the Hinge Demand-Capacity Ratio, Fifteen-Story Reference Frame

The reference frame carries 1,530 plastic hinges. Table C.3 reports, at selected steps of the uniform-pattern pushover saved at 20 mm increments, the largest D/C ratio among all hinges and the number of hinges whose D/C ratio exceeds unity.

Table C.3 Hinge D/C evolution, reference frame.

Step	**Roof displacement (mm)**	**Base shear (kN)**	**Largest D/C**	**Hinges with D/C > 1**
0	0.0	0.0	0.000	0
10	200.0	4,071.7	0.000	0
20	400.0	7,467.6	0.141	0
30	600.0	10,081.7	0.295	0
40	800.0	12,169.5	0.436	0
50	1,000.0	13,804.1	0.585	0
60	1,200.0	15,257.9	0.759	0
67	1,340.0	16,135.6	0.975	0
68	1,360.0	16,251.8	1.014	6
70	1,400.0	16,480.3	1.090	8
80	1,600.0	17,447.9	1.497	80
90	1,800.6	18,318.0	1.903	146
100	2,000.0	18,994.2	2.344	166

The largest D/C ratio reaches unity between steps 67 and 68, which gives $\Delta_{max,C}$ = 1,352.80 mm by Equation (6.14). Up to step 67 no hinge has exceeded its Collapse-Prevention criterion; at the end of the analysis, at 2.0 m, 166 of the 1,530 hinges have.

APPENDIX D FEMA 356 DISPLACEMENT COEFFICIENT METHOD: COEFFICIENT VALUES

This appendix documents the coefficients used in Method B of Chapter 6 and the resulting target displacements. The target displacement of FEMA 356, Section 3.3.3.3.2, Equation 3-15, is

$$\delta_t = C_0 \, C_1 \, C_2 \, C_3 \, S_a \, (T_e^2 / 4\pi^2) \, g \tag{D.1}$$

D.1 Basis of Each Coefficient

Three of the four coefficients are fixed by the standard for the structures examined here, and are not free parameters of the study.

Table D.1 Basis of the displacement modification coefficients.

Coefficient	Value	Basis
C_1	1.00	FEMA 356 Section 3.3.3.3.2: $C_1 = 1.0$ for $T_e \geq T_s$. With $S_{DS} = 0.40$ g and $S_{D1} = 0.20$ g, $T_s = 0.50$ s, and the effective period of every model exceeds it.
C_2	1.00	FEMA 356 Table 3-3, Framing Type 2. The special moment frames of this study contain none of the degrading components that define Framing Type 1. The standard additionally permits $C_2 = 1.0$ for nonlinear procedures.
C_3	1.00	FEMA 356 Section 3.3.3.3.2: $C_3 = 1.0$ for buildings with positive post-yield stiffness. The capacity curve has a positive slope at the target displacement in every model.
C_0	Computed	FEMA 356 Table 3-2 permits the tabulated value; the standard states that explicit calculation from the deflected shape is preferred. C_0 was computed from the first mode of the nonlinear model in the direction of loading for every model (Section D.2).

D.2 Computation of C_0

FEMA 356 defines C_0 as the first-mode participation factor evaluated at the control node. Using the elastic first-mode shape, and denoting by Γ the modal participation factor in the direction of loading and by φ_{roof} the mode-shape ordinate at the roof under the same normalization,

$$C_0 = \Gamma \cdot \varphi_{roof} \tag{D.2}$$

The SAP2000 modal analysis normalizes each mode shape to unit modal mass, so the participation factor Γ (in the units of the program output) and the roof ordinate φ_{roof} (in m) may be combined directly; their product C_0 is dimensionless and independent of the scaling convention.

Table D.2 Modal properties and target displacement.

Model	**T_e (s)**	**Γ**	**φ_{roof}**	**$C_0 = \Gamma \varphi_{roof}$**	**S_a (g)**	**S_d (mm)**	**δ_t (mm)**	**Δ_y (mm)**
Four-story	1.205	46.109	0.027561	1.271	0.1660	59.88	76.09	48.43
Six-story	1.561	56.670	0.022824	1.293	0.1281	77.58	100.35	76.41
Fifteen-story reference	3.667	86.608	0.015424	1.336	0.0545	182.26	243.48	223.67
Model 4	3.667	86.608	0.015424	1.336	0.0545	182.26	243.48	222.13
Model 5	3.667	86.608	0.015424	1.336	0.0545	182.26	243.48	223.67
Model 6	3.676	86.560	0.015416	1.334	0.0544	182.69	243.78	224.78
Model 7	3.669	86.372	0.015634	1.350	0.0545	182.36	246.24	226.22

The spectral acceleration is evaluated on the constant-velocity branch of the design spectrum, $S_a = S_{D1} / T_e$, which applies because the effective period of every model lies between $T_s = 0.50$ s and the long-period transition period $T_L = 4$ s. The yield displacement listed is that of the Method B idealization, with $\Delta_u = \delta_t$ (Section 6.5.2).